Technical Report
TR-23-23
December 2024

Evaluation and modelling report of Task 10.2.1 – Geometric evaluation and prediction of fracture surfaces and aperture distributions

Task 10 of SKB Task Force GWFTS – Validation approaches for groundwater flow and transport modelling with discrete features

Stefan Finsterle
Milan Hokr
Aleš Balvín
Jakub Jankovec
Libor Gvoždík
Jeffrey Hyman
Hari Viswanathan
Matthew Sweeney
Tai-Tien Wang
Po-Kai Chen
Chia-Hsiang Tu
Seungbeom Choi
Chae-Soon Choi
Yong-Ki Lee
Kyung-Woo Park
Sung-Hoon Ji
Brandon Stock
Andrew Frampton

SVENSK KÄRNBRÄNSLEHANTERING AB

SWEDISH NUCLEAR FUEL
AND WASTE MANAGEMENT CO

Box 3091, SE-169 03 Solna
Phone +46 8 459 84 00
skb.se

SVENSK KÄRNBRÄNSLEHANTERING

ISSN 1404-0344
SKB TR-23-23
ID 2058558
December 2024

Evaluation and modelling report of Task 10.2.1 – Geometric evaluation and prediction of fracture surfaces and aperture distributions

Task 10 of SKB Task Force GWFTS – Validation approaches for groundwater flow and transport modelling with discrete features

Stefan Finsterle[1], Milan Hokr[2], Aleš Balvín[2], Jakub Jankovec[3], Libor Gvoždík[3], Jeffrey Hyman[4], Hari Viswanathan[4], Matthew Sweeney[4], Tai-Tien Wang[5], Po-Kai Chen[5], Chia-Hsiang Tu[5], Seungbeom Choi[6], Chae-Soon Choi[6], Yong-Ki Lee[6], Kyung-Woo Park[6], Sung-Hoon Ji[6], Brandon Stock[7], Andrew Frampton[7]

1 Finsterle GeoConsulting, LLC
2 Technical University of Liberec (TUL)
3 PROGEO Ltd.
4 Los Alamos National Laboratory
5 National Taiwan University, Department of Civil Engineering
6 Korea Atomic Energy Research Institute (KAERI)
7 Department of Physical Geography, Stockholm University

Keywords: Pragmatic validation, Fractured rock, Flow channelling, Roughness/aperture.

Abstract

This report evaluates the modelling and analysis work on Task 10.2.1 performed by five Modelling Groups participating in the SKB Task Force GWFTS. The overall goal of Task 10 is to (1) improve the understanding of fluid flow through single fractures and fracture networks, and (2) exercise the steps of a proposed pragmatic model validation approach.

The specific objectives of Task 10.2 are (1) to develop concepts and models for flow and transport at the single-fracture scale, (2) to consider the importance of hydro-mechanical coupling on flow and transport, and (3) to develop modelling approaches for the prediction of flow and transport in single fractures as well as fracture properties upscaled from the borehole to the deposition hole scales.

Task 10.2.1 is the first step in the road map for Task 10.2, focusing on geometric evaluation of fracture surfaces and aperture distribution on a borehole scale and predicting fracture surface topography and aperture distributions on a metre scale. The main objectives of Task 10.2.1 are (1) to get familiar with the fracture surface datasets and provide the opportunity to develop appropriate tools and concepts, (2) to develop methods for building a description of the fracture roughness and fracture void space (together with an assessment of relevant uncertainties) for the purpose of flow and transport simulations, (3) to investigate scaling of fracture surface properties from borehole to metre scale, and (4) to start to consider the influence of fracture normal closure on this void space description, which will be a topic for Task 10.2.2.

The introductory Task 10.2.1 establishes the workflow for the pragmatic validation of the fundamental fracture characterisation data and their pre-processing methods for the derivation of properties that are subsequently used in the flow simulations of Task 10.2.2. Both subtasks support the aim of Task 10.2, which focuses on mechanical effects and flow through a single fracture, which in turn supports the overall goals of Task 10 to better understand fluid flow in fracture networks based on a suite of pragmatically validated submodels.

Task 10.2.1 considers the characterisation of a single fracture based on high-resolution surface roughness measurements. This analysis of roughness data involves the development of a simplified geometrical or mathematical representation of the fracture based on a set of high-resolution measurements of fracture topography. The underlying assumptions and formulas are the basis for generating upscaled aperture distributions, which are subsequently used for flow and transport modelling with focus on capturing channelling effects. The individual steps of the workflow need to be tested using a model validation approach, which is pragmatically tailored to the ultimate modelling purpose.

Five Modelling Groups participated in Task 10.2.1; the modelling reports, written by the individual Modelling Groups, are included in this evaluation report as Appendices. The Modelling Group's work and its evaluation is briefly summarised as follows:

1. The SÚRAO Modelling Group from the Technical University of Liberec (TUL) and PROGEO Ltd. followed the guidance of the Task Description and did a detailed analysis of fracture surface topography as the basis for estimating aperture distributions and effective transmissivities. The analysis and documentation provide the information needed to gain insights into the validity of the chosen approach and the use of the generated single-fracture aperture fields for model validation and subsequent use. It is recommended that SÚRAO compare the calculated, upscaled performance metrics with the corresponding values from the three large fractures, thus completing the prediction-outcome exercise.
2. The DOE Modelling Group from Los Alamos National Laboratory (LANL) calculated some statistical measures of the fracture surface heights using a geostatistical method. However, questions related to uncertainty propagation to flow-relevant representations of fractures, flow channelling, or model validation were not addressed.
3. The Modelling Group from the National Taiwan University (NTU) performed detailed and sophisticated analyses to characterize the fracture surfaces, generate upscaled property fields, and derive aperture distributions as a function of different loading forces. The workflow and methods presented by NTU likely contain useful information that improve fundamental system understanding and help

making pragmatic decisions about abstraction steps that need to be taken as the scale and complexity of the fracture system increases in subsequent subtasks. However, the absence of formal sensitivity analyses makes it difficult to identify the relative relevance of the processes, fracture characteristics, and model simplifications in support of the ultimate modelling purpose. The excellent modelling work should be supplemented with a detailed discussion and interpretation of the results to arrive at actionable conclusions and a defensible, pragmatic model validation.

4. The Modelling Group from the Korea Atomic Energy Research Institute (KAERI) diligently pre-processed the provided data sets, calculated various measures describing the characteristics of the fracture surfaces and corresponding aperture fields, developed a two-step workflow to derive upscaled fields of surface heights, and used a simplified approach to account for aperture changes in responses to different normal stresses. Flow simulations were also performed. Initial steps towards the validation of the derived aperture field and upscaled surface heights were taken by comparing the derived surface heights to pressure film data, albeit without testing against formal validation acceptance criteria. KAERI's work in Task 10.2.1 will likely assist subsequent tasks if properly supplemented by methods that support pragmatic model validation across different modelling spaces.
5. The SKB Modelling Group from Stockholm University developed data pre-processing, analysis, and upscaling procedures based on sophisticated theoretical concepts. More relevant, the assumptions underlying these concepts are well described, tested, or otherwise justified, with limitations and uncertainties discussed. Surface roughness, pressure film data, and derived aperture distributions were used in prediction-outcome exercises to evaluate the proposed analysis and upscaling procedure. Sensitivity and uncertainty analyses were performed to examine the impact of modelling decisions on the predicted performance metrics. Recommendations about future work and changes to the proposed workflow were also made in preparation for the application of the workflow in subsequent subtasks.

In general, the modelling needed to develop a defensible upscaling procedure for deriving fracture surface roughness and/or aperture distributions in support of the simulation of fluid flow and analysis of channelling effects are conceptually and numerically very challenging. Interpretation of the computational results and the workflow of pragmatic validation requires additional understanding and skills. Moreover, documentation of both the modelling and validation work is arguably difficult and arduous. Most Modelling Groups demonstrated their deep understanding and computational capabilities in data pre-processing and modelling analyses. Despite this diligent work on data processing, only some of the Modelling Group supplied results in support of the main two goals of Task 10.2.1: (1) understanding of the impact of small-scale fracture topography on flow and channelling effects, and (2) pragmatic model validation, which requires uncertainty propagation and the comparison of relevant performance metrics to validation acceptance criteria. This suggests that pragmatic model validation remains difficult to understand, conduct, and/or document. It is therefore recommended that future exercises be carefully planned by both the Task Force Secretariat and the Modelling Groups so that the results of the Modelling Group's considerable efforts provide practical workflows and useful insights into both fluid flow and transport in fractured media and pragmatic model validation.

Sammanfattning

Denna rapport utvärderar modellerings- och analysarbetet angående Modelleringsuppgift 10.2.1 som utförts av fem modelleringsgrupper som deltar i SKB Task Force GWFTS. Det övergripande målet för Modelleringsuppgift 10 är att (1) förbättra förståelsen av vätskeflöde genom enstaka sprickor och spricknätverk och (2) utöva stegen i en föreslagen pragmatisk modellvalideringsmetodik.

De specifika målen för Modelleringsuppgift 10.2 är (1) att utveckla koncept och modeller för flöde och transport på skalan av enstaka sprickor, (2) att undersöka vikten av hydromekanisk koppling på flöde och transport, och (3) att utveckla modelleringsmetoder för att kunna förutsäga flöde och transport i enstaka sprickor samt sprickegenskaper uppskalade från borrhåls- till deponeringshålsskalan.

Uppgift 10.2.1 utgör det första steget i färdplanen för Uppgift 10.2, med fokus på geometrisk utvärdering av sprickytor och aperturfördelningar i borrhålsskalan samt prediktion av sprickytstopografi och aperturfördelningar i meterskalan. Huvudsyftet med Uppgift 10.2.1 är (1) att bekanta sig med datauppsättningarna för sprickytor samt ge möjlighet att utveckla lämpliga verktyg och koncept, (2) att utveckla metoder för att skapa en beskrivning av sprickgrovheten och sprickhålrummet (tillsammans med en bedömning av relevanta osäkerheter) med syfte att utföra flödes- och transportsimuleringar, (3) för att undersöka skalning av sprickytsegenskaper från borrhåls- till meterskalan, och (4) för att börja betrakta inverkan av en last i spricknormalens riktning på förslutningen av hålrummet i sprickan, vilket kommer att vara ett ämne för Uppgift 10.2.2.

Den inledande modelleringsuppgiften 10.2.1 etablerar arbetsflödet för den pragmatiska valideringen av fundamentala sprickkarakteriseringsdata samt deras förbearbetningsmetoder för härledning av egenskaper som sedan kan användas i flödessimuleringar i Uppgift 10.2.2. Båda deluppgifterna stödjer syftet med Uppgift 10.2, som fokuserar på mekaniska effekter och flöde genom en enskild spricka, vilket i sin tur stödjer de övergripande målen för Uppgift 10 dvs att bättre förstå vätskeflöde i spricknätverk baserade på en uppsättning pragmatiskt validerade delmodeller.

Uppgift 10.2.1 undersöker karakteriseringen av en enskild spricka baserat på högupplösta ytjämnhetsmätningar. Denna analys av grovhetsdata innefattar utvecklingen av en förenklad geometrisk eller matematisk representation av sprickan baserat på en uppsättning högupplösta mätningar av sprickytopografin. De underliggande antagandena och formlerna utgör grunden för att generera uppskalade aperturfördelningar, som sedan används för flödes- och transportmodelleringar med fokus på att beskriva kanaliseringseffekter. De individuella stegen i arbetsflödet måste testas med hjälp av en modellvalideringsmetod, som är pragmatiskt skräddarsydd för det slutgiltiga modelleringssyftet.

Fem modelleringsgrupper deltog i Uppgift 10.2.1. Modelleringsrapporterna, skrivna av de enskilda modelleringsgrupperna, ingår i denna utvärderingsrapport som bilagor. Modelleringsgruppernas arbete och dess utvärdering kan sammanfattas kort på följande sätt:

1. SÚRAO-modelleringsgruppen från det tekniska universitetet i Liberec (TUL) och PROGEO Ltd. följde anvisningarna i modelleringsuppgiftsbeskrivningen och gjorde en detaljerad analys av spricktopografin som grund för att uppskatta aperturfördelningar och effektiva transmissiviteter. Analysen och dokumentationen ger den information som behövs för att få insikter i giltigheten av det valda tillvägagångssättet och användningen av genererade apertursdata för enskilda sprickor i modellvalidering och efterföljande användning. Dock, det rekommenderas att SÚRAO jämför de beräknade och uppskalade karaktäristiska mätetalen med motsvarande värden från de tre stora sprickorna, för att på så sätt slutföra prediktion-resultatövningen dvs jämförelse av prediktioner mot experimentella resultat.
2. DOE:s modelleringsteam från Los Alamos National Laboratory (LANL) beräknade några statistiska mått på sprickytans höjder med hjälp av en geostatistisk metod. Frågor relaterade till propagering av osäkerheter angående flödesrelevanta representationer av sprickor, flödeskanalisering eller modellvalidering behandlades dock inte.
3. Modelleringsteamet från National Taiwan University (NTU) utförde detaljerade och sofistikerade analyser för att karakterisera sprickytorna, generera uppskalade sprickegenskaper och härleda aperturfördelningar som en funktion av graden av belastningskraft. Arbetsflödet och metoderna

som presenteras av NTU innehåller troligen användbar information som förbättrar den grundläggande systemförståelsen och hjälper till att de fatta pragmatiska beslut om abstraktionssteg som måste tas när spricksystemets skala och komplexitet ökar i efterföljande modelleringsuppgifter. Dock, frånvaron av formella känslighetsanalyser gör det svårt att identifiera processernas relativa relevans, sprickegenskaper och modellförenklingar till stöd för det ultimata modelleringssyftet. Det utmärkta modelleringsarbetet bör kompletteras med en detaljerad diskussion och tolkning av resultaten för att komma fram till genomförbara slutsatser och en försvarbar pragmatisk modellvalidering.

4. Modelleringsteamet från Korea Atomic Energy Research Institute (KAERI) förbearbetade idogt de tillhandahållna datamängderna, beräknade olika mått som beskriver egenskaperna hos sprickytorna och motsvarande aperturfält, utvecklade ett arbetsflöde i två steg för att härleda uppskalade fält av sprickytans höjder och använde ett förenklat tillvägagångssätt för att ta hänsyn till aperturförändringar som svar på olika nivåer av belastningen i normalriktningen. Även flödessimuleringar utfördes. De första stegen mot validering av det härledda aperturfältet och uppskalade sprickytshöjder togs genom att jämföra de härledda sprickytsythöjderna med tryckfilmsdata, dock utan testning mot formella valideringsacceptanskriterier. KAERI:s arbete i Subask 10.2.1 kommer troligen att underlätta utförandet av efterföljande modelleringsuppgifter om de kompletteras på rätt sätt med metoder som stöder pragmatisk modellvalidering av olika fall i modelleringsrymden.
5. SKB:s modelleringsteam från Stockholms universitet utvecklade dataförbearbetning, analys och uppskalningsprocedurer baserade på sofistikerade teoretiska koncept. Än mer relevant är att de antaganden som ligger bakom dessa begrepp är väl beskrivna, testade eller på annat sätt motiverade, samt med en diskussion av begreppens begränsningar och osäkerheter. Ytjämnhet, tryckfilmsdata och härledda aperturfördelningar användes i prediktion-resultatövningar för att utvärdera den föreslagna analys- och uppskalningsproceduren. Känslighets- och osäkerhetsanalyser utfördes för att undersöka effekten av modellbeslut på de förutsagda karaktäristiska mätetalen. Rekommendationer angående framtida arbete och ändringar av det föreslagna arbetsflödet gjordes även som förberedelser för tillämpningen av arbetsflödet i efterföljande modelleringsuppgifter.

Generellt sett är den modellering som krävs för att utveckla en försvarbar uppskalningsprocedur för att generera sprickytor och/eller aperturfördelningar till stöd för simulering av vätskeflöden och analys av kanaliseringseffekter begreppsmässigt och numeriskt mycket utmanande. Tolkning av beräkningsresultaten och arbetsflödet för pragmatisk validering kräver ytterligare förståelse och färdigheter. Dessutom är dokumentation av både modellerings- och valideringsarbetet utan tvekan svårt och mödosamt. De flesta modelleringsgrupperna visade sin djupa förståelse och beräkningsförmåga i dataförbearbetning och modelleringsanalyser. Trots detta idoga arbete med databearbetning, levererade endast några av modelleringsgruppen resultat till stöd för de två huvudsakliga målen för Task 10.2.1: (1) förståelse av effekten av småskalig spricktopografi på flödes- och kanaliseringseffekter, och (2) pragmatisk modellvalidering, vilket kräver propagering av osäkerheter och jämförelse av relevanta karaktäristiska mätetal inklusive deras valideringsacceptanskriterier. Detta tyder på att pragmatisk modellvalidering fortfarande är svår att förstå, genomföra och/eller dokumentera. Det rekommenderas därför att framtida övningar planeras noggrant av både Task Force-sekretariatet och modelleringsgrupperna så att resultaten av modelleringsgruppernas avsevärda insatser ger praktiska arbetsflöden och användbara insikter om både vätskeflöden och transport i sprickiga medier samt pragmatisk modellvalidering.

Contents

1 Introduction

Understanding, characterising, simulating, and predicting fluid flow and solute transport through fractured rock is relevant for supporting the safety case for a repository of radioactive waste in crystalline formations. These flow and transport processes in fractured host rocks are inherently complex, as they occur over multiple spatial scales, i.e., within the aperture field of a single fracture, along geometrically controlled or dynamically changing flow channels, within and across fracture intersections, and through the network of interconnected fractures of different scales and properties. Moreover, fluids and radionuclides interact with the adjacent rock mass, exchanging mass and energy, which affects the transport time and repository-induced thermal effects.

Numerical modelling is an essential tool for generic and site-specific analyses of flow and transport in fractured porous media. Based on characterisation data describing only certain aspects of the system at discrete points in space and time, a conceptual and numerical model has to be developed that is expected to be able to make inferences or predictions at specific locations and on different spatial and temporal scales. Due to the limited data support, this extrapolation to a different model space may lead to predictions that are biased, qualitatively deficient, or quantitatively erroneous. Each step during model development is based on simplifying assumptions and affected by uncertainties. This includes not only the conceptual model and formulation of physical processes, but also the derivation of model-specific, process-related, and scale-dependent parameters, such as geometric and hydraulic properties of single fractures and fracture networks.

It is necessary to test the ability of the extrapolated model (and each of its submodels) to make reasonable predictions for the intended purpose of the model, a process referred to a “pragmatic model validation.”

The SKB Task Force has historically examined experimental data and modelling approaches that study flow and transport in fractured porous media. Task 10 continues this line of investigation but focuses on demonstrating to which extent these models are suitable for the specific purpose for which they have been developed. A pragmatic model validation approach has been proposed (see Task 10.1; Lanyon et al., 2021, 2024; Finsterle and Lanyon, 2022); it is being exercised as part of Task 10.2 and subsequent modelling tasks.

Task 10 consists of multiple subtasks of increasing scale and complexity regarding both the geometry of the system and the physical processes to be considered, as illustrated in Figure 1-1. Task 10.1 develops and documents the fundamental concept of the proposed pragmatic validation approach and its applicability to Task 10. Task 10.2, which is the subject of this evaluation report, is concerned with the characterisation of a rough fracture, and how fundamental geometric information about the fracture’s surface roughness measured on a relatively small sample is used as the basis for deriving flow and transport properties of a single fracture on a larger scale and under different stress conditions. The task is also seen as an opportunity to develop and test pre-processing and modelling capabilities. Note that in Task 10.2, the pragmatic validation approach is mainly exercised on the processing of geometric data rather than fluid flow and transport through a single facture. The methods established in Task 10.2.1 are then applied in Task 10.2.2 to develop flow models on a larger scale and apply the pragmatic validation approach by comparing predicted flow rates in a single fracture to corresponding measured data are obtained by a dedicated laboratory experiment. In Task 10.3 and its various subtasks, the scale of the problem is further increased from a single, small fracture to a small network of discrete, deterministically known fractures. Following a bridge task that ensures that the lessons learned from Tasks 10.2.1 and 10.2.2 are transferred to Task 10.3, a 3D printed physical model containing a network of artificial fractures is used to provide flow data for the prediction-outcome exercise. In later subtasks, the geometry and physical processes increase. First, the focus is on a single discrete structure (Structure #20 in the TASS tunnel, Hardenby and Sigurdsson, 2010), which is intersected by a few other structures or fractures, with the goal to validate the corresponding model by comparing its predictions to measured total flow rate and conservative tracer data. This exercise is followed by the modelling of a small network of several fractures that form compartments. Data from the TRUE Block Scale experiment (Andersson et al. 2002ab, 2007) are used for the prediction-outcome comparison.

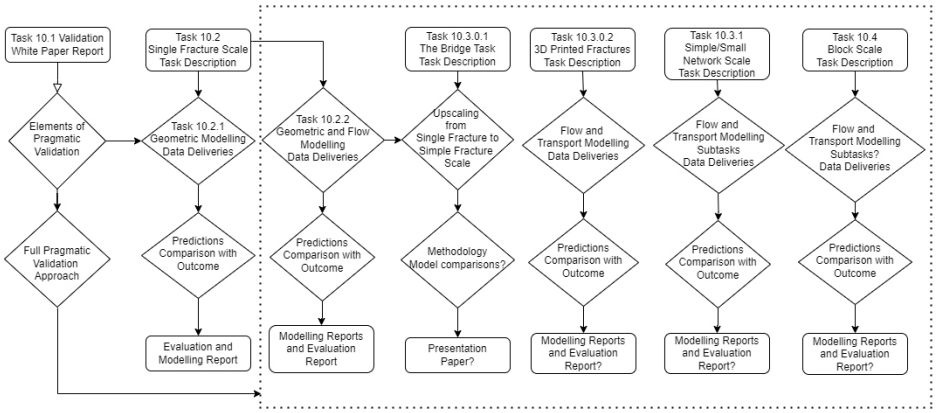

Figure 1-1. *Overview of Task 10 subtasks.*

It should be noted that while the scale and complexity increase with each subtask, the degree of abstraction, i.e., simplifying assumptions that need to be made for implementation in a predictive model, tend to increase also, highlighting the importance of an objective-driven pragmatic validation approach and adapting the acceptance criteria applied at each intermediate step. It also requires that uncertainties identified in one subtask be qualitatively acknowledged or quantitatively propagated to the model of the next subtask.

This evaluation report is only concerned with Task 10.2. The first step, Task 10.2.1, considers the characterisation of a single fracture based on high-resolution measurements of the fracture's surface topography. Surface roughness and the related aperture distributions and transmissivity fields are expected to be fundamental characteristics that impact flow rates and channelling effects in a single fracture. While no dynamic fluid flow or radionuclide transport simulations are performed in this initial subtask, it is important to realize that the analysis and interpretation of fundamental geometric information about the fracture requires the development of several – mainly conceptual, but also computational – models. Moreover, the ultimate use of this information for the assessment of a radioactive waste repository requires multiple upscaling steps, from the scale of measurements to the scale of the fracture sample to a larger fracture to a fracture network and potentially to the site scale of the repository. Moreover, on each of these scales, numerical models may be used that employ spatial resolutions different from the resolution of the underlying measured, calculated, and upscaled property data. This clearly indicates that each of the conceptual decisions and each of the (sub)models that are built as part of this process requires model validation with a level of detail and strictness that depends on how the results of a particular (sub)model will be used in subsequent steps, be that the direct calculation of a measure of interest, or the generation of input parameters for the next model in the sequence.

The pragmatic validation approach will also reveal whether the set of measured data provides relevant information for the model to fulfil its dedicated purpose, whether the data set is complete or requires auxiliary information, assumptions, and hypotheses, whether its accuracy or resolution is sufficient or can be reduced, and whether residual uncertainties in the measured and/or derived data are influential, can be accepted, or are irrelevant.

Fracture roughness data are intuitively considered essential for the development of a model for flow and transport in fractured porous media. Exercising the pragmatic validation approach for the initial steps of analysing surface roughness data is useful, as it demonstrates the validation workflow and likely provides some fundamental insights into how information contained in measured data propagates through a cascade of models of varying complexity. This process may be more transparent for this initial step, as only relatively simple concepts and calculations are involved rather than complex, dynamic, and computationally expensive numerical models that will need to be used in subsequent steps involving flow and transport simulations.

Task 10.2 focuses on channelling processes in a single fracture, considering hydro-mechanical coupling and upscaling. Task 10.2.1 is the first step in the road map for Task 10.2, focusing on geometric evaluation of fracture surfaces and aperture distribution on a borehole scale and predicting fracture surface topography and aperture distributions on meter scale.

The main objectives of Task 10.2.1 are to:

1) Get familiar with the fracture surface datasets and provide the opportunity to develop appropriate tools and concepts.
2) Develop methods for building a description of the fracture roughness and fracture void space (together with an assessment of relevant uncertainties) for the purpose of flow and transport simulations.
3) Investigate scaling of fracture surface properties from borehole to metre scale.
4) Start to consider the influence of fracture normal closure on this void space description, which will be a topic for Task 10.2.2.

Task 10.2.1 is the first step in setting up a single-fracture model based on available surface roughness data from four rock samples. As these data and their analysis are fundamental to the subsequent dynamic modelling of flow and transport processes, it is essential to gain confidence in the way the data are used to provide input to or otherwise condition the flow models.

For the processing, analysis, and prediction of the geometric quantities defining Task 10.2.1, reproducing the measured surfaces provides a test of the analysis and fracture characterization approach, while the extrapolation to the larger scale (upscaling) can be viewed as a type of prediction-outcome exercise, which is an important part of the pragmatic model validation approach.

According to the Task Description (Bruines, unpublished[1]), the validation process requires (a) a clear definition of the model purpose, (b) the documentation of decisions made during the development of the conceptual model, (c) the examination of alternative models, and (d) an understanding of the influence of uncertainties in model parameters and assumptions on the relevant performance metrics.

The model purpose of Task 10.2.1 is to assess if single-fracture observations made on the scale of a pilot borehole can be used to make predictions of single-fracture properties on the deposition-hole scale. The main focus is on the fracture surface roughness and the derived aperture distribution.

The specific objectives of Task 10.2.1 are to (a) introduce the fracture surface data sets, (b) develop a workflow and tools for characterising the fracture's aperture distribution and/or channel dimensions for subsequent use in a flow and transport model, (c) determine the uncertainty of these data-derived, flow-relevant fracture characteristics, (d) investigate the upscaling of these characteristics from the borehole (centimetre scale) to the deposition-hole (metre) scale, and (e) comment on the impact of normal fracture closure on the void space distribution.

The Task Description and associated Data Deliveries include information on (a) surface roughness from four fractures of dimensions 100×70 mm^2, (b) contact pressure measurements using pressure-sensitive films, (c) high-resolution photographs of apertures along the edges of the fracture, (d) results from normal loading tests, and (e) additional background information about sample preparation, the measurement process, sampling frequency, accuracy and resolution, initial postprocessing of the raw data, and potential sources of uncertainties and errors. Corresponding data from three samples of size 500×300 mm^2 will be made available for the prediction-outcome exercise.

The Task Description proposes to calculate specific roughness measures, so they can be used as performance metrics for model comparisons and the evaluation of the prediction-outcome exercise. Moreover, the resulting flow-relevant parameters (e.g., average or distribution of mechanical apertures, contact or flow-wetted surface area, transmissivity) should be reported. Other performance metrics can be provided if considered relevant for the ultimate purpose of the study, which is to inform the subsequent development of flow and transport models.

Finally, as no specific validation acceptance criteria have been formulated, the Modelling Groups are requested to provide a description of the uncertainties of the prediction and contemplate on what a reasonable spread for each performance measure would be. This involves identifying (through sensitivity or uncertainty propagation analyses) which factors – model choices, assumptions,

[1] Bruines, P. SKB Task Force on Modelling of Groundwater Flow and Transport of Solutes: Description of Task 10.2. SKB R-23-10, Svensk Kärnbränslehantering AB, Stockholm, Sweden. Unpublished.

parameters – are most influential on the results of the analysis. The Task Description makes various recommendations and provides templates for reporting results and submitting deliverables. It encourages the Modelling Groups to focus on clear and complete documentation of the model and analysis steps, to interpret and discuss results, to make recommendations, and to perform a self-evaluation.

Despite the relative simplicity of this initial subtask, it is acknowledged that the efforts of reviewing the available data, performing the analysis, and providing the information requested by the pragmatic validation approach, as detailed in the Task Description, are substantial. Five of the ten participating Task 10 Modelling Groups conducted all or parts of the exercise.

Short comments about these analyses are summarized in the following subsections.

2 Models and parameters

2.1 Introduction

Task 10.2.1 requires a geometric evaluation of fracture surfaces and information needed to derive the corresponding aperture distributions on the borehole scale, which will then be extrapolated to estimate the fracture surface relief and a description of the void space on the metre scale. The models to be developed and validated in this exercise are therefore not numerical flow and transport models, but relatively simple equations, such as averaging, interpolation, mapping and correction formulas used during pre-processing of the data, models to relate the upper and lower fracture surfaces and their vertical and lateral adjustments to generate aperture distributions, contact models to estimate normal deformation under changed loading, geostatistical characterization models and methods to generate additional realisations, upscaling methods, etc.

While the Modelling Groups are encouraged to explore any approach considered suitable for the task, it is essential for model development – and specifically model validation – to clearly describe and test assumptions underlying the chosen model or approach.

Similarly, the parameters of the model, either fixed or adjusted during the analysis, need to be clearly identified, and their expected uncertainty discussed. Section 2.2 provides a short summary of the chosen modelling approaches as well as input data and parameters used by each of the participating Modelling Groups.

2.2 Summary of input from Modelling Groups

2.2.1 Modelling Group SÚRAO (Czech Republic) – Roughness analysis and surface generation

The Modelling Group of SÚRAO used approaches and analysis tools to (a) process the laser-scanning data of the fracture surfaces, (b) calculate composite surface-roughness measures, (c) estimate heterogeneous fracture aperture fields, (d) generate synthetic surface-roughness fields, (e) develop relations of surface-roughness parameters across scales, and (f) evaluate hydraulic properties, including channelling, for the measured rock samples. Estimates of larger-scale rough fracture surfaces are provided in preparation for the prediction-outcome exercise, in which comparisons to the measured data from the three 500×300 mm^2 fracture samples are to be made.

Before processing the available data, SÚRAO recognized some general limitations. One of the uncertainties related to potential biases from end-effects, SÚRAO extracted two subsets of the data, one capturing the maximum number of data points in a bounding rectangle common to both surfaces in a given sample, and the other a reduced subset with a 2 mm cropping distance from the previous rectangle's sides. The data were further prepared for analysis by the software packages Surfer and Surface Roughness Calculator, which were used for calculating composite and directional roughness performance measures, respectively (see Section 3.2). The second data set used for the analysis are the pressure film data, which were provided as colour-coded bitmaps.

In addition to these two sets of raw data, SÚRAO reported on key assumptions, including (a) treatment of the fracture as a two-dimensional, planar object, (b) local applicability of the cubic law, (c) self-similarity of the roughness field, (d) adjustment of relative position of the two fracture surfaces by translation along the two coordinate axes (but no rotation), treated as adjustable parameters, (e) adjustment of surface separation value (mean aperture) by vertical displacement, conditioned on pressure film data, (f) choice of the minimal aperture threshold value (both for the pressure film data and the numerical distance measure), and (g) numerical grid resolution.

SÚRAO describes the roughness metrics as input parameters to the model used for the prediction-outcome exercise. This is appropriate, as these parameters (i.e., Hurst exponent and root-mean-squared error) are input to the fractal model that is used to make the upscaled predictions for the larger fracture surfaces. It should be noted that these parameters are derived from the analysis of the small-scale

roughness data, i.e., they are also uncertain output variables. As described by the pragmatic model validation approach, this is the reason why estimation uncertainties need to be quantified and then propagated through the sequence of downstream models to arrive at an understanding of the modelling study's consistency with validation data.

Details about SÚRAO's modelling and analysis can be found in Appendix A.

2.2.2 Modelling Group LANL (DOE/USA) – Geostatistical analysis of surface roughness

The LANL Modelling Group performed a geostatistical analysis of the fracture surface data as an initial step for characterizing flow and transport parameters (i.e., aperture distribution and upscaled transmissivities, flow channelling metrics, etc). The fracture surface data provided by the Task Force's data-release package were used as input to the geostatistical analysis; the pressure film data were not used, and no additional data needs were identified. LANL noted as a specific objective of their work to examine the sufficiency of the sample size as a basis for extrapolation. No additional objectives were given, and no limitations were identified.

The data were pre-processed to obtain surface elevation values on a regular grid. A geostatistical analysis approach was employed to calculate empirical statistics of fracture heights and their spatial correlation structure under the assumptions of isotropy and stationarity. A spherical semi-variogram model was matched to the empirical semi-variogram. No generation of upscaled surfaces, calculation of aperture or transmissivity fields, or flow simulations were attempted. Since no calculations involving an extrapolation beyond the existing data space were performed and no uncertainty quantification was performed, no questions related to pragmatic model validation could be addressed.

Details about LANL's modelling and analyses can be found in Appendix B.

2.2.3 Modelling Group NTU (TPC/Taiwan) – Geometric evaluation of fracture surfaces and aperture distributions under loading

The Modelling Group of the National Taiwan University (NTU) pre-processed the data from four fractures to be able (a) to calculate fracture surface roughness parameters, (b) to develop aperture fields based on pairs of fracture surfaces and describe them statistically, (c) to evaluate the changes in aperture distributions in response to increasing normal loading, and (d) to upscale the roughness maps based on a statistical theory and the empirical roughness indices.

Pre-processing of geometric fracture surface data involved trimming of the data domain and applying an iterative transformation approach to align the surfaces such that the average aperture is minimized with the overlap of the surfaces being limited to 1 %. Various roughness indices were calculated for each fracture surface, and the statistics of the aperture field were reported.

Finally, the roughness parameters from the 70×100 mm^2 fractures were upscaled to the 1 m scale. It was assumed that the logarithm of the maximum roughness amplitude increases with the logarithm of the scale, implying that the aperture increases with fracture size.

Details about NTU's modelling and analyses can be found in Appendix C.

2.2.4 Modelling Group KAERI (Korea) – Evaluation of geometric properties of rock fractures and proposal for upscaling process

The Modelling Group of the Korea Atomic Energy Research Institute (KAERI) conducted studies on geometric fracture characterisation (roughness, aperture, and spatial correlation), upscaling of one of the fracture's surface areas based on fractal theory combined with a geostatistical method (co-kriging) to maintain spatial correlation of the second surface area, followed by fluid flow simulations for aperture fields affected by normal stress changes.

The fracture surface data were analysed using fast Fourier transform (FFT) under the assumption of self-affinity to determine the Hurst coefficient. Semi-variograms and a co-variogram between the primary variable – the roughness of the second surface to be upscaled – and the secondary variable – the upscaled roughness of the first surface – were calculated as input data to the two-step upscaling procedure.

Data pre-processing required alignment of the upper and lower surfaces using the Iterative Closest Point algorithm, followed by detrending and interpolation onto a regular mesh with 0.2 mm grid spacing. Finally, the boundaries of the model were trimmed to arrive at a sample size of 100×70 mm^2.

Details about KAERI's modelling and analyses can be found in Appendix D.

2.2.5 Modelling Group of Stockholm University (SKB, Sweden) – Methodology for pre-processing surface scan data and presentation of an updated method for generating rough surfaced aperture

The Modelling Group of Stockholm University pre-processed the fracture surface scan data by interpolating the point cloud onto a regular grid with a spatial resolution of 0.1 mm using different interpolation methods (linear, nearest neighbour, and cubic spline interpolation; ultimately, linear interpolation was selected for the subsequent analyses). The samples were cropped. The upper surface was translated relative to the lower to increase the minimum negative value; finally, the upper surface was vertically shifted so that the resulting aperture visually corresponded to the patterns shown by the pressure film data. Negative values were set to zero and assumed to be contact areas between the upper and lower surface. This methodology induced significant corrections to the scanned surfaces, so that the resulting calculated and processed aperture fields more closely resembled the natural fracture aperture field.

Details about Stockholm University's modelling and analyses can be found in Appendix E.

3 Results and discussion

3.1 Introduction

The types of results expected to be produced by Task 10.2.1 are essentially given by the objectives of the study, which were outlined in the Task Description. However, intermediate results depend on the particular approach taken by the individual Modelling Groups.

The results are described in the Modelling Groups' modelling reports, which can be found in the Appendices; they are not repeated here in detail other than listing what type of modelling output was calculated and how it was discussed and interpreted.

3.2 Modelling Group SÚRAO (CZ) – Roughness analysis and surface generation

The SÚRAO Modelling Group calculated statistical roughness measures (including directional metrics) for the four samples (eight surfaces). Roughness measures were compared between the upper and lower surfaces and across the four samples. The results were grouped, and representative parameters for each of the groups were identified for the generation of upscaled fracture surfaces. Next, multiple aperture fields were generated for different supporting data sets, but also different correction procedures. This sensitivity analysis revealed the significance of excluding potential edge effects (damage along block edges), and the impact of the correction procedure on calculated contact areas and thus the resulting aperture distributions, despite the conditioning on the pressure film data. Average apertures were calculated for each of the examined variants.

The aperture distributions were converted to heterogeneous transmissivity fields by locally applying the cubic law. Flow simulations were performed. The resulting flow fields were used to infer an effective transmissivity and channelling metric. Again, the analysis was performed for multiple variants regarding supporting data sets and correction procedure. Moreover, grid resolution effects were examined. Finally, the transmissivities inferred from the flow simulations were compared to those calculated directly from the average aperture.

3.3 Modelling Group LANL (USA) – Geostatistical analysis of surface roughness

The analysis resulted in sample statistics (mean, variance, skewness, kurtosis) and spatial information (correlation length, mean curvature). The shape of the empirical semi-variogram does not resemble that of a spherical correlation structure; consequently, the matching of a spherical semi-variogram did not produce meaningful correlation lengths and sill values, and therefore cannot be used as a basis for the generation of synthetic fracture surfaces.

3.4 Modelling Group NTU (Taiwan) – Geometric evaluation of fracture surfaces and aperture distributions under loading

The NTU Modelling Group highlighted that while surface roughness data are important, they are insufficient to derive the flow-relevant aperture field without additional information or assumptions, specifically a contact area ratio.

Changes in the initial aperture distribution (calculated for an overlap ratio of 1 %) in response to increasing values of normal loading were calculated accounting for deformations at contact points based on the contact area and the granite's Young's modulus. In a first scenario, only vertical force

equilibrium was considered with vertical deformations. In a second scenario, two horizontal moment equilibria were considered in addition to the vertical force equilibrium. The model describing the loading effects confirmed the expected behaviour that increased loading resulted in reduced apertures.

3.5 Modelling Group KAERI (Korea) – Evaluation of geometric properties of rock fractures and proposal for upscaling process

The processed data (see Section 2.2.4) were analysed to quantify surface elevation, roughness, mechanical aperture, and spatial correlation. Surface elevation data showed a unimodal but slightly skewed distribution. Various two-dimensional, directional roughness indices were evaluated. The upper and lower surfaces showed overall similar roughness indices. Empirical directional semi-variograms were generated and matched to spherical and Gaussian variogram models, indicating the presence of a nugget effect and an average correlation length of approximately 40 mm, with orientation-dependent variations around this value.

The initial mechanical aperture was calculated under the assumption that 1 % of the fracture surface areas are in contact with each other. The aperture showed a negative exponential distribution, qualitatively matching the patterns observed by the pressure film data. The average initial apertures for the four samples range between 0.15 and 0.4 mm.

A two-step upscaling procedure was proposed. The first fracture surface is upscaled by fractal theory. However, applying the same procedure independently to the other surface is likely to violate the correlation between the two surfaces. The second surface is upscaled by co-kriging, taking into account the co-variogram between the second surface and the upscaled distribution of the first surface. Multiple realisations of the upscaled surfaces were compared to the measured data on the 200×200 mm^2 scale, showing general similarity, but with the predicted, upscaled surfaces underestimating the surface height.

Flow simulations were conducted based on the measured data from the 200×200 mm^2 fracture sample, with the raw data pre-processed as described above. The initial (unloaded) mean aperture was set to 0.46 mm. Contact mechanics under uniaxial compressive stress was simulated assuming elastic properties of the rock mass. Parameters were adjusted to approximately reflect the observed stress-strain relationship. The Stokes equation was solved to simulate fluid flow across the aperture field for different flow directions and normal stress. Calculated outflow rates were reduced by approximately a factor of 5 when increasing the normal stress from 2 to 8 MPa. The derived average hydraulic aperture was found to be slightly lower than the mechanical aperture.

3.6 Modelling Group Stockholm University (Sweden) – Methodology for pre-processing surface scan data and presentation of an updated method for generating rough surfaced aperture

The underlying concept used in the geometric analysis of fracture apertures is to generate two self-affine fractal surfaces, representing the upper and lower surfaces of a fracture, using fractal scaling information derived from roughness measurements of natural fractures. To obtain a variable aperture field, the two generated surfaces must be only partially correlated to each other, such that there is high correlation between the surfaces for large-range roughness and lower correlation at smaller scales. A range of Hurst coefficients and scaling parameter values was determined from various trace profiles across the fracture surfaces. Multiple realisations were generated, and statistics of fracture roughness, Hurst exponent and their correlation to the scaling parameter were determined and compared to the corresponding measured values.

The generated aperture distributions were compared to the measured aperture distributions on both the original and upscaled fields. The upscaling methodology yields significantly smaller apertures as surface topography is reduced on the larger scale.

The goal of the work was to develop a method for reproducing naturally occurring rough surfaced fractures with variable apertures using information obtained from 3D scans of natural rock fractures. Although the surfaces could be accurately reproduced, the resulting aperture ensemble distributions of the generated fractures tend to deviate from the measured distributions to a varying extent. It is hypothesized that the main reason of the discrepancies is the correlation between the upper and lower surfaces, which may be inaccurately calculated because of the rock break-outs in the samples.

It was concluded that surface roughness data are useful as they can be used to generate aperture distributions that correspond to measured aperture fields. To generate an aperture field that is representative of reality, the correlation between the upper and lower surface is important, so is the alignment between the two fracture surfaces. Consequently, it may be preferable to focus on aperture distribution rather than solely on surface roughness of individual surfaces. Without the correlation structure, one surface is not useful for generating fractures with variable apertures and hence for subsequent modelling of flow and transport through heterogeneous aperture fields.

4 Evaluation

4.1 Introduction

The evaluation of the work by the Task Force 10 Modelling Groups is done with respect to the goals of Task 10.2.1 as outlined in the Task Description. While the Task Description offers suggestions of the type of analyses that could be undertaken to reach these goals, the choice of the workflow and approaches was left to the Modelling Groups. However, it is expected that results are discussed in sufficient detail so they provide a basis for a pragmatic model validation of this subtask, which will also be a basis for the validation of models developed as part of the subsequent subtasks.

4.2 Modelling Group SÚRAO (CZ) – Roughness analysis and surface generation

The declared overall objectives of the modelling were consistent with goals outlined in the Task Description. While committing to these goals, the Modelling Group also indicated anticipated limitations of the study as a result of small sample size along with uncertainties and ambiguities in the input data.

Limitations, modelling assumptions, and potential sources of errors and uncertainties were listed and further discussed if considered to have a critical influence on the results. The Modelling Group identified which of these factors are choices made by the modellers, are inherent in the supplied data sets, or remain unknown. This information is most useful and provides valuable background when evaluating the suitability of the model results for subsequent use. It is an essential part of the pragmatic model validation approach. However, no formal uncertainty analysis was performed.

The Modelling Group justified their choices of the performance metrics they evaluated and discussed potential shortcomings. No direct comparison of the calculated performance metrics with the corresponding values on the upscaled fractures could be made. Nevertheless, the contribution to this prediction-outcome exercise remains valuable, as it is based on a truly blind prediction, and the evaluation can still be made in the future. Moreover, a comparison of the generated fracture surfaces with the actual roughness data was made, providing confidence that the chosen analysis approach and its execution yielded synthetic surfaces that can be considered consistent with the supporting real fractures on the same scale.

The Modelling Group made an effort to verify that the statistics of the generated surfaces are consistent with both the provided input parameters and the statistics of the measured surfaces. They referred to this check as model verification. It provided confidence that no substantial errors were introduced during the multi-step analysis process, and that the fracture generation software performed as expected. This is considered an important, relatively easy-to-perform test that significantly increases the confidence in the appropriateness of the overall approach and the correctness of the calculations.

They also considered alternative options to calculate upscaled fracture surfaces, where either the parameter sets from each of the four small-scale fracture sets are used individually or are combined into a single set of effective statistical parameters, which also reflects spatial variability. To guide the decision on which approach should be used, the Modelling Group examined and grouped the results from the analysis of the small-scale fracture samples. This seems a sensible way not only to justify a modelling decision, but also to obtain additional information about spatial variability.

To make surface roughness data useful for flow and transport simulations – which is the ultimate purpose of taking the measurements and performing these initial pre-processing steps – the two surfaces must be related to each other so that an aperture field (and later a transmissivity field) can be determined. The Modelling Group described the individual analysis steps in detail, integrating the pressure film measurements into the determination of the separation distance between the two surfaces and the void-space distribution. They developed and applied an optimization method to

condition their aperture model on the available pressure film data. They visualised the objective function, clarifying the approach and providing insights into the quality of the solution; this addresses an important requirement of the pragmatic model validation approach.

Multiple aperture fields were generated for different supporting data sets, but also different correction procedures, which can be considered part of a sensitivity analysis, providing insights into relevant parameters and assumptions.

The local cubic law was applied to the inferred aperture field, assuming a planar fracture, and saturated water flow was simulated with gradients applied in two orthogonal directions to determine effective, anisotropic transmissivities and channelling factors. All model assumptions, including adjustments made to address computational issues, were documented to a level of detail that is sufficient to reproduce the results and to enable a peer review in support of pragmatic model validation.

Interpretations of the results were qualified by comments that reflect the author's confidence. Alternative explanations were offered if the interpretation is ambiguous. The modelling report does not contain a final section that summaries the study, its results or conclusions, and no recommendations were provided.

Overall, the work by the Modelling Group is technically sound and clearly aimed at providing information and interpretations needed to perform and assess pragmatic model validation.

4.3 Modelling Group LANL (USA) – Geostatistical analysis of surface roughness

The geostatistical analysis provided some composite statistical measures of the fracture surface roughness. It was concluded that the sample size was sufficiently large to reveal a correlation length.

However, it is not discussed how these composite statistical measures will be used in support of the ultimate modelling purpose of predicting flow and channelling effects in a single, upscaled fracture. Moreover, this initial fracture roughness characterization is insufficient to address the questions needed to contribute to an evaluation of the approach in support of pragmatic model validation. While the need to identify potential sources of uncertainties is occasionally mentioned, uncertainties are not quantified. Instead, it was asserted that the key uncertainty comes from the measurements (and some effects from the small-scale discretization and interpolation schemes used for the initial mapping step). The mismatch of the spherical semi-variogram to the empirical semi-variogram is a clear indication that uncertainties in the chosen conceptual model – which is the subject of model validation – dominate the uncertainties in the predicted aperture field, transmissivities, and channelling behaviour (if such predictions had been attempted). A proper conditioning or calibration of the chosen conceptual model (i.e., geostatistical representation of the data using a spherical semi-variogram) is a prerequisite for a meaningful pragmatic model validation exercise. Alternative conceptual models, their representativeness of the actual data, and the uncertainties in predicted, upscaled surface roughness values could be readily examined as a pre-step to generating aperture and transmissivity fields, and eventually flow simulations.

4.4 Modelling Group NTU (Taiwan) – Geometric evaluation of fracture surfaces and aperture distributions under loading

The analysis of fracture surface data, their description by various roughness indices, the upscaling of one of these indices, and the calculation of aperture distributions as a function of different loading forces are valuable initial steps to support the modelling of fluid flow through a single, rough fracture.

While the results appear reasonable, their interpretation is minimal, and no conclusions are drawn or recommendations are made. The stated, generic objectives of the study can be considered met, i.e., the Modelling Group became familiar with the available fracture data and calculated geometric

metrics of surface roughness and aperture distributions. However, it would be useful to expand the discussion and interpretation section, arriving at conclusions that are supported by the analysis, and recommendations that can be used by the Modelling Group and other interested parties to develop an effective workflow that supports the ultimate objectives of the project, ready to be applied once site-specific data become available.

For example, it would be useful to learn (a) how the upscaled joint roughness coefficient (JRC) measure would be used to generate upscaled aperture distributions, (b) whether aperture changes due to loading are substantial enough so they significantly affect fluid flow and channelling (this assessment should account for the uncertainty in the data and analysis approach), (c) how the calculated uncertainties will be used in a validation study and propagated to subsequent analysis steps and subtasks, and (d) whether the different approaches to calculate the loading-dependent aperture fields yield significantly different results that may affect flow, i.e., whether the simplified approach based on vertical deformation is sufficient, or whether lateral momentum equilibria need to be accounted for. Some of this information can readily be found in or derived from the presented results, supporting the next subtasks as part of Task 10 and work related to actual site characterization, performance assessment calculations, and model validation.

4.5 Modelling Group KAERI (Korea) – Evaluation of geometric properties of rock fractures and proposal for upscaling process

KAERI diligently pre-processed the provided data set and calculated various measures describing the characteristics of the fracture surfaces and corresponding aperture fields. These aperture fields were visually compared to patterns from the pressure films for a qualitative validation of the first characterisation step – the determination of the unloaded aperture distribution for the small fracture samples. A two-step workflow was developed to derive upscaled fields of surface heights. The distribution of these heights was then compared to the height measurements from the larger fracture sample. The aperture distributions were adjusted using a simplified approach to account for different normal stresses. Flow simulations were also performed – albeit using measured surface roughness data rather than upscaled apertures – and effective, load-dependent average hydraulic apertures and corresponding flow rates were calculated.

KAERI's pre-processing and analysis approaches appear sound. Two steps towards the validation of early characterisation and modelling tasks were undertaken: (1) The validation of the aperture field using pressure film data, and (2) the validation of upscaled surface heights by comparison of statistical measured from the scanned 200×200 mm^2 fracture. The question of whether the models would have passed or failed validation was not addressed, as no validation acceptance criteria were defined. The results of the flow simulations (absolute flow rates or change in flow rates as a function of stress) were not yet compared to corresponding experimental data (these data became available as part of Task 10.2.2).

It remains unclear whether the detailed analysis of fracture surface data (e.g., accounting for anisotropy and the inclusion of covariances during the upscaling step) are relevant for an improved performance of the upscaled model when simulating fluid flow and/or evaluating channelling. These questions could be addressed by performing systematic sensitivity analyses, or by comparing flow simulation results obtained with the upscaled aperture field to those obtained using the measured surface roughness data.

Overall, KAERI's development of a workflow for fracture characterisation, upscaling, and fluid flow simulation are likely to support subsequent analyses as part of Task 10, supplemented by methods that support pragmatic model validation across different modelling spaces.

4.6 Modelling Group Stockholm University (Sweden) – Methodology for pre-processing surface scan data and presentation of an updated method for generating rough surfaced aperture

Stockholm University described their data pre-processing and analysis methods clearly and concisely. The resulting performance metrics were statistically tested and compared among the various surfaces, fractures, and scales. The key assumptions underlying their methodology to generate variable aperture fields based on surface roughness data were clearly stated. The validity of some of the assumptions was tested, and the impact of related uncertainties on the resulting aperture fields was examined.

The robustness of the chosen interpolation schemes was tested, so were various decisions made as part of the upscaling method. The generation of fracture roughness distributions was compared to measured data by calculating composite performance metrics. Pressure film data were used to validate the initially generated aperture field. The discrepancies were then used to adjust (calibrate) some of the parameters (vertical shift and lateral translation of the two fracture surfaces). Residual uncertainties were discussed and used as explanation and justification of the conclusions. Validation of the upscaled aperture field was described elsewhere (Stock and Frampton, 2023).

Considerable insights were gained about the sensitivity of upscaling results on procedural decisions (e.g., the chosen percentile for the Hurst coefficient and scaling parameter). The calculation and comparison of numerous performance metrics is valuable, but – given that they suggest different outcomes regarding the method's performance – raises the question which ones are most suitable as validation acceptance criteria.

Even though the authors concluded that the proposed method could generate fracture surfaces based on high-resolution 3D fracture surface scans that are representative of natural rock fractures, they also acknowledged that the generated aperture ensemble distributions tend to deviate from the measured distributions. The question remains, therefore, whether the proposed approach is considered validated and applicable to models whose purpose is to predict fluid flow and channelling effects, specifically if the procedure is based on small-scale data and applied to larger-scale fractures or fracture networks – questions that need to be addressed in subsequent subtasks of Task 10.

5 Summary and conclusions

The topic of Task 10 is two-fold: First, the understanding of fluid flow through a single fracture and fracture networks should be improved, with special attention to channelling effects; and second, the models developed to improve that understanding should be assessed following a pragmatic model validation approach as outlined in Task 10.1 (Lanyon et al., 2024).

Flow through fractures and associated channelling effects are expected to depend, in part, on the small-scale characteristics of the fracture surfaces and corresponding aperture field. (This presumption of the importance of small-scale fracture characterisation data for performance assessment may still need to be conclusively demonstrated.) Characterisation of fracture properties and the representation of these characteristics as part of the conceptual and numerical model are therefore important initial steps, as they provide the transfer of information from the measured data to the model. The data analysis itself can be viewed as modelling, as it involves the development of a simplified mathematical representation of reality, which is then used to make inferences and predictions. The decisions, assumptions, and uncertainties inherent in these initial modelling steps will affect all the downstream models – should fracture surface roughness turn out to be an influential aspect of the ultimate prediction of repository safety. It is therefore essential that the assumptions, formulas, models, and the analysis workflow should be clearly described and tested as part of this overall pragmatic model validation exercise.

The SÚRAO Modelling Group followed the guidance of the Task Description and did a detailed analysis of fracture surface topography as the basis for estimating aperture distributions and effective transmissivities. They discussed their assumptions and commented on potential systematic impacts and uncertainties, based on which they selected alternative scenarios to be examined. They verified that their description and reproduction of fracture surfaces on the scale of the data samples is reasonable, before they generated fracture models on the larger scale. They performed flow simulations and evaluated effective transmissivities and channelling metrics. These efforts targeted the key goal of Task 10, namely exercising the pragmatic validation approach. The analysis and documentation provide the information needed to gain insights into the validity of the chosen approach and the use of the generated single-fracture aperture fields for model validation and subsequent use. It is recommended that SÚRAO compare the calculated, upscaled performance metrics with the corresponding values from the three large fractures, thus completing the prediction-outcome exercise.

The LANL Modelling Group calculated some statistical measures of the fracture surface heights using a geostatistical method. They matched a spherical semi-variogram to the corresponding empirical data. No further analyses were performed, i.e., no questions related to uncertainty propagation to flow-relevant representations of fractures, flow channelling, or model validation were addressed.

The NTU Modelling Group evaluated various roughness indices, upscaled one of these indices, and calculated aperture distributions as a function of different loading forces. It would be useful if a more detailed discussion and interpretation of these results were presented, and recommendations were made on how they can be used in support of model validation, either using the geometric data available from the one-meter-scale fractures, or how the lessons learned can be used in the next subtasks.

The KAERI Modelling Group also followed a detailed pre-processing workflow to characterise the surface topography. They developed a two-step approach for deriving aperture distributions, where the first step consisted of upscaling of one of the fracture's surface areas based on fractal theory, followed by a second step, in which a geostatistical method (co-kriging) was used to maintain spatial correlations between the two surface areas. Finally, fluid flow simulations were performed with various aperture fields affected by normal stress changes. Partial validations of some of the intermediate analysis steps were performed. While the models needed for the analysis of fracture surface data as input to flow and transport models are relatively simple (in comparison to subsequent models that will make use of the results of Task 10.2.1), the analysis and documentation demands needed for pragmatic model validation appear difficult or onerous. While no clear statements about model validation, the relevance of features and parameters, or the propagation of uncertainty were derived, KAERI's development of a workflow for fracture characterisation, upscaling, and fluid flow simulation are likely to support subsequent analyses as part of Task 10.

The Stockholm University Modelling Group used a suite of sophisticated analysis methods and evaluation metrics to describe the surface roughness data, generate realisations of aperture fields, and perform upscaling. They also comprehensively documented and analysed the impact of assumptions and modelling decisions on the performance metrics and validated some of the steps using independent data or derivations of the aperture fields that are more closely related to the measured surface trace data.

Overall, the modelling and analysis work performed by the Modelling Group is technically sound and of high quality. Unfortunately, documentation of the work occasionally lacks the technical clarity needed to convey the complex scientific concepts involved in the subtasks. Even in the case when approaches and results were presented in detail, the reporting often lacked a comprehensive interpretation or the formulation of findings and conclusions. In many cases, the work itself and/or its documentation focused on data pre-processing and modelling issues rather than the execution of the pragmatic model validation workflow, which is one of the explicit purposes of Task 10.

While the individual evaluations of the Modelling Group's work on Task 10.2.1 varied somewhat as described in Sections 2 to 4, the general impression can be summarised as follows:

The modelling needed to develop a defensible upscaling procedure for deriving fracture surface roughness and/or aperture distributions in support of simulations of fluid flow and analyses of channelling effects are conceptually and numerically very challenging. Interpretation of the computational results and the workflow of pragmatic validation requires additional understanding and skills. Moreover, documentation of both the modelling and validation work is arguably difficult and arduous. Most Modelling Groups demonstrated their deep understanding and computational capabilities in data pre-processing and modelling analyses. Despite this diligent work on data processing, only some of the Modelling Groups supplied results in support of the main two goals of Task 10: (1) understanding of the impact of small-scale fracture topography on flow and channelling effects, and (2) pragmatic model validation, which requires uncertainty propagation and the comparison of relevant performance metrics to validation acceptance criteria. This suggests that pragmatic model validation remains difficult to understand, conduct, and/or document. It is therefore recommended that future exercises be carefully planned by both the Task Force Secretariat and the Modelling Groups so that the results of the Modelling Groups' considerable efforts provide practical workflows and useful insights into both fluid flow and transport in fractured media and pragmatic model validation.

The results, insights, and experiences gained by the participating Modelling Groups can be directly transferred to and used as the basis for Task 10.2.2, which is concerned with the prediction and validation of flow in a single fracture of larger size and under changed loading conditions. Gaining confidence in the pre-processing and upscaling of fundamental fracture characterisation data is essential and provides a solid basis the use of these or similar data sets in a flow and transport model. The stepwise pragmatic model validation approach exercised in Task 10.2.1 enables the transfer of this information along a suite of related models of increasing scale and complexity (see Figure 1-1).

References

SKB's (Svensk Kärnbränslehantering AB) publications can be found at www.skb.com/publications.

Andersson P, Byegård J, Dershowitz B, Doe T, Hermanson J, Meier P, Tullborg E-L, Winberg, A (ed), 2002a. Final Report of the TRUE Block Scale Project 1. Characterisation and model development. SKB TR-02-13, Svensk Kärnbränslehantering AB.

Andersson P, Byegård J, Winberg A, 2002b. Final Report of the TRUE Block Scale Project 2. Tracer tests in the block scale. SKB TR-02-14, Svensk Kärnbränslehantering AB.

Andersson P, Byegård J, Billaux D, Cvetkovic V, Dershowitz W S, Doe T, Hermanson J, Poteri A, Tullborg E-L, Winberg A (ed), 2007. TRUE Block Scale Continuation Project Final Report. SKB TR-06-42, Svensk Kärnbränslehantering AB.

Barton N, 1981. Shear strength investigations for surface mining. In: Proceedings of the 3rd International Conference on Surface Mining, SME, Vancouver, 171–196.

Barton N, Choubey V, 1977. The shear strength of rock joints in theory and practice. Rock Mechanics and Rock Engineering, 10(1), 1–54.

Barton N, Bandis SC, 1982. Effects of block size on the shear behavior of jointed rock. In: 23rd U.S. Symposium on Rock Mechanics, 739–760.

Březina J, Stebel J, Flanderka D, Exner P, Hybš J, 2020. Flow123d version 3.0.4, https://flow123d.github.io (accessed January 10, 2023).

Brown S R, 1987. Fluid Flow through Rock Joints: The Effect of Surface Roughness. *Journal of Geophysical Research: Solid Earth* 92 (B2): 1337–47. https://doi.org/10.1029/JB092iB02p01337

Brown S R, 1995. "Measuring the Dimension of Self-Affine Fractals: Example of Rough Surfaces." In *Fractals in the Earth Sciences*, edited by Christopher C. Barton and Paul R. La Pointe, 77–87. Boston, MA: Springer US. https://doi.org/10.1007/978-1-4899-1397-5_4

Candela T, François R, Michel B, Alexandre B, David M, Jean S, Christophe V, 2009. Characterization of Fault Roughness at Various Scales: Implications of Three-Dimensional High Resolution Topography Measurements. *Pure and Applied Geophysics* 166 (10–11): 1817–51. https://doi.org/10.1007/s00024-009-0521-2

Esaki T, Du S, Jiang Y, Wada Y, Mitani Y, 1998. Relation between mechanical and hydraulic apertures during shear-flow coupling test. Proceedings of the 10th Japan Symposium on Rock Mechanics, Osaka, January 1998.

Finsterle S, Lanyon B, 2022. Pragmatic validation of numerical models used for the assessment of radioactive waste repositories: A perspective. *Energies*, *15*, 3585, doi: 10.3390/en15103585, https://www.mdpi.com/1996-1073/15/10/3585/pdf

Geuzaine C, Remacle J-F, 2009. Gmsh: A 3-D finite element mesh generator with built-in pre- and post-processing facilities. International Journal for Numerical Methods in Engineering, 79(11), 1309–1331. https://doi.org/10.1002/nme.2579

Glover P W J, Matsuki K, Hikima R, Hayashi K, 1998a. Fluid Flow in Synthetic Rough Fractures and Application to the Hachimantai Geothermal Hot Dry Rock Test Site. *Journal of Geophysical Research: Solid Earth* 103 (B5): 9621–35. https://doi.org/10.1029/97JB01613

Glover P W J, Matsuki K, Hikima R, Hayashi K, 1998b. Synthetic Rough Fractures in Rocks. *Journal of Geophysical Research: Solid Earth* 103 (B5): 9609–20. https://doi.org/10.1029/97JB02836

Golden Software, 2023. Surfer, available from: https://www.goldensoftware.com/products/surfer-Magsipoc E., Zhao Q., Grasselli G. (2020) 2D and 3D Roughness Characterization, Rock Mechanics and Rock Engineering (2020) 53:1495–1519.

Hardenby C, Sigurdsson O, 2010. Äspö Hard Rock Laboratory. The TASS-tunnel. Geological mapping. SKB R-10-35, Svensk Kärnbränslehantering AB.

Lanyon G W, Davy P, Dershowitz W S, Finsterle S, Gylling B, Hyman J D, Neretnieks I, Uchida M, 2021. Pragmatic Validation Approach for Geomechanics, Flow, and Transport Models in Fractured Rock Masses. Paper (DFNE 21-2369) presented at the 3rd International Discrete Fracture Network Engineering Conference, Virtual, June 2021.

Lanyon G W, Davy P, Dershowitz W, Finsterle S, Gylling B, Hyman J, Neretnieks I, Uchida M, 2024. White Paper essays on model validation. Task 10 of SKB Task Force GWFTS – Validation approaches for groundwater flow and transport modelling with discrete features. SKB TR-22-04, Svensk Kärnbränslehantering AB.

Li B, Jiang Y, Koyama T, Jing L, Tanabashi Y, 2008. Experimental study of the hydro-mechanical behavior of rock joints using a parallel-plate model containing contact areas and artificial fractures. *International Journal of Rock Mechanics and Mining Sciences*, *45*(3), 362–375.

Magsipoc E, Zhao Q, Giovanni G, 2020. 2D and 3D Roughness Characterization. *Rock Mechanics and Rock Engineering* 53 (3): 1495–1519. https://doi.org/10.1007/s00603-019-01977-4

Malinverno A, 1990. A Simple Method to Estimate the Fractal Dimension of a Self-Affine Series. *Geophysical Research Letters* 17 (11): 1953–56. https://doi.org/10.1029/GL017i011p01953

Marsch K, Fernandez-Steeger T M, 2021. Comparative Evaluation of Statistical and Fractal Approaches for JRC Calculation Based on a Large Dataset of Natural Rock Traces. *Rock Mechanics and Rock Engineering* 54 (4): 1897–1917. https://doi.org/10.1007/s00603-020-02348-0

Ogilvie S R, Isakov E, Glover P W J, 2006. Fluid Flow through Rough Fractures in Rocks. II: A New Matching Model for Rough Rock Fractures. *Earth and Planetary Science Letters* 241 (3–4): 454–65. https://doi.org/10.1016/j.epsl.2005.11.041

Power W L, Tullis T E, 1991. Euclidean and Fractal Models for the Description of Rock Surface Roughness. *Journal of Geophysical Research: Solid Earth* 96 (B1): 415–24. https://doi.org/10.1029/90JB02107

Renard F, Voisin C, Marsan D, Schmittbuhl J, 2006. High Resolution 3D Laser Scanner Measurements of a Strike-Slip Fault Quantify Its Morphological Anisotropy at All Scales. *Geophysical Research Letters* 33 (4). https://doi.org/10.1029/2005GL025038

Stigsson M, Mas Ivars D, 2019. A Novel Conceptual Approach to Objectively Determine JRC Using Fractal Dimension and Asperity Distribution of Mapped Fracture Traces. *Rock Mechanics and Rock Engineering* 52 (4): 1041–54. https://doi.org/10.1007/s00603-018-1651-6

Stock B, Frampton A, 2023. Fracture Aperture Generation Using Surface Scan Measurements of Natural Rock Samples. Preprint. https://doi.org/10.22541/essoar.169566449.99205257/v1

Tatone B S A, Grasselli G, 2009. A method to evaluate the three-dimensional roughness of fracture surfaces in brittle geomaterials. *Review of Scientific Instruments*, 80:125110.

Tse R, Cruden D, 1979. Estimating joint roughness coefficient. International Journal of Rock Mechanics and Mining Sciences & Geomechanics Abstracts. 16(5), 303–307.

Wan T, Du S, Xu Y, Xu G, Li Z, Chen B, Gao Y, 2019. RGB-D point cloud registration via infrared and color camera. *Multimedia Tools and Applications*, *78*, 33223–33246.

Yu X, Vayssade B, 1991. Joint profiles and their roughness parameters. *International Journal of Rock Mechanics and Mining Sciences & Geomechanics Abstracts*. *28*(4), 333–336.

Appendix A

Modelling Group SÚRAO (CZ) – Roughness analysis and surface generation

Milan Hokr[1], Aleš Balvín[1], Jakub Jankovec[2], Libor Gvoždík[2]

[1] Technical University of Liberec (TUL), Liberec, Czech Republic

[2] PROGEO Ltd., Roztoky, Czech Republic

A1 Introduction

Participation of modellers in Task 10 is covered by SÚRAO, the Czech national waste management organization. The Czech deep geological repository (DGR) concept considers crystalline host rock where the prediction of rock fracture transmissivities will be one of the substantial issues to be addressed. Therefore, the generic idea of Task 10.2 to extrapolate the drillcore-scale fracture surface and aperture observations to the larger scale of the whole fracture plane is followed as it addresses the aim relevant to SÚRAO's safety case.

Many of the theories, procedures and data sets related to the Task Description were beyond the authors' experience for modelling groundwater flow in fractured rock. Therefore, the participation of the authors in Task 10.2.1 was limited to studying the literature, searching for software and gaining relevant experience. The chosen methods are partly controlled by the functions available in the used software. To provide blind predictions and comparisons to data within the project, there was a preliminary version of the report with incomplete results to record the state before data disclosure. This version combines the procedures used and results obtained after the date data became available; however, no part of the work explicitly used the additional data.

The report discusses the following topics:

- Processing of laser-scanning data of rough surfaces.
- Calculation of roughness measures based on the surface geometry data.
- Estimation of heterogeneous fracture aperture (as input for the flow and solute transport models).
- Generation of synthetic rough surfaces (general approach).
- Relation of roughness parameters across scales (including the issue of larger-scale generation from smaller-scale measured data).
- Theoretical evaluation of hydraulic properties, including channelling, of the measured fracture samples.

The solution excludes in particular:

- Generation of synthetic aperture field (without regard of scale).
- Stochastic approaches (considering inputs and outputs as probabilistic distributions, uncertainty ranges etc).
- Validation against the measured large-scale surfaces (the additional data provided after the blind prediction stage).

The main, detailed description of the modelling procedure and results is contained in Sections A5.7 and A6, while the previous sections mostly provide an overview of the corresponding features; therefore, some terms may be mentioned before their full explanation.

A2 Objectives of Task 10.2.1

The model purpose of Task 10.2.1 is to confirm if single-fracture observations made on the scale of a pilot borehole can be used to make predictions of single-fracture properties on the scale of a deposition hole. The main focus will be on the fracture roughness distribution and its relation to aperture, transmissivity and channelling effects. A secondary purpose is to develop workflows for upcoming modelling tasks, focusing on aperture distribution and pragmatic model validation.

A3 Limitation of Task 10.2.1

The number of physical samples is small and therefore does not allow for stochastic processing. General differences between the samples are therefore difficult to explain. There are several uncertainties related to the real geometry of the fracture surfaces before rock extraction and fracture splitting (discussed below).

The hydraulic properties of the fracture cannot be validated against (hydraulic) experimental data with the present extent of the task.

A4 Data description

A4.1 Data pre-processing

The laser scan data of individual surfaces were obtained in two formats – ASCII files (point cloud with X, Y, Z coordinates) and STL files (triangulation). Since the latter covered all rock block sides (not just the fracture surface) and it would be difficult to detect and extract the fracture surface sub-set, the ASCII files were used for creation of a regular grid using the Surfer software (Golden Software, 2023). Eight data sets were processed: four blocks 1N1–4N4, each with an upper and lower scanned surface. The resolution was set to 0.1 mm, and kriging was used as the interpolation method.

It was not clear a-priori, how the edges of the fracture are defined and where the limit of influence of the rock sample cutting is. Therefore, two model rectangles were chosen for each fracture sample:

- “full-range”: a technical minimum crop of the data plane, i.e., a rectangle with coordinates in multiples of 0.1 mm that fits between the minimum and maximum data coordinates (there can still be grid points outside of the convex data hull, but no such case was recognized). A common rectangle was defined for both the upper and lower surfaces, but individual rectangles were defined for each rock sample.
- “cropped”: a crop of 2 mm from each side with respect to the “full-range” rectangle.

Surfer evaluates statistics as part of the gridding output. The standard deviation was recorded, which corresponds to the R_q surface roughness measure (root mean square, RMS) and is used below for the synthetic surface generation.

Next, the data were converted and processed to comply with the input format of the free software “Surface Roughness Calculator” (SRC) (Magsipoc et al., 2020).

- Export of the grid into STL format: The triangles are constructed by splitting each grid square along its diagonal.
- Construction of line profiles: “slices” in steps of 5 degrees between 0 and 180 degrees were calculated by Surfer (Figure A-1). The slices go from the centre to the edges of the data rectangle, i.e., they have variable lengths. There is one profile for each direction for use in directional roughness calculations, which are not available for area STL input, limited by partly manual processing.

The second set of the supporting data consisted of “pressure films”. Pressure films consist of layers of pressure-sensitive material, which, after assembling between and pressing against the two fracture surfaces, can be interpreted as capturing the asperity contacts, or even expressing the magnitude of aperture. These were provided in a bitmap image format with colour scale.

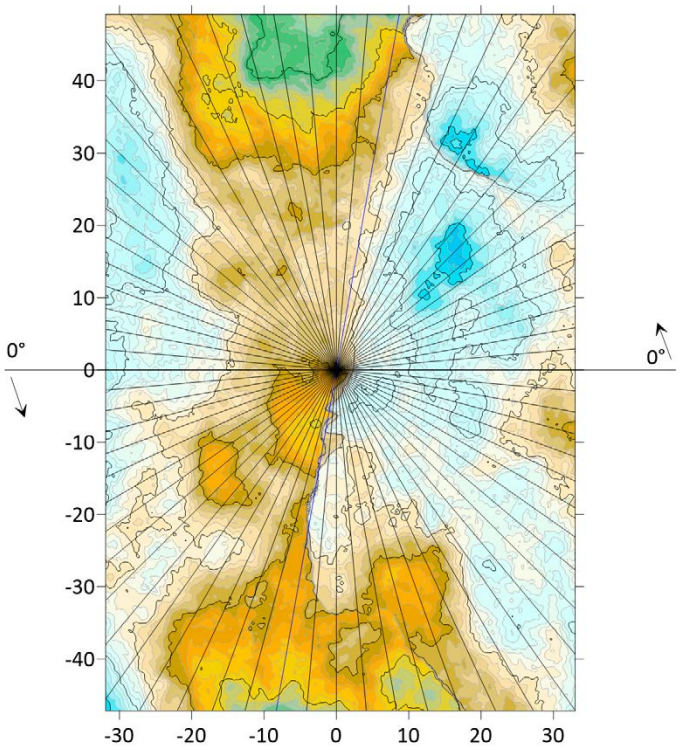

Figure A-1. *Selection of line profiles for directional roughness measures evaluation.*

A5 Modelling and methodology

A5.1 Model purpose

Within the framework of the objectives of Task 10.2.1, the model and analysis procedure should demonstrate how the transmissivity and the channelling factor can be determined based on geometric data of two fracture surfaces and determine what other data and assumptions are needed.

A5.2 Model description

The modelling work addresses the following topics:

- Determination of the surface roughness measures as a direct application of standard methods to the data with eventual input variants and evaluation of observed features in the results.
- Generation of upscaled synthetic surfaces, followed by application of the same roughness measure calculation and comparison to the source rock samples.
- Calculation of the fracture aperture fields and their basic statistical measures.
- Calculation of the fracture transmissivity as the basis for flow simulations within a heterogeneous, plane fracture.

The roughness measures to be evaluated were based on the assignment from the Task Description, extended as necessary to allow for upscaling and synthetic surface generation, but limited by the functionalities of the available software.

Details of the roughness and aperture measures and their calculation, as well as of the fracture flow model, are provided in Section A5.7.

Determination of the aperture from the two surfaces required some ad-hoc data corrections, also specified below. More variants of results are obtained depending on processing choices.

Key processes: The problem to be solved is to determine the impact of geometry and statistics of the fracture-plane roughness on water flow processes as transmissivity is controlled by fracture surface geometry.

Assumptions: The fracture is simplified as a 2D plane, using the local cubic law to calculate transmissivity. For the synthetic surface generation, the choice of the method (in particular the fractal model explained below) defines an abstraction of reality and introduces the assumption of ideal self-similarity across spatial scales. Although the measured surface geometry is used as "fixed", there are some adaptations described below (relative position of the two surfaces, irregularities near the boundaries, numerical thresholds). The position correction considers displacements only, but not rotations. Potential changes of the surfaces due to sample handling, resulting in non-fitting surfaces, caverns, etc are not considered during the processing.

Key parameters: Input data include the X, Y, Z surface coordinates and the colour pressure film maps. The roughness measures, for both the planar data and the line profiles, and the aperture statistics are derived by standard formulas. The generator does not require additional parameters except the previously evaluated roughness measures. There are free parameters of choice for the surface relative position correction, numerical lower threshold of the aperture, and numerical grid discretisation. The interpretation of the pressure film scale is a matter of choice, i.e., the level defining the contact is a chosen parameter.

Uncertainties: Uncertainties are due to potential damage of the surface, relative displacement of the two surfaces, conceptual errors of the local cubic law and the 2D model, numerical errors from the discretisation, stochastic nature of the measured surfaces and the synthetic realizations (only selected images of the real fracture are investigated). Moreover, the physical samples and measurements cover only a subset of the spatial scales, so the application of the fractal model introduces uncertainty and potential bias as the data are extrapolated.

A5.3 Determination of critical aspects

We ask the question: What aspects could cause the resulting fracture properties (primarily the transmissivity) to be unrealistic or inaccurate? Some answers to this question include:

- Validity of the local cubic law and horizontal projection to represent fracture geometry.
- Without at least one measurement of hydraulic phenomena, the transmissivity determined from the aperture field is affected by the free parameters of the relative position of the two surfaces.
- The surface geometry may not be a precise image of the fracture's natural state before block splitting and core extraction.
- Although the upscaling of the single surface can be somehow validated by comparison of the measured and synthetic data in both scales, aperture distributions have not yet been evaluated.
- Validity of the fractal model (consistent self-similarity across all relevant scales). For example, there may be just one or two channels per fracture, which is not a basis for stochastic approaches.

A5.4 Definition of performance measures and criteria

In general, the performance measures should be comparisons of model predictions and their counterpart measurements. Relevant performance measures for this work include:

- Comparison of the surface roughness measures of the real large-scale fracture samples (1 m scale) versus the roughness measures of the synthetically generated surfaces on the same scale (1 m × 1 m). We consider that the direct, deterministic comparison of the surfaces as a geometric set is not meaningful, so the comparison of stochastic measures would be the appropriate approach. However, this would require many measurements of large-scale surfaces for calculation of the statistics.
- Evaluation of aperture statistics of the real large-scale fracture versus synthetically generated fracture aperture fields, with all the comments from the previous point valid here as well.
- Comparison of the predicted hydraulic properties from the aperture with the measurement based on the pressure difference and the flow rate.

None of the criteria in the list above were available in this particular subtask. The large-scale measured surfaces require filtering; these data could not be processed due to limited time for this report. Hydraulic measurements were not planned for Task 10.2.1 but will be available as part of Task 10.2.2 together with the stress influence.

Some of the comparisons made below could be understood as "partial" performance measures:

- Comparison of roughness measures of the synthetic fractures versus the same measures in the physical samples used for derivation of the input data controlling the generator. This is shown in Table A-3 and Figure A-11.
- Comparison of the aperture field derived from the two measured surfaces and the pressure film. This is shown in Figure A-12 to Figure A-15, but the comparison was not actually made using a numerical criterion; instead, the interpreted contact area size was used as a fitting parameter for aperture processing (correction of the two surfaces position, so not available as the performance measure), and the spatial distribution was not processed as a quantitative comparison.

A5.5 Identification of influential factors

Some of the potentially influential factors result from evaluation of more data processing variants and parameter choices.

- The zones of the fracture along the rock sample sides are not (or little) affected in term of surface roughness measures but significantly affected in terms of aperture and transmissivity.
- The correction of the relative position of the two surfaces is a fitting parameter with a strong effect on the aperture distribution and hydraulic and transport parameters.
- Possible losses of material when dismantling the blocks can lead to locally unrealistic apertures ("caverns"), which affect the statistics of apertures and of roughness. Also, minor movements of mineral crystals at the surface at the level of the laser scan resolution can cause shifts in the surface numerical grids which yields unrealistic block position corrections.

A5.6 Uncertainty analyses

No formal uncertainty analyses were performed.

A5.7 Prediction-outcome exercise

This section summarizes the analysis procedure, parameter values, and corresponding results for the variants described above.

Surface roughness

The measures available in the software "Surface Roughness Calculator" (SRC) (Magsipoc et al., 2020 and references therein) are:

- $Z_2 = \sqrt{\frac{1}{L}\int_L \left(\frac{dz}{dx}\right)^2}$ for the line profiles only (*z(x)* the profile function, *L* the profile length, input as a two-column ASCII file).
- Root-mean-square (RMS) ($R_q = \sqrt{\frac{1}{L}\int_L z^2}$) for the line profiles only.
- Roughness metric $\theta_{max}^*/(C+1)$ where θ_{max}^* is the maximum inclination angle and *C* is a fitting parameter of the inclination angle distribution, for both line profiles and planar data (STL file input), includes 5-degree steps for the latter (directional-dependent metric).
- Fractal model parameters for both kinds of input – fractal dimension *D* and proportionality factor *A*, defined by power regression $S(w) = Aw^H$ of the RMS dependence *S(w)* on the window size *w* [m], where the Hurst exponent $H = 3\text{-}D$ (for planar surface) or $H = 2\text{-}D$ (for line profile).

The Z_2 and the roughness metric (third point) are among those required in the assignment and the data delivering template. The RMS is mentioned in the assignment but not compulsory in the template. The fractal model is added and together with the RMS, its parameters are used as the input for the synthetic surface generation.

The directional roughness metric $\theta_{max}^*/(C+1)$ for the whole area is calculated from the statistical distribution of dip angles of the triangular discretisation, the effect of direction is included by projection of the true dip of triangles to their apparent dip in the direction (Magsipoc et al., 2020). This is contrary to Z_2 which is only based on the line profile and therefore sensitive on the profile position.

The following data are filled in the Excel file for delivery of 16 datasets (8 surfaces and two rectangle dimension variants):

- Z_2 values from SRC for line profiles in orientations from 0 to 175 degrees in 5-degree steps. These are for test purposes only, with a single instance of line profiles in each direction and only the half circle range (mirror non-symmetry was not considered).
- Roughness metric $\theta_{max}^*/(C+1)$ evaluated for STL surface in SRC, for direction in 5-degree steps between 0 and 360 degrees.
- RMS (R_q) evaluated by Surfer from the grid format of the whole surface.
- Fractal parameters H and A evaluated for STL surface in SRC.

For verification of the procedure, the roughness metric $\theta_{max}^*/(C+1)$ and RMS were also evaluated in SRC for the set of individual line profiles (to be compared with their counterpart from surface data input).

Synthetic surface generation

The fractal model was used for the generation of rough surfaces, as the one available in the SRC software and containing the scaling in its concept. Larger-scale surfaces were generated as a part of the assignment, and same-scale surfaces for verification purposes.

While the output of the roughness analysis in SRC contains D and A for the fractal model, the SRC generator tool requires H and R_q as input. It was previously verified, by processing the generated point cloud into a grid in Surfer, that for any R_q used as the generator input, the resulting "standard deviation" in the grid statistics of Surfer is equal to this input R_q. Therefore, it is possible to use the standard deviation of the measured data calculated by Surfer as the input for surface generation in SRC.

On the other hand, considering that the fractal model is based on a power relation of the problem scale and the standard deviation, the input R_q for the generator should be rescaled when generating a larger fracture than the analysed one:

$$R_q^{(2)} = R_q^{(1)} \left(\frac{w_2}{w_1}\right)^H \qquad \text{(A-1)}$$

where w_1 [m] is the analysed rock sample size, w_2 [m] the generated model size, $R_q^{(1)}$ is the standard deviation of the analysed surface and $R_q^{(2)}$ is the scaled input for the generator.

There could be more options how to process the individual rock samples and surfaces, getting an image on the surface prediction uncertainty. One way would be to first evaluate a statistic of the roughness measures for the whole set of measured surfaces, get a single input for the generator and generate one set of realizations of the same kind. An alternative option would be to take each rock sample measure as individual generator input and compare the results between the realization sets of different generator inputs. The final choice was expected to be decided based on visual evaluation of the differences between the individual measured surfaces. It is a subject of the results and discussion section, but to allow the description of the next procedure steps, we note in advance that there were two groups of measured surfaces with similar roughness measures within the group and well separated from others. The decision was to ignore the effect of cropping, and to set two input sets for the generator, mainly differing by the Hurst exponent.

For each group, five realizations of generated surfaces were evaluated. Additionally, for verification, synthetic surfaces of the "same" size (square of 85 mm side length) were generated with R_q without scaling. Another "self-verification" is available from the output fractal parameters – ideally the H from the analysis should be equal to the controlling H for the generator (the equality of the input and output R_q was mentioned above as verified prior the overall workflow design).

Fracture aperture

The aperture grids of 1N1–4N4 were obtained by subtraction of the z coordinate of the lower from the upper grid. The grids of the upper and lower surfaces consist of identical rectangles, so that the upper and lower grid points fit to each other without additional interpolation.

The relative position of blocks (alignment of coordinate systems of upper and lower surfaces, separately described for z and for x,y coordinates) was considered uncertain. As the reference case, the relative position included the measuring the holder distance in the z coordinate reported in the assignment as 9.92 mm, i.e., Aperture = Upper grid – Lower grid + 9.92 mm.

Additional correction was derived from the measured contact by the pressure film. The colour range was considered qualitative and only the "highest" colour on the range was defined as the area corresponding to the zero aperture – the background idea is that the "real" contact area should be rather small, otherwise the two surfaces would fit more accurately one onto another (assuming no significant rock deformation). The provided pressure film bitmap files were analysed by the online software Pixel Colour Counter (townsean.github.io, Figure A-2), which outputs the number of pixels of each colour of the palette (i.e., of the colour scale). This was visualized by means of cumulative distribution functions and the ratio in % for the highest level was evaluated.

The correction of the relative upper and lower surface shift in z was made by guessing an additive constant to the aperture field (with respect to the reference case with 9.92 mm added distance). We consider the negative aperture from the subtraction as the contact area. Surfer's function "grid volume" provides an output of "positive area" and "negative area" (parts of $z(x,y)$ function surface above and below the $z = 0$ plane, respectively). With that, the additive constant was iteratively changed until the negative area (contact) was equal to that obtained from the pressure film (with 10 % accuracy). The contact area ratios for samples 1N1–4N4 ranged from 3 to 8 %, and the fitted displacements from 0.02 mm to 0.53 mm (increasing the reference aperture field), see Table A-1. The area ratio was evaluated for horizontal projections.

For the $z(x,y)$ intersection with $z = 0$, Surfer calculates both the "real" surface area in 3D (considering a slope) and the horizontal projection area. The calculation for the intersection requires as input two functions $z_1(x,y)$ and $z_2(x,y)$ (i.e., the plane is a special case), which could be theoretically applied for the two rough surfaces, but it was found that Surfer version 11 transforms the problem so that it evaluates a fictitious surface equal to the z_1 and z_2 difference against the horizontal plane (this is equivalent to the use of the aperture field as the surface and it is only correct for the horizontal projection area, not the surface in 3D). Therefore, the flow-wetted area was calculated as a workaround: The total "real" area in 3D was calculated for the upper and lower surfaces individually (without intersection and evaluation of "positive"/"negative" parts) and then the sum of the upper and lower area was multiplied by the complement of the ratio of the contact area and the total area in the horizontal projection (evaluated in the previous paragraph) to 100 %. We note that a value for the double surface in mm^2 is provided in the delivered Excel file.

Next, the relative movement in X and Y direction was also considered (this was made after the date of the blind prediction but with no relevance to the new data). First, the Z (vertical) correction above was applied. Then, an optimization problem was solved: for relative shifts in discrete steps of 0.1 mm (equal to grid resolution) in each direction (XY matrix) within the range of −0.6 mm to 0.6 mm, the number of grid points with "negative aperture" (surface penetration) was counted and the relative XY shift with this criterium (area with penetration) minimized was considered as the proper surface position (Figure A-3 – all other cases with similar pattern of a unique minimum), temporarily without regard to the Z position and the pressure film contact area. A significant shift was only needed for 1N1 (here the misfit was at first visible on the line profiles), while for others it was just one or two grid steps. As seen in Table A-2, the improvement of the fit in terms of the contact/penetration area is always clearly visible. Then, the Z position correction was applied once more, to get the contact area equivalent to that of the pressure film. As a consequence of the optimization, the surfaces are always closer to each other compared to the case without the XY position correction (Table A-1 the last column).

Finally, the spatial patterns of the pressure film were also visually compared to the aperture contour maps (Figure A-7 to Figure A-10), in two variants with either Z coordinate shift (normal to the fracture) or both X-Y and Z coordinate shift.

Table A-1. Fit of contact area (positive shift means a movement out – increasing aperture).

Physical rock sample	Contact area ratio (pressure film)	Z shift distance (optimized)	Z shift distance with XY shift (2nd iteration)
1N1	8.1 %	0.02 mm	−0.036
2N2	3.0 %	0.415 mm	0.389
3N3	2.5 %	0.265 mm	0.243
4N4	4.8 %	0.53 mm	0.5195

Table A-2. Position correction in the X and Y coordinate (total number of grid points is approximately 700 000).

Physical rock sample	X shift of the upper surface [mm]	Y shift of the upper surface [mm]	Penetration points before	Penetration points after
1N1	0.1	0.4	57 272	2 346
2N2	0	0.2	21 452	10 328
3N3	0.1	0	16 675	6 542
4N4	0.1	0	36 447	18 472

For computation of flow in Flow123d code (Březina et al., 2020) the GMSH (Geuzaine and Remacle, 2009) file format was necessary. Firstly, a GMSH geometry file ".geo" defining the rectangle of the desired size was created and then it was meshed with 0.2 mm resolution. Then an input file in the format ".bln" (see the Surfer documentation) containing the mesh points and element centres was prepared in MS Excel and the function Residuals in Surfer was used, projecting the aperture from the grid onto the element centres. Then the part of input ".msh" (GMSH native mesh format) file in MS Excel was designed (according to Flow123d file format documentation) and the transmissivity section was compiled using the local cubic law for individual mesh elements.

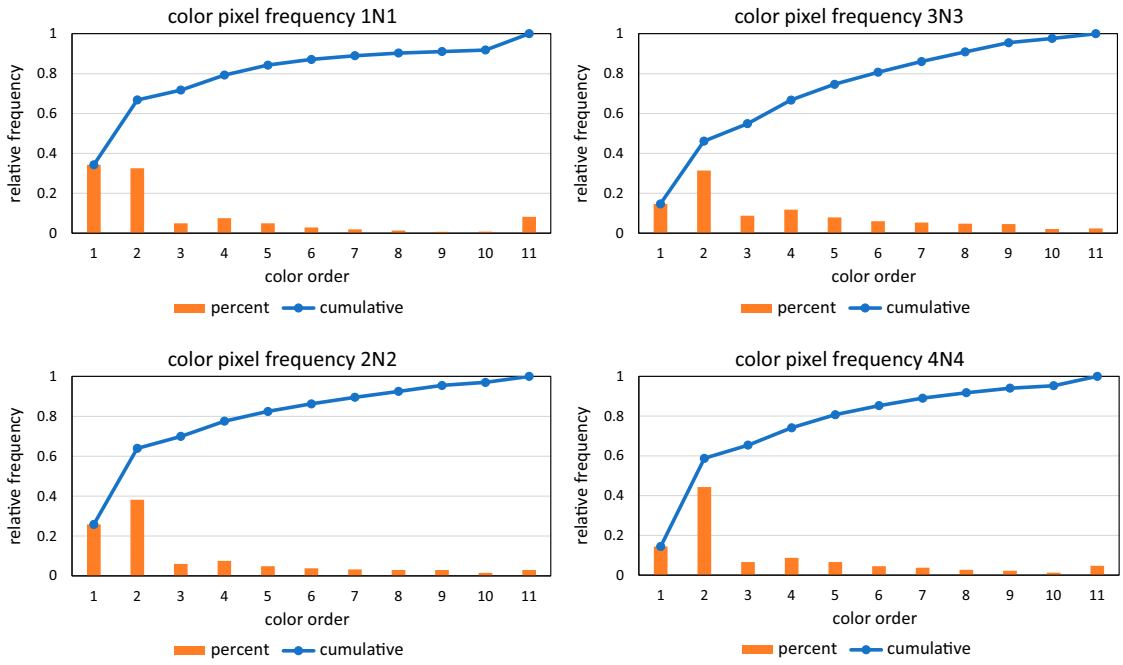

Figure A-2. Cumulative distribution functions of the pressure film colour range (the tightest contact on the right – no. 11, data used for Table A-1).

neg_nmr	-6	-5	-4	-3	-2	-1	0	1	2	3	4	5	6	dx
-6	126794	123553	121049	119222	118264	118725	120438	122616	125865	130283	135108	140543	146048	
-5	117312	112753	109309	106697	105035	104938	106229	108916	112992	118096	123984	130389	136754	
-4	107783	102156	97246	93129	90487	89458	90450	93461	98490	104842	112265	119603	127349	
-3	98395	91458	84833	79294	74955	72727	73121	76693	82837	90736	99614	108662	117653	
-2	89170	80741	72437	65266	59046	55362	54974	58922	66439	75996	86601	97315	108192	
-1	81097	71450	61575	52059	43844	38366	36950	40823	49783	61438	73979	86822	99353	
0	74557	63859	52502	41142	30868	23602	21452	25129	34840	48417	62730	77234	91063	
1	70411	58729	46108	33311	21929	14144	12133	15667	24885	39026	54245	69652	84405	
2	68314	56578	43774	30333	18769	11679	10328	13248	21663	34889	49754	65032	79802	
3	68409	57401	45472	32983	21914	15061	13746	17232	24809	35923	49517	63848	77909	
4	70542	60628	49851	38954	29678	24131	22814	25730	32067	41401	52816	65469	78488	
5	73610	64675	55497	46741	39753	35261	33787	35736	41022	48732	58014	68751	80549	
6	77580	69929	62321	55311	49662	46020	44757	46186	50229	56555	64393	73551	83478	
dy														

Figure A-3. *Example of blocks mutual XY position optimization for 2N2 – number of grid points with "negative aperture" (surface penetration) depending on the upper surface shift in grid steps of 0.1 mm.*

Transmissivity calculation

The purpose of flow simulations is to examine the impact of the aperture distribution on the hydraulic behaviour of the fracture. Flow simulations were only performed for the "measured" aperture field (no aperture fields were generated for the synthetic surfaces). Among the required outputs, the transmissivity and the channelling factor were obtained as postprocessing of these flow simulations.

We consider a planar fracture model (XY plane) with apertures *b(x,y)* obtained from the Z positions of the surfaces, from which local transmissivities were determined based on the cubic law. Therefore, all data (distances, velocities) are considered as projections to the XY plane or to the fracture normal. For general non-horizontal fracture surfaces, this simplification overestimates the aperture and the hydraulic gradient, based on the same factor of cosine of the surface angle – to compensate the effect, it could be needed to decrease the flow rate by one over square of this factor. This was not applied in the reported calculations.

To get a numerically well-posed problem, the aperture and transmissivity fields need to be above certain positive limit (threshold). A value of 0.001 mm was chosen for the minimum aperture, the corresponding transmissivity is approximately 8×10^{-13} m^2/s. Such a transformation is also necessary to calculate the geometric mean required in the data submission template. The provided data on the aperture distribution are evaluated using the same lower limit only for the case of the geometric mean while the presented arithmetic mean, standard deviation and min/max values are based on the original set.

Flow123d developed at the Technical University of Liberec was used for the flow calculations (Brezina et al., 2020). Pre-processing was described in the previous section.

Two configurations of boundary conditions were used to generate X and Y gradients, respectively. A pressure-head difference of 1 m (just a scaling factor for the linear problem) was specified across two of the opposite fracture sides, and zero flux for the other two sides. The resulting fluxes in both directions provide some visualization of channelling and an indication of anisotropy, but they do not take into account the eventual deviation of the permeability tensor's principal directions from the coordinate system.

The reported transmissivities are in the sense of effective transmissivity on the rock sample scale: obtained from back-calculation of the flow rate and problem dimensions with uniform transmissivity. All "full range" data sets are evaluated as 100 mm and 69 mm dimensions and all "cropped" data sets are evaluated as 96 mm and 65 mm dimensions.

The channelling factor is defined in the Task Description. The formula is evaluated based on the mesh discretisation used for the computation, the element-wise velocity magnitudes and element areas, but the actual calculation was simplified so that all element areas were equal (the areas were not directly available in the data files).

Calculations were done for several variants:

- Apertures with only Z position correction: with “cropped” rectangle size and with Y hydraulic gradient (4 in total).
- Apertures with both XY and Z position correction.
  - With “full range” size (smaller by the amount of mutual shift in X and Y) and both gradient directions (8 in total).
  - With “cropped” size and both gradient directions (8 in total).
- Some cases with different mesh resolution (0.2–0.5 mm).

A6 Results, discussion and conclusions

A6.1 Outcomes and deliverables

According to the task assignment and the Excel template, the following deliverables are expected:

- Various surface roughness criteria of the measured samples and generated realizations.
- Images of the contour map of surface height and the shaded reliefs.
- Statistic data of aperture fields and hydraulic properties.

In the text below, the results are presented with the structure corresponding to Section A5.7. Partial comparisons are explained, and the effects of parameters and expected relevance to reality are discussed.

A6.2 Measured surface roughness evaluation

Roughness measures were evaluated for the 16 surface data sets (meant as variants of representation of physical rock samples and their surfaces). One of the introductory questions was how the quantities are distributed among these surfaces – relation of upper and lower surfaces of the same fracture, differences between four fracture samples, and the effect of area boundary cropping. Next, we compared directional roughness metric $\theta_{max}^*/(C+1)$ evaluated for the area and for the line profiles on the same surface, as a step of verification of the roughness metric formulas.

Figure A-4 shows the Hurst exponent (for the fractal model) and R_q, the generic measure of the surface coordinate standard deviation. It is clearly visible that the cropping effect is minor for H in all cases and for R_q except for sample 2N2.

The situation becomes more complicated for comparison of upper and lower surfaces of the same fracture. In terms of H, surfaces of 1N1 have almost the same value, 2N2 and 4N4 have different values and for 3N3 surfaces have a smaller difference. The R_q values upper versus lower are similar for 3N3 and 4N4 while different for 1N1 and 2N2. In general H and R_q are not visually correlated.

There is a common H level of about 0.87 for 1N1 upper, 1N1 lower and 4N4 upper. On the opposite side of the range, a value of 0.80 is common for 2N2 lower and 3N3 lower. Disregarding R_q, we consider these as characteristic values, to which the remaining surfaces can be assigned to form two groups illustrated in Figure A-4. The averages within these groups, $H = 0.86$ with $R_q = 1.10$ mm and $H = 0.86$ with $R_q = 1.11$ mm, can be used as two representative inputs to generate synthetic surfaces. Although R_q is similar for both and cannot be considered to distinguish the type of surface, H is considered to determine the lower and higher bounds of roughness: the lower H value corresponds to a higher fractal dimension, i.e., more contributions from higher frequencies compared to lower frequencies, meaning a more “irregular” surface, and vice versa. For visual comparison with measured surfaces, 1N1 upper and 3N3 upper are used as representatives of the groups.

The directional dependence of roughness is evaluated in Figure A-5. The “roughness metric” $\theta_{max}^*/(C+1)$ is delivered in the Excel file from the whole area evaluation in SRC but was also evaluated for individual profiles. The comparison for 1N1 and 3N3 (more and less rough representatives based on H) is shown. The direction dependence for line profiles is very irregular because a single line of the given direction is very sensitive to particular irregularities along the path. The overall magnitude is consistent, but directions of minima and maxima are not. Higher and lower values of the metric correspond to lower and higher Hurst exponent respectively, as expected.

All area results for 8 surfaces (cropped only cases) are plotted in Figure A-6, sorted by the Hurst exponent. The two groups defined based on the *H* exponent are consistently sorted to lower *H* and higher roughness versus higher *H* and lower roughness, but still there are some overlaps.

In general, some anisotropy is observed on the directional roughness data, but the directions are quite irregular, so it was difficult to evaluate, especially with a relatively small anisotropy ratio (max to min directional value). A detailed evaluation would be deteriorated by undocumented rock sample orientation from the source granite block.

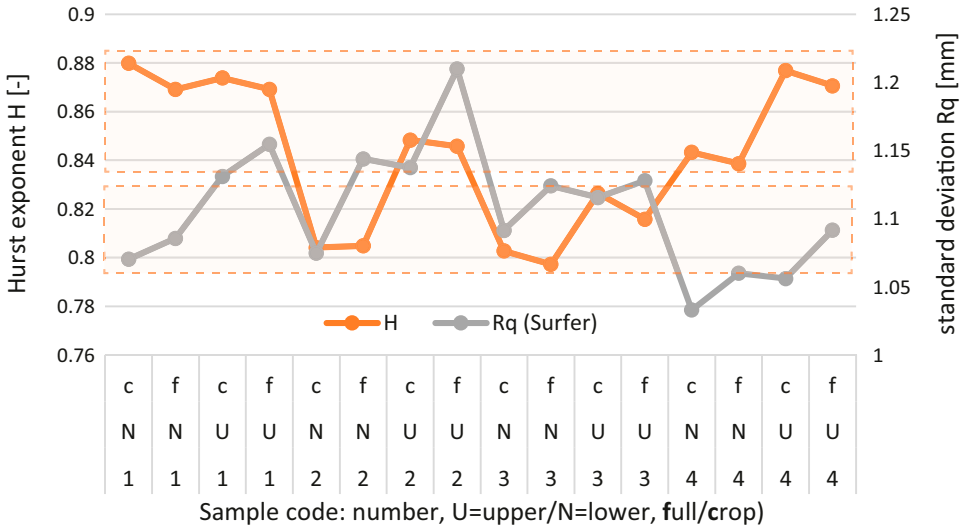

Figure A-4. *Evaluated roughness measures – standard deviation of vertical coordinates (Rq) and the Hurst exponent H of the fractal model. The dashed frames show two considered groups represented by selected H values.*

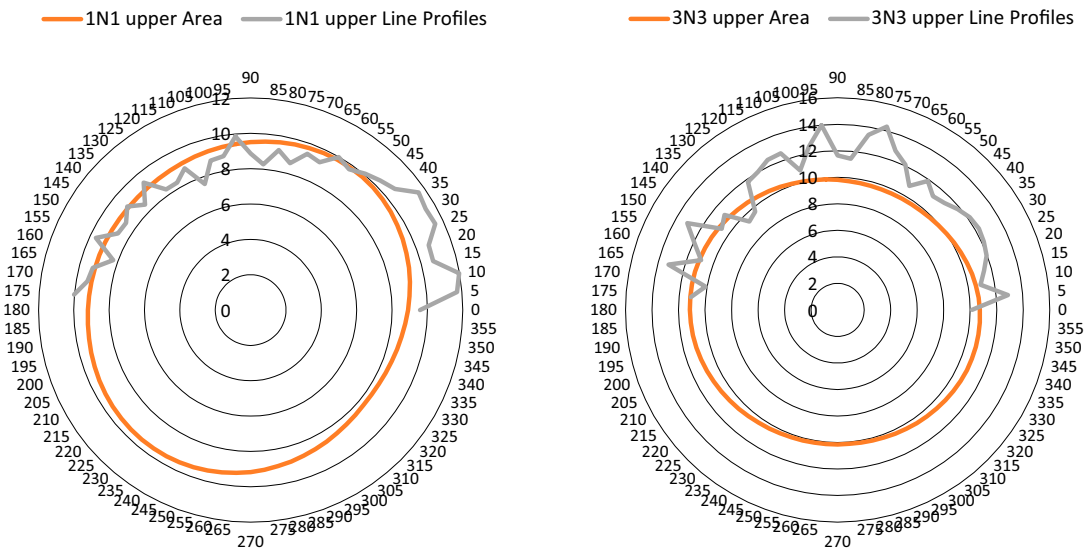

Figure A-5. *Evaluated directional "roughness metric", compared results from area processing and from individual line profiles. The left with lower roughness (area data) corresponds to high Hurst exponent (more "regular" surface) and the right with higher roughness to lower Hurst exponent (more "irregular" surface). The individual profile roughness cannot be interpreted this way.*

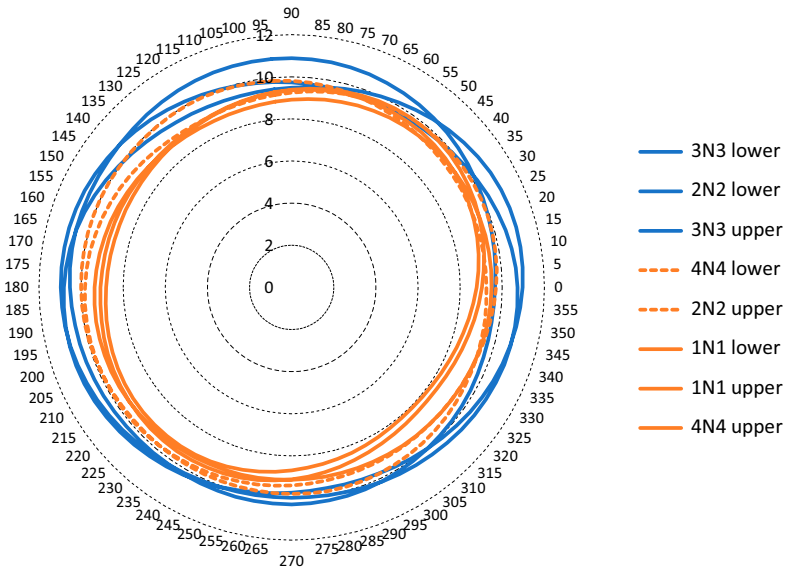

Figure A-6. *Directional "roughness metric" for all measured surface samples sorted by the Hurst exponent. The blue lines represent the group of lower H and orange lines represent the group of higher H.*

A6.3 Generated roughness evaluation

Generated realizations of 1 m times 1 m synthetic surfaces are denoted a01–a05 for the first case of the higher Hurst exponent (lower roughness) and b01–b05 for the lower H value (higher roughness). Two examples are shown, Figure A-7 for the former and Figure A-8 for the latter. Visually, the difference of roughness is not easily recognized. We suppose the reason is that the contours do not show well the "higher frequency" pattern, which could be an important component for lower H. Pictures of the remaining surfaces are contained in the data delivery Excel file.

To verify the statistical consistency between the generated surfaces roughness and the measured roughness of the actual fractures used as the basis (generator input), the Hurst exponent was evaluated for the generated surfaces and compared to the input Hurst exponent (representing a group of measured roughness data), in Table A-3. The Hurst exponent values are not transferred precisely, but the two groups "axx" and "bxx" keep the systematic difference corresponding to the input. In general, generated surfaces have lower H in the analysis compared to the generator input value of H, for the 1-m realizations. The standard deviation is reproduced almost exactly.

Additionally, two realizations of surface roughness were generated for the same scale as the characterized real fracture surfaces. They verify the effect of scaling on the R_q: as shown below, the directional roughness metric has about the same magnitude for the measured and generated surfaces for the reported generator input of R_q (1.10 mm for the same-scale surface and 9.22 mm for the upscaled surface in the "axx" set, by Equation (1) representing the fractal) while it becomes order of magnitude off if the unscaled R_q was used for the large surfaces (not shown).

The reason for a systematically lower H exponent of the generated surfaces is not fully clear. One hypothesis could be related to limited range of scales by the surface size and by the discretization: If looking at the regression which is the source for the H determination and represents the power function as fractal property of the data (Figure A-10), there are systematic deviations of the data approaching a concave curve instead of the line. If data without the largest length scale are fitted, they are almost on the line and the exponent (i.e. the determined H) is significantly higher. The H value used for the surface generation control lies between the two fitted exponents of the generated surface. Therefore, the deviation of the generated surface H value is within the uncertainly of the regression and corresponds to non-ideal surface properties with respect to the fractal model (exact power dependence). As in the example, the largest scale is the whole model surface which is only one instance to evaluate R_q (no statistic). The discretization determines the lowest scale which can be evaluated.

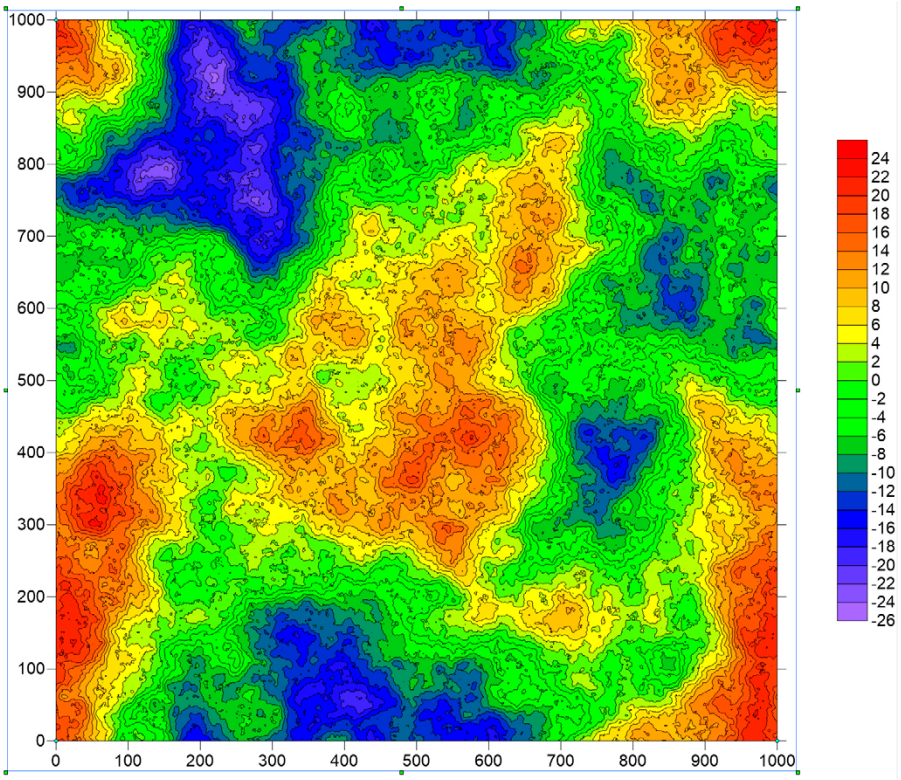

Figure A-7. *Contour map of the surface z coordinate [mm] of generated realization a01 (higher H input), dimensions and colour scale in mm.*

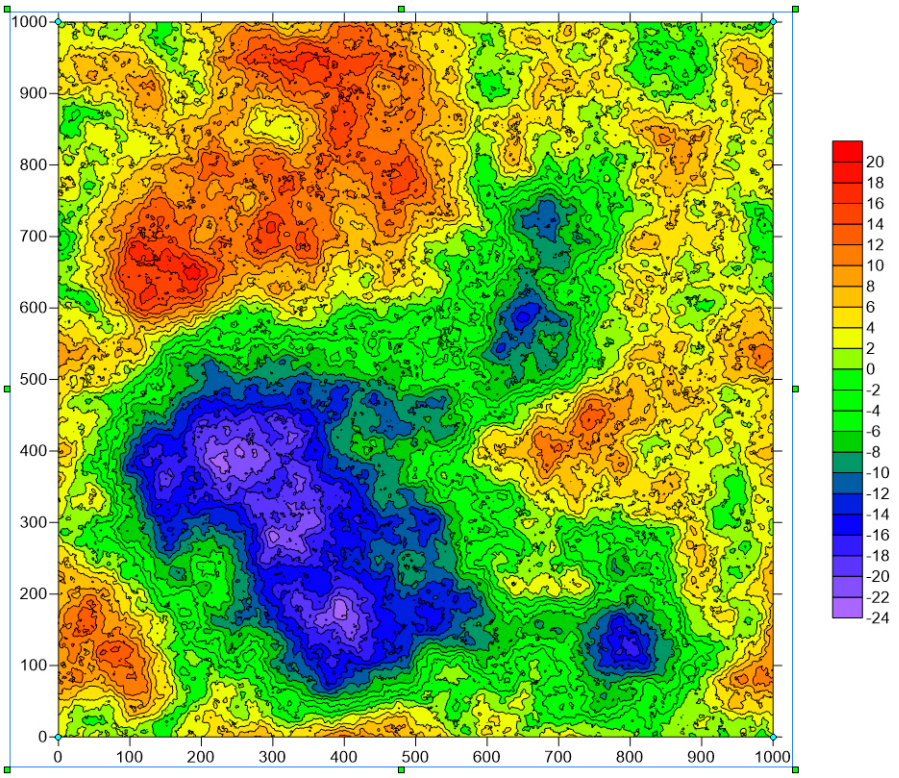

Figure A-8. *Contour map of the surface z coordinate [mm] of generated realization b01 (lower H input), dimensions and colour scale in mm.*

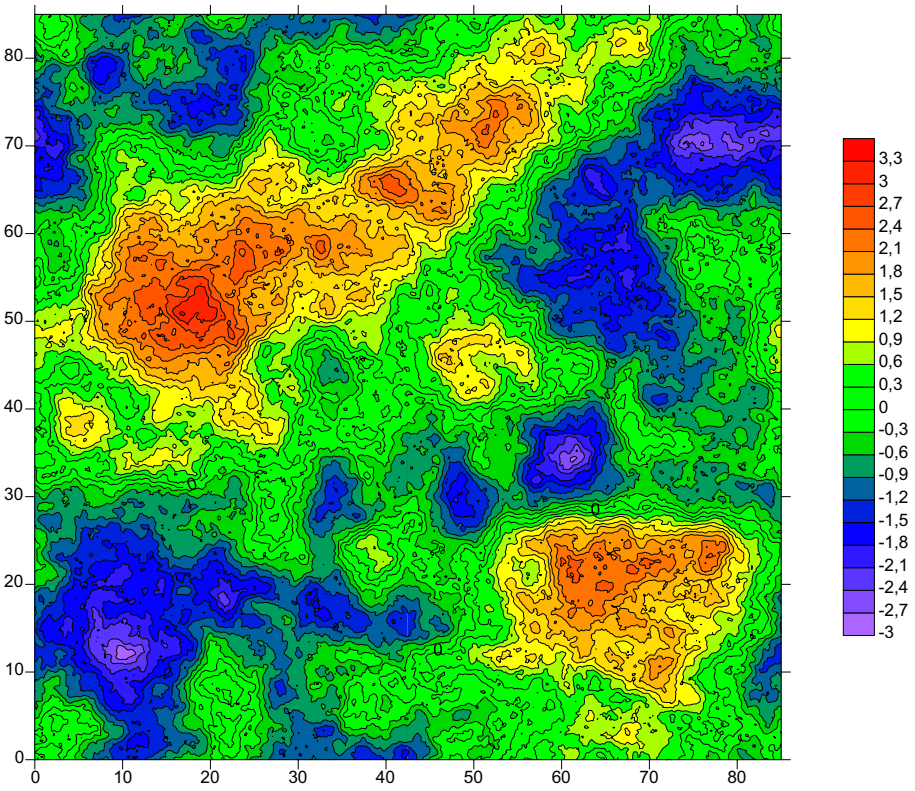

Figure A-9. *Contour map of the surface z coordinate [mm] of the same-scale generated sample, dimensions and colour scale in mm.*

The directional roughness metric of the generated surfaces and the real surfaces used for *H* determination is plot on Figure A-11 for both groups "axx" and "bxx". There are some instances with good fit and some with significantly higher roughness metric than the reference of the measured surfaces. The outlier circles are for the identical generated realizations as those with outliers *H* (a04 of higher *H* than the group and b02 and b04 of lower *H* than the group).

Table A-3 Comparison of controlling parameters for the fractal surface generation with the values for generated realizations.

Generated instance	H input	Rq input	H analysed	Rq analysed
a01	0.86	9.22	0.758	9.220
a02	0.86	9.22	0.757	9.220
a03	0.86	9.22	0.772	9.220
a04	0.86	9.22	0.827	9.220
a05	0.86	9.22	0.755	9.220
b01	0.81	8.16	0.728	8.160
b02	0.81	8.16	0.676	8.160
b03	0.81	8.16	0.735	8.160
b04	0.81	8.16	0.656	8.173
b05	0.81	8.16	0.729	8.160
85 mm test	0.86	1.10	0.784	1.10
85 mm test	0.81	1.11	0.833	1.11

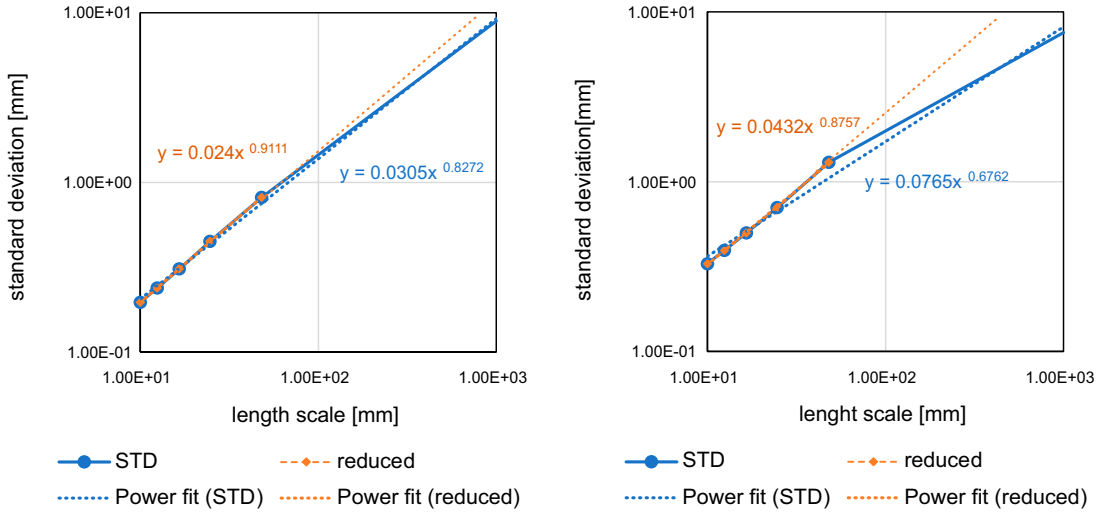

Figure A-10. *Derivation of H by power function fitting (H is the exponent). On the left is the a04 realization with the highest H, and on the right is the b02 realization with the second lowest H. The power-law fit (blue dotted line) includes all points, yielding the H exponent shown in Table B-3); A "reduced-scale" power-law fit that excludes the highest length scale data point is shown as an orange-dotted line.*

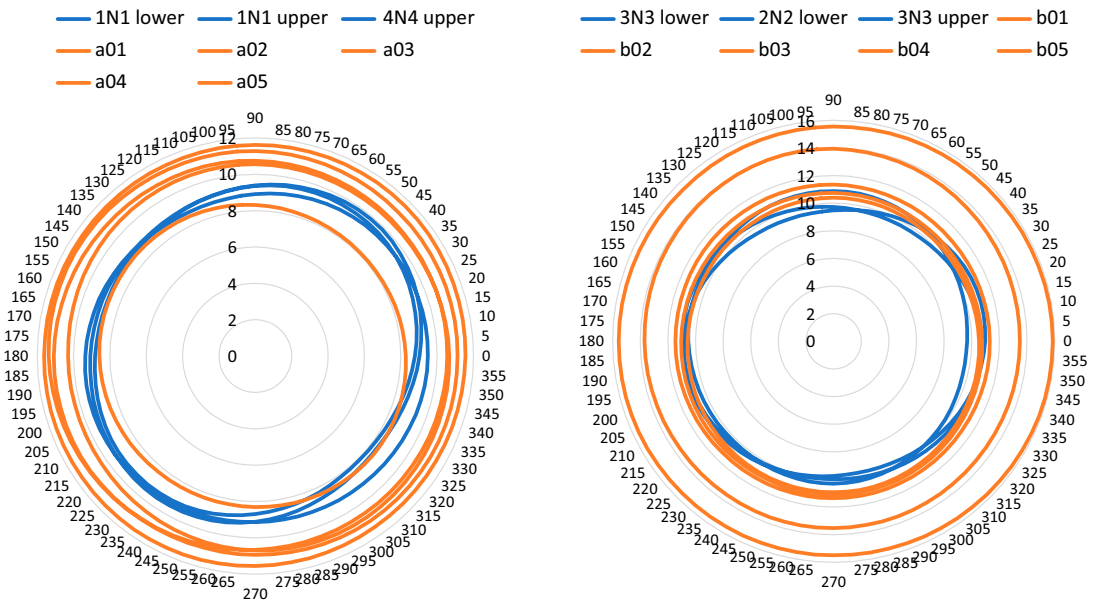

Figure A-11. *Directional roughness metric for measured (blue) and generated (orange) surfaces in the two roughness groups, the left plot for all a01–a05 (higher H) and corresponding measured surfaces and the right plot for all b01–b05 (lower H) and corresponding measured surfaces.*

A6.4 Aperture analyses

In the delivered file, aperture data for 24 variants (6 for each fracture) are present – combinations of the full size and cropped and with or without the additional correction of relative surface positions in XY and/or Z direction, based on the pressure film contact measurement. The results for corrected XY positions and all the transmissivity and channelling calculations were included after the data from the large, fractured blocks were disclosed (practically, the processing has been done without any use of the data). The mean apertures are shown in Table A-4 for cases with either variant of block position correction. Without the correction using the pressure film results, the two model fracture surfaces for 2N2, 3N3, and 4N4 were clearly in a position that does not correspond to a realistic configuration of physical fracture surfaces (model surfaces largely intersecting each other). Within the correction procedure, the "negative aperture" values (surface data subtractions) are understood as expression of the contact,

which means all the surface intersections (penetrations) are interpreted as measurement errors or uncertainties. If, instead, the positiveness of surface subtraction was strictly required as a condition of correction, any individual outlier point in the fracture surface scan data representation would cause the surfaces to be rather far apart from each other with one or few discretisation points with contact.

There are more visible differences between the full-size and the 2 mm-cropped surfaces in the aperture data compared to the roughness data. With cropping, the mean and standard deviation are reduced and the maxima significantly smaller in some cases. It means there could be possibly channels along the sides not detectable as irregularities on the roughness of the surfaces. The effect is similar for both cases of Z-correction and XYZ-correction. The effect of XY correction on the mean aperture is similar to the corresponding change of the Z position of the blocks (tens of micrometres, Table A-1). The effect of cropping is also visible on the contact area ratio (in the delivered Excel file only). After cropping, while keeping the same Z position determined for the, uncropped, full-size data set, the ratio of contact increases.

The contour plots of apertures after the correction to the pressure film results and optionally after the XY position correction optimizing the upper/lower surface fit are shown in Figure A-12 to Figure A-15. It is observed that even very small XY shifts (one grid step of 0.1 mm) lead to a change of contact area and a different pattern of smallest apertures. For 1N1, the XY correction improves the fit of the contact distribution to the pressure film data. For all other rock samples, the difference (aperture map versus pressure film) is larger and the change by the block shift also changes other pattern features.

For all rock samples, the aperture contour map shows dominant “tight” areas with apertures less then 0.1 mm. The (arithmetic) mean apertures are therefore not representative characteristics, as they are biased by the “caverns” with apertures larger than 1 mm. This also makes the standard deviation larger (exceeding the mean). The following specific patterns are observed:

- The surfaces defining fracture 4N4 are closer than those of other fractures, which also corresponds to both lower arithmetic and geometric mean apertures and to lower transmissivity (next section).
- Fractures 2N2 and 3N3 have chains of caverns in X and Y direction, respectively, which create channels and cause larger transmissivities in the respective direction (next section).

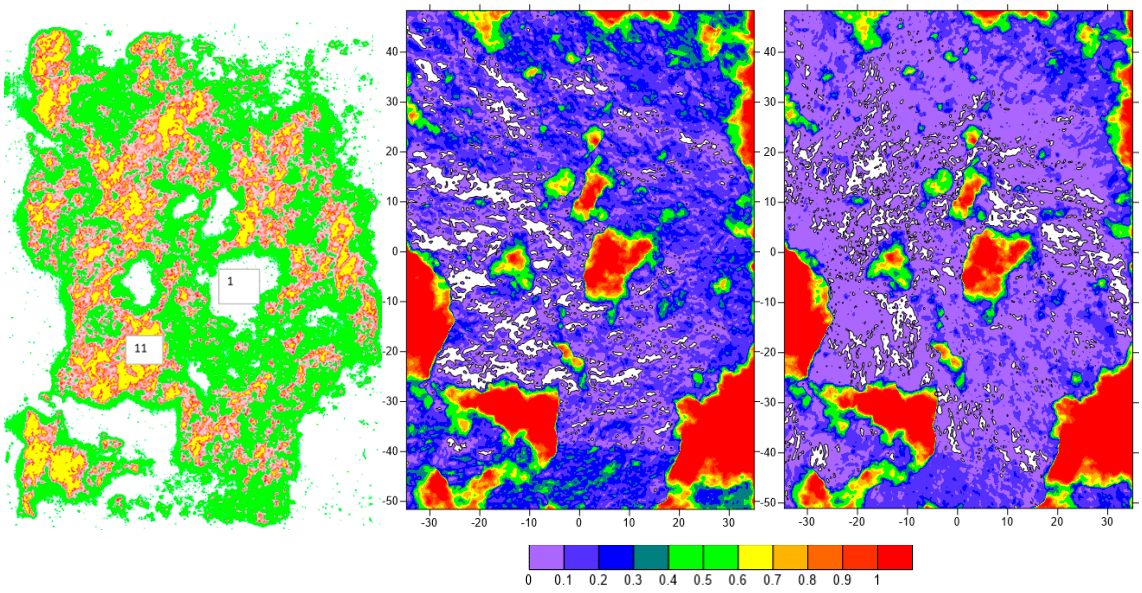

Figure A-12. *1N1 Pressure film picture (left) and the aperture field adapted to the size of the contact area: middle by the Z coordinate correction, right by all X,Y,Z coordinates correction. For the pressure film, min/max numbers in the colour palette and histogram are shown, yellow is interpreted as the contact. Aperture is in mm with cropped range to the same with the figures of 2N2, 3N3, and 4N4 below – white represents a contact or penetration.*

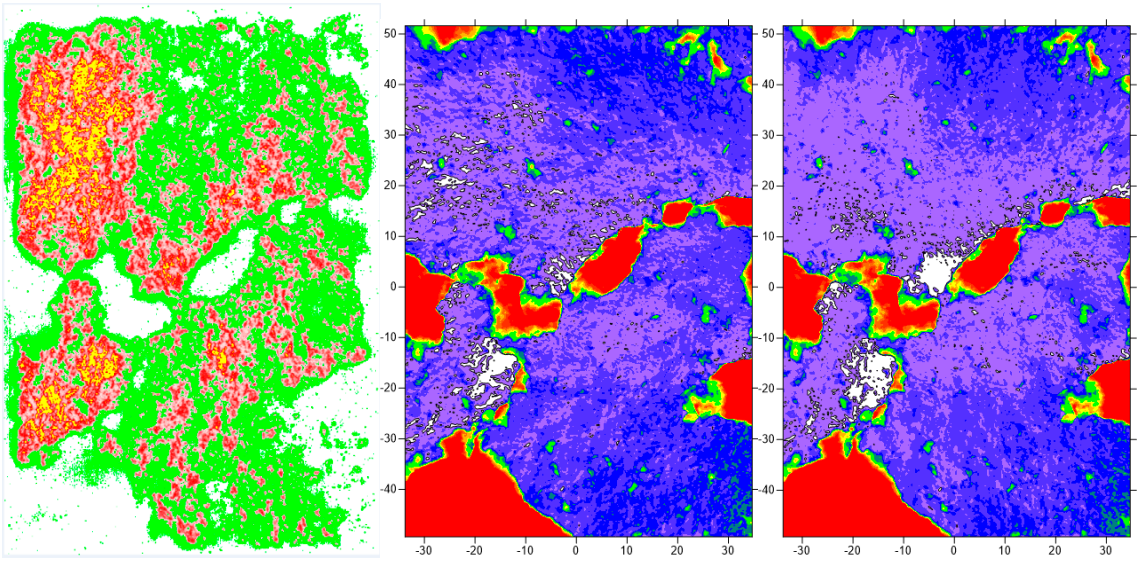

Figure A-13. *2N2 Pressure film picture (left) and the aperture field adapted to the size of the contact area: middle by the Z coordinate correction, right by all X,Y,Z coordinates correction. Aperture scale 0–1 mm is shown above, white represents a contact or penetration.*

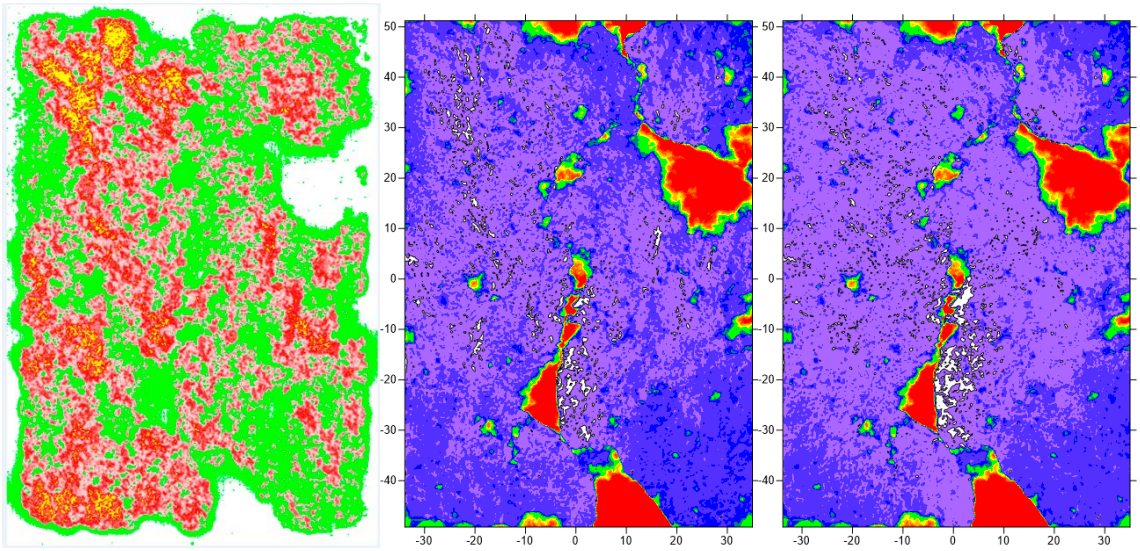

Figure A-14. *3N3 Pressure film picture (left) and the aperture field adapted to the size of the contact area: middle by the Z coordinate correction, right by all X,Y,Z coordinates correction. Aperture scale 0–1 mm is shown above, white represents a contact or penetration.*

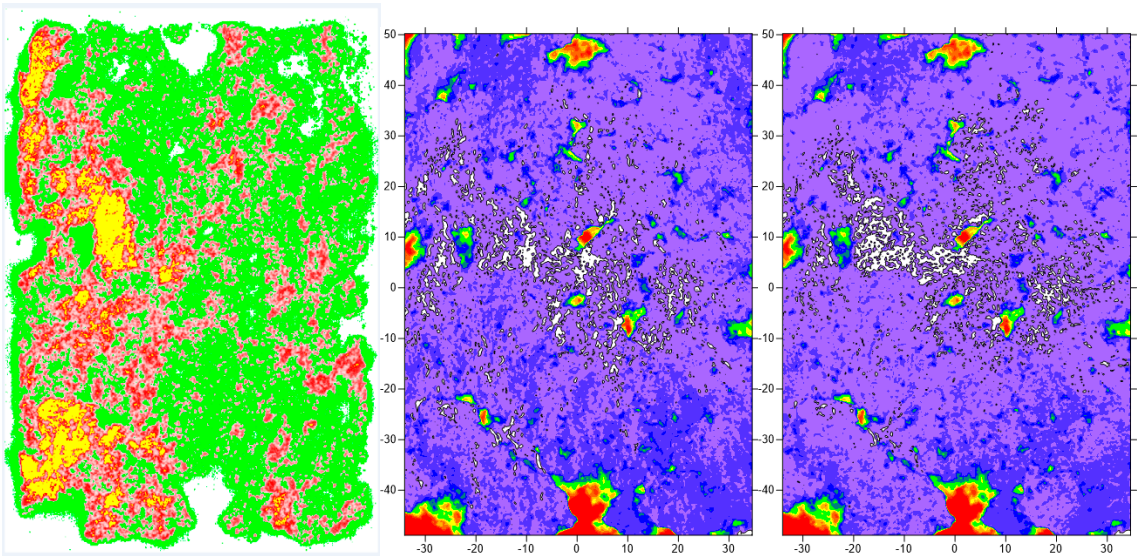

Figure A-15. 4N4 Pressure film picture (left) and the aperture field adapted to the size of the contact area: middle by the Z coordinate correction, right by all X,Y,Z coordinates correction. Aperture scale 0–1 mm is shown above, white represents a contact or penetration.

Table A-4. Average apertures [mm] for various rock sample processing.

Sample	Variant Z-correction full	Variant Z-correction + crop	Variant XYZ-correction full	Variant XYZ-correction + crop
1N1	0.334	0.301	0.274	0.244
2N2	0.391	0.348	0.368	0.327
3N3	0.219	0.203	0.198	0.182
4N4	0.126	0.113	0.115	0.103

A6.5 Flux and transmissivity computation

This section has been completed after the large-scale data disclosure, but practically, no ideas, decisions, or numerical data were related to the new measured surfaces.

Numerical flow computation with the element-wise cubic law application based on the aperture from the two measured surfaces, in the horizontal plane model, was intended to estimate the fracture transmissivity. The following issues were examined:

- Variability among the physical samples which is understood as a random effect.
- Anisotropy which is also quite variable among the samples.
- Effect of surface data crop (eventual damage and larger aperture channels along block edges).
- Effect of two surfaces fitting by XY shift optimization.
- Effect of discretisation.

The transmissivity data are delivered in the Excel file for all evaluated cases (not all possible combinations, the calculations were more focused on the XYZ-corrected blocks). Here the data are shown graphically: In Figure A-16, the effect of data cropping is shown, and the two gradient directions are compared. Overall, the calculated transmissivities for all four fractures and including both directions lie within two orders of magnitude; for a given direction, the range is slightly more than one order of magnitude. There is a systematic effect of lower transmissivities for cropped fractures, which confirms the presence of more fracture openings along the block edges. However, except for the large effect of the visible channel along one side of the 1N1 model in the Y direction, these do not form continuing channels. The removal of the 1N1 side “channel” with the rectangle crop also strongly

affects the channelling factor of the 1N1 in Y direction. The remaining cases have the channelling factor range between 0.15 and 0.25. There is no visible correlation with the transmissivity, except for 2N2 in X direction, where the larger transmissivity is related to more uniform flow (i.e., higher channelling factor), which is contrary to intuitive observation of the openings chain in the middle of the fracture as a single, strong channel. It can be easily explained that the caverns are hydraulically not sufficiently connected to form a channel but are visibly separated by low-aperture zones.

Figure A-17 shows the effect of the position correction. The better fit of the two surfaces using the XYZ correction procedure decreases the transmissivity by a factor between 2 and 10, with the strongest effect for 1N1, which required the largest relative shift of the two surfaces. The channelling factor is either similar or slightly decreased (1N1, 4N4), which means a stronger channelling effect that could be explained by the creation of tighter contact areas acting as barriers to flow.

Additionally, an effect of discretisation (numerical mesh for flow calculation to which the same data from 0.1 mm step grid are projected) is determined as being very small, as shown in Table A-5.

Figure A-18 shows the calculated pressure and velocity fields for the full-size rectangle models and XYZ position correction. The velocity range is adapted for increased visibility: very low velocities are hidden, and the number of arrow symbols is reduced 20:1. The range is common so that the rock samples are comparable (for 3N3, some of the velocities are out of this range, but the effect on the view is negligible). The pressure field is very uneven, with small zones of large gradient and large areas of small gradient. This is an effect of a distribution of flow barriers near "contact" areas of the minimum (threshold) aperture. The areas in between of these barriers form the flow channels, which are just few visually in each sample.

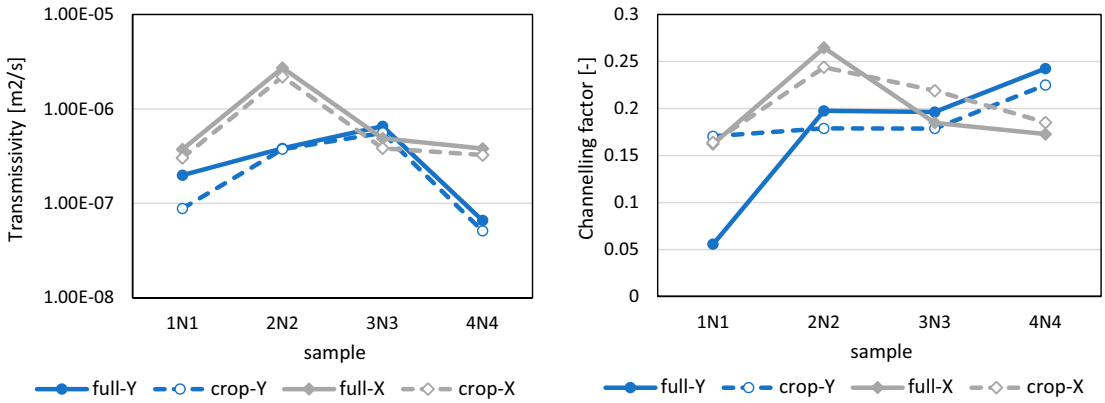

Figure A-16. *Calculated transmissivity and channelling factor for individual physical samples, gradient directions, and data processing variants (full-size and 2 mm border crop).*

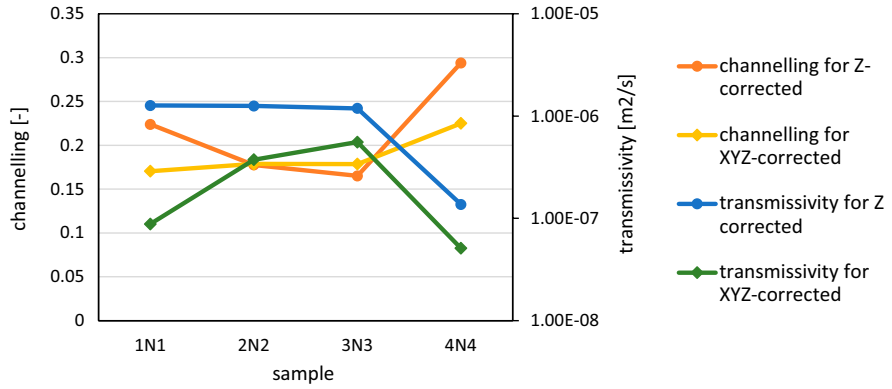

Figure A-17. *Comparison of calculated transmissivity and channelling factor between cases of two surfaces fitting (either by Z shift only or by all XYZ shifts), for cropped rectangle domain variants.*

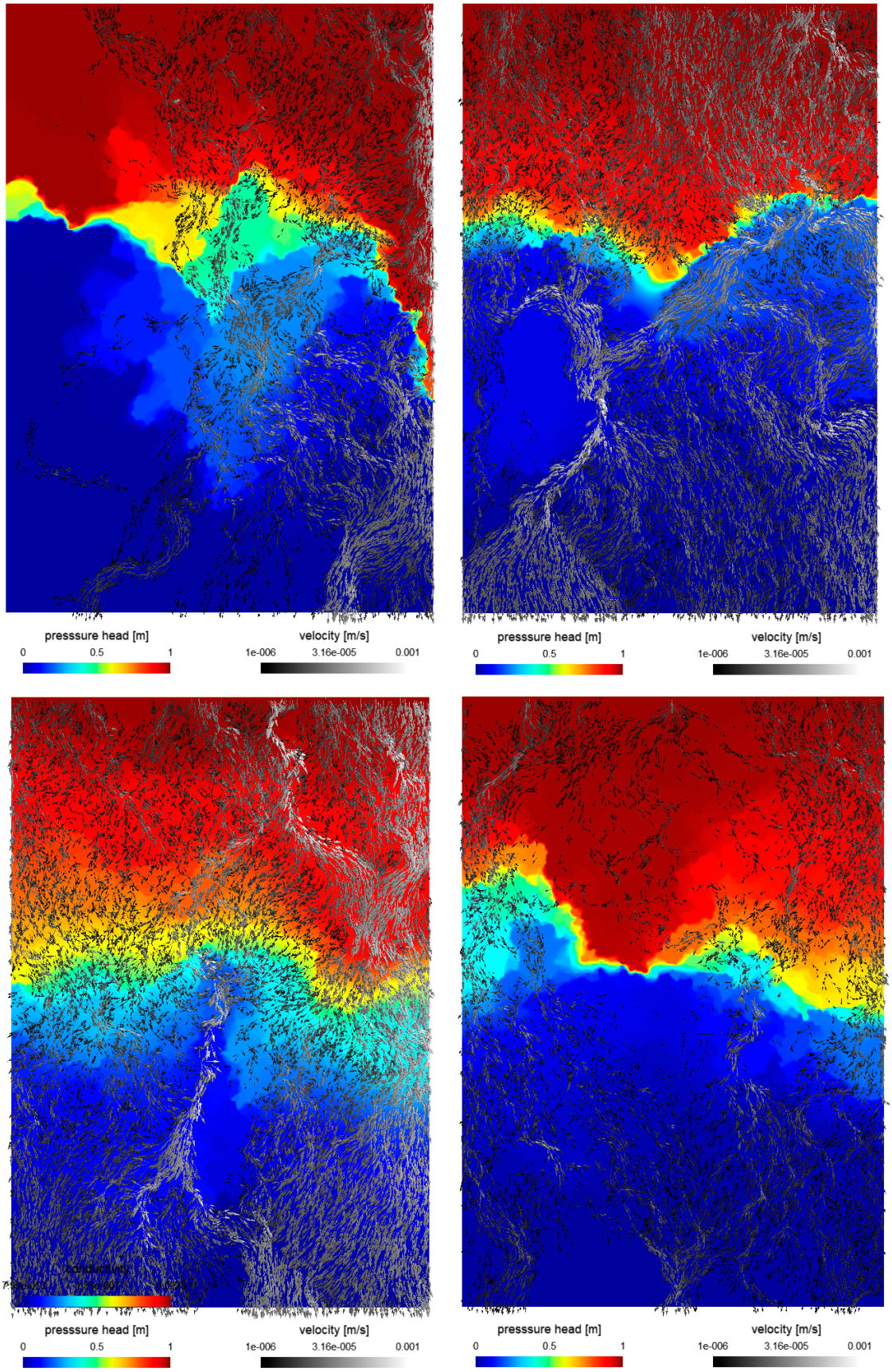

Figure A-18. *Calculated pressure and velocity fields in Y (vertical in the view) pressure gradient for all four fractures 1N1, 2N2, 3N3, 4N4 ordered by rows. The velocity range is cropped to a common range to improve visibility.*

The geometric means of aperture were used for one additional comparison. If a hypothetical transmissivity was calculated by application of the cubic law to the geometric mean, this is compared in Figure A-19 with the numerical simulation with the respective aperture field. The data are related within about an order of magnitude, and mostly respect the ordering of less and more permeable, also the linear regression statistic for the whole data is not satisfactory unless e.g., the 2N2 rock sample is excluded. It would need more detailed study with larger set of data to evaluate the properties of the geometric-mean-based transmissivity.

Table A-5. Discretisation effect for 1N1 example.

Mesh element size [mm]	Transmissivity [m²/s]	Channelling factor [-]
0.5	1.272E−06	0.224
0.4	1.306E−06	0.223
0.3	1.335E−06	0.222

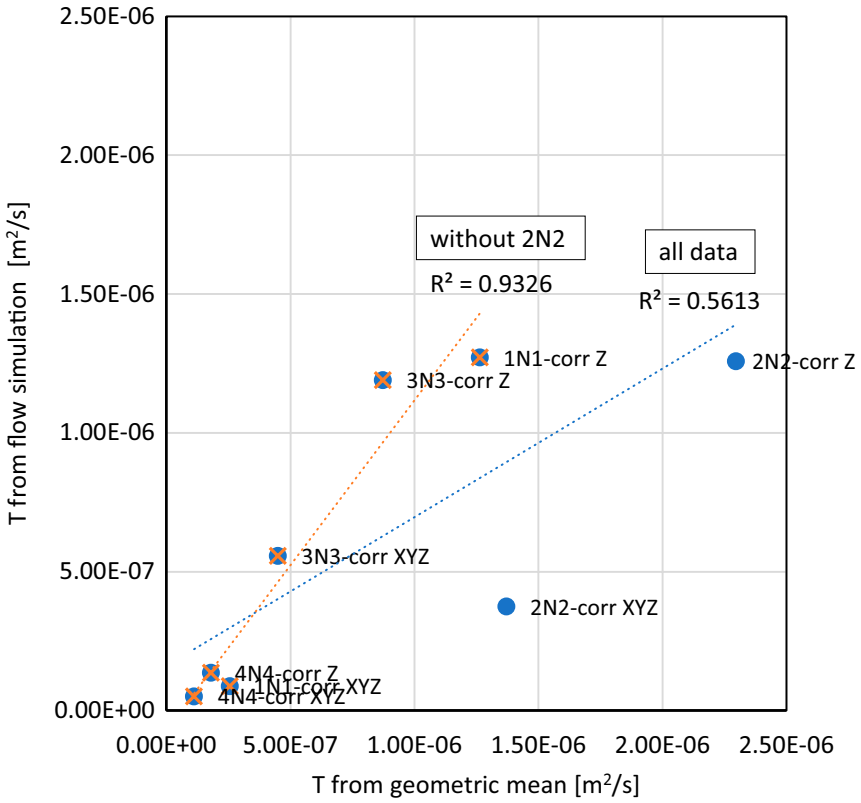

Figure A-19. *Comparison of calculated transmissivity from flow simulation and applying the cubic law on the geometric mean of the aperture field (both with 0.001 mm lower limit on the aperture). Linear regression of all data and of a subset excluding the 2N2 rock sample.*

Appendix B

Modelling Group LANL (USA) – Geostatistical analysis of surface roughness

Jeffrey Hyman, Hari Viswanathan, Matthew Sweeney

Los Alamos National Laboratory

22 December, 2022 – LA-UR-23-20001

B1 Introduction

The primary goal of task 10 is to build confidence and "validation" of models for flow and transport in fractured rock and the phenomenon of flow channelization. Prior to evaluation of the flow and transport models, however, there needs to be characterization of the fractured rock itself. To this end, our focus in Task 10.2.1 is to perform a geo-statistical characterization of the samples provided by the Task Force. This quantification step is essential because: (1) if one wants to go beyond the characterization of flow channels and link their formation with geological information, the geological properties need to first be characterized and (2) limited observations of host rock require the creation of numerical models for said host rock to develop flow models at scales of interest. Our approach is to obtain statistical information from the sample surfaces and the projected aperture field between the surfaces. This information can be used to develop computational techniques to generate rough fracture surfaces at scale, and then characterize and compare the synthetic and real samples in terms of both metrics considered and not considered in the generation.

B2 Objectives of Task 10.2.1

No additional objectives considered.

B3 Limitation of Task 10.2.1

No additional limitations noted.

B4 Data description

No additional data considered.

B5 Modelling and methodology

B5.1 Model purpose

In addition to the purpose put forth in the Task Description, our goal is a comprehensive geostatistical description of the samples to determine if they are of sufficient size to extrapolate information to the meter scale. Information such as correlation length and moment stabilization will be considered to this end.

B5.2 Model description

Our model is broken up into two steps. The first is pre-processing the data for projection onto a regular quadrilateral grid from the unstructured quadrilateral mesh obtained using profilometry. Once the surface is obtained on this regular grid, we measure surface heights to compute the empirical probability density function, i.e., the distribution of fracture heights, and spatial correlations of the surface.

Part 1) We use the LANL software named LaGriT (Los Alamos Girding Toolbox) https://lanl.github.io/LaGriT/ to handle the data. LaGriT is a library of user callable tools that provide mesh generation, mesh optimization and dynamic mesh maintenance in two and three dimensions. LaGriT is used for a variety of geology and geophysics modeling applications including porous flow and transport model

construction, finite element modeling of stress/strain in crustal fault systems, seismology, discrete fracture networks, asteroids, and hydrothermal systems. The general capabilities of LaGriT can also be used outside of earth science applications and applied to nearly any system that requires a grid/mesh and initial and boundary conditions, setting of material properties and other model setup functions. It can also be used as a tool to pre- and post-process and analyze vertex and mesh-based data.

The data processing portion of the workflow is broken up in the following steps:

1. Import Data: We read in the ascii data for the x and y coordinates to create a set of points in 3D space.
2. Create Surface: This point set is triangulated to create a 2D surface. The z-coordinate is added as a point-based attribute.
3. Project surface to 3D: We create a 3D surface by projecting the z-coordinate of the surface, which was uniformly 0, to the position provided by the data.
4. Generation of uniform mesh: We generate a uniform resolution grid of quadrilaterals at the scanner resolution.
5. Interpolation: We interpolate the z coordinates from the initial unstructured surface to the uniform quadrilateral mesh.

Part 2) Geospatial Analysis
For each sample, top and bottom, we determine the distribution of surface heights and treat them as a probability density.

We consider the autocorrelation function of the surfaces in the x and y directions, to look for any anisotropy in the samples. We used the discrete estimation defined as

$$R(\delta) = \frac{1}{(n-k)\sigma^2} \sum_{i=1}^{n-k} (z_i - \mu)(z_{i+k} - \mu)$$

where μ is the mean of the surface and σ^2 is the variance, and a lag distance of δ.

We compute the two-point radial empirical semi variogram of the surfaces, defined as

$$\gamma(\delta) = \frac{1}{2|N(\delta)|} \sum_{(i,j)\in N(\delta)} |z_i - z_j|^2$$

where z_i are the samples, N is the number of samples, at a lag distance of δ.

Finally, we look at the local curvature of the surface defined using the magnitude of the second derivative of the surface.

$$\kappa = \left\| \nabla^2 z \right\|$$

Note that the local curvature is one possible two-dimensional definition of the joint roughness coefficient (JRC).

B5.3 Determination of critical aspects

The characterization and model assume that a geo-statistical approach is sufficient to characterize the surfaces. Underpinning this choice is the assumption that the surfaces can be treated as correlated random fields. The adopted forms of the autocorrelation function and semi-variogram also assume stationarity.

Model parameters

In the data processing, two modelling parameters are used. The first is the resolution of the regular quadrilateral grid. By selecting the scanner resolution, this choice helps mitigate issues in upscaling the data or removing sub-grid scale features. However, its influence was not characterized. Second, is the choice of interpolation scheme. We use an interpolation method where the obtained value is the sum of vertex values multiplied by the relative volume of elements formed by the sink point location on or inside the found element. The element is divided into volumes as determined by the sink point location and its relationship to the vertices of the enclosing element. Other interpolation schemes could be selected, and the influence of that choice on the metrics presented above could be characterized. Within each of the interpolation schemes, there are user parameters, the downstream effects of which would also need to be characterized.

B5.4 Definition of performance measures and criteria

We adopted the definitions of the performance measures in the TD. We did not participate in the blind predictions at the 1 m scale.

B5.5 Identification of influential factors

We do not model roughness; rather our method is used to characterize roughness based on the presented measurements. In turn, we cannot say what are the influential factors that determine the roughness. This is outside of the scope of information that can be gleaned from the data.

B5.6 Uncertainty analyses

The primary uncertainties in our analysis are from data measurement, rather than model parameters. Any sub grid-scale information that was not provided could not be considered. In comparison, the choice of mesh resolution, beyond matching the scanner data, and interpolation scheme, are likely lesser contributors to uncertainty in the data. The mathematical forms for our metrics are standard. Furthermore, the limited independent data, only 4 samples, means that there are large uncertainties in any stable statistical measurements taken over the small ensemble. In fact, the number of samples is so small that the confidence intervals will naturally be quite large. The limited data is the largest source of uncertainty in predictions at the meter scale.

B5.7 Prediction-outcome exercise

Not performed.

B6 Results, discussion, and conclusions

B6.1 Data Processing

Figure B-1 shows Steps 1, 2, and 3 of our data processing workflow for one surface sample. The scanner data triangulated into a 2D surface is shown on the left, and the projected 3D data on the right.

Figure B-2 shows Steps 4 and 5 of our data processing workflow. The z coordinates interpolated onto the uniform 2D quad mesh is shown on the left and the projected 3D version on the right.

Figure B-3 shows a comparison of the provided surface data (left) with the interpolated data (right). The primary features of the surface are retained.

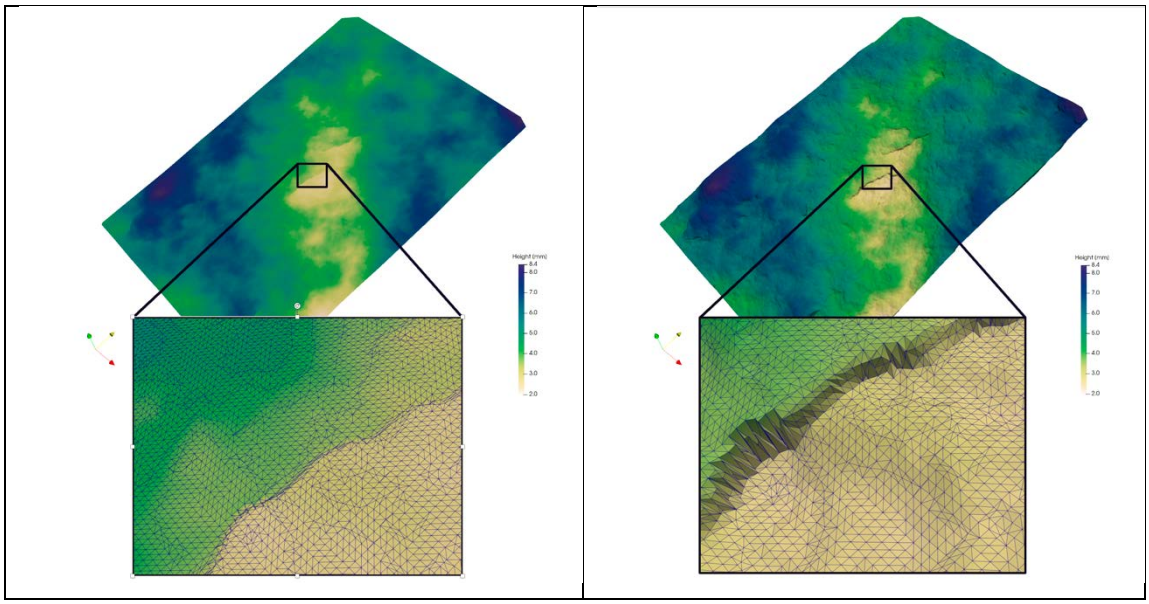

Figure B-1. *Steps 1, 2, & 3 of the workflow.*

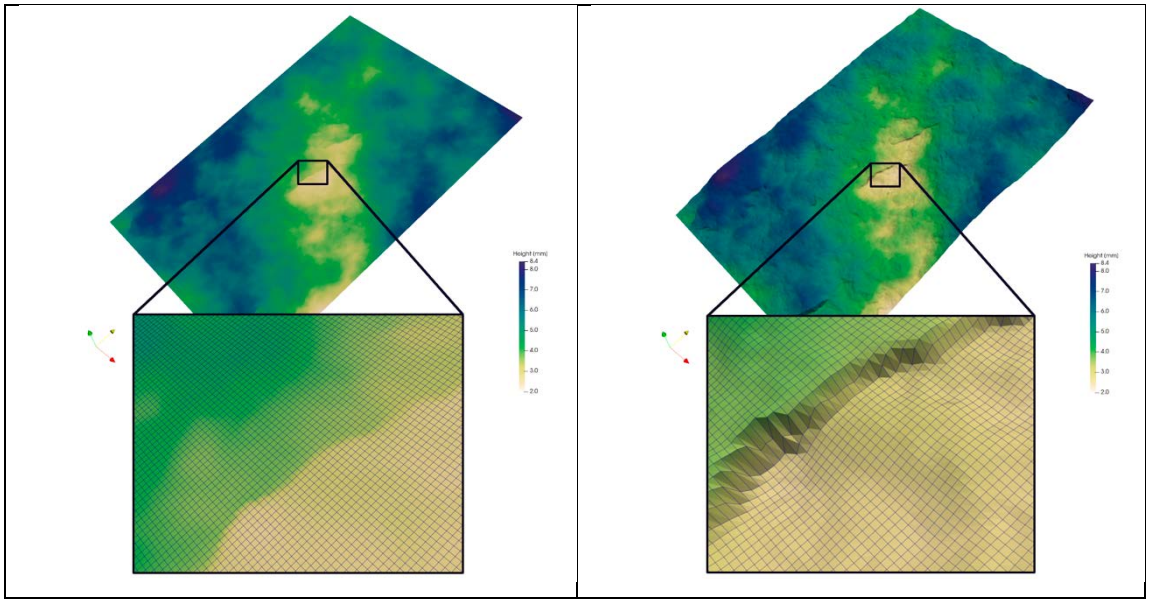

Figure B-2. *Steps 4 and 5 of the workflow.*

B6.2 Geostatistical analysis

The probability densities of the N- and U-surfaces are shown in Figure B-4 and Figure B-5, respectively. Units along the x-axis are in mm where the mean value has been subtracted to highlight deviations from the mean.

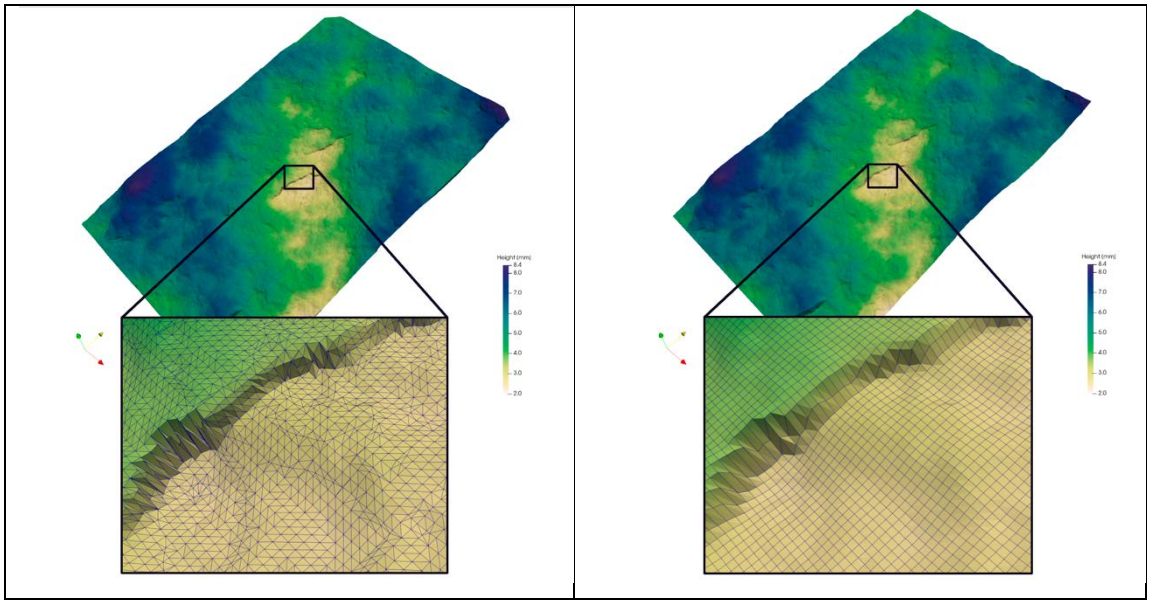

Figure B-3. Comparison of provided data (left) and interpolated surface (right).

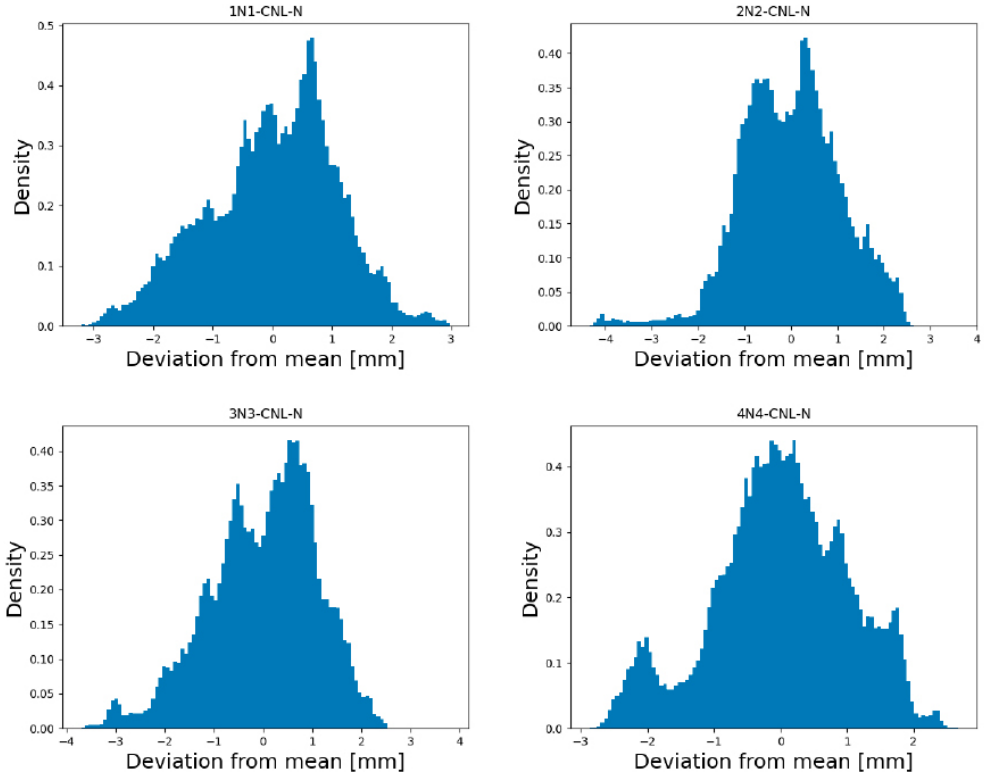

Figure B-4. Probability Density Functions for the N-Surfaces.

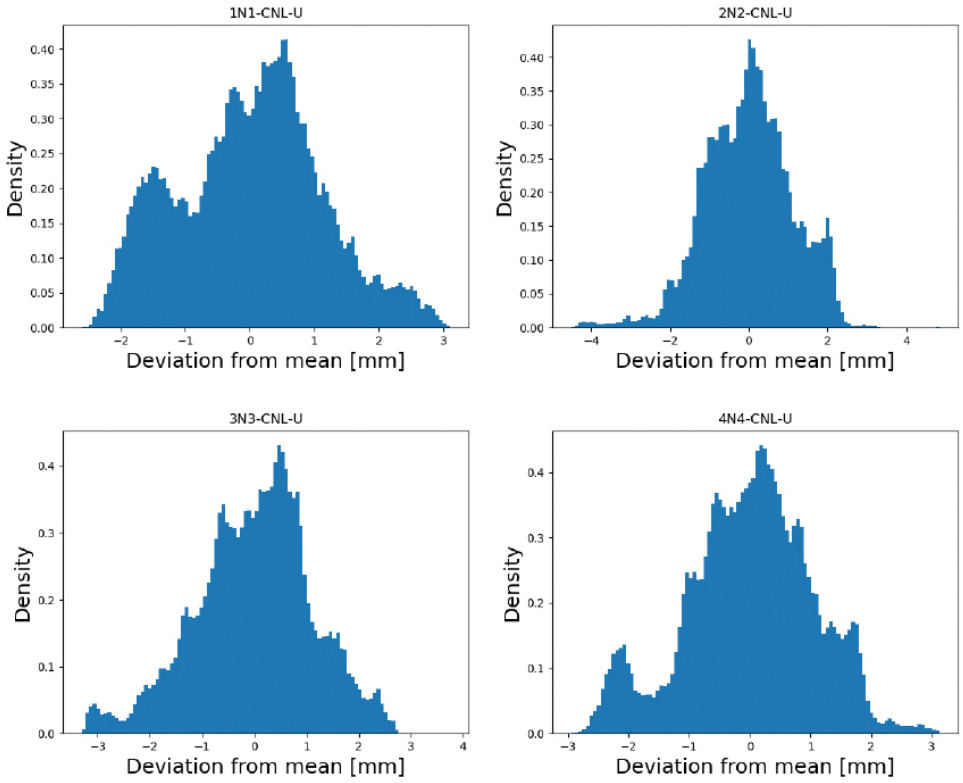

Figure B-5. *Probability Density Functions for the U-Surfaces.*

The first four moments, mean/variance, skewness/kurtosis, are presented in the Table B-1. Units refer to mm.

Table B-1. Geostatistical parameters.

Moment	1N1-N	1N1-U
Mean	5.37e+00	4.27e+00
Variance	1.15e+00	1.29e+00
Skewness	−2.69e−01	−1.10e−01
Kurtosis	−2.93e−01	−4.23e−01

Figure B-6 presents the autocorrelation functions for the surfaces. If one adopts the first zero crossing to be an indication of correlation length, then all samples (except 2N2) are sufficiently large to have multiple correlation lengths.

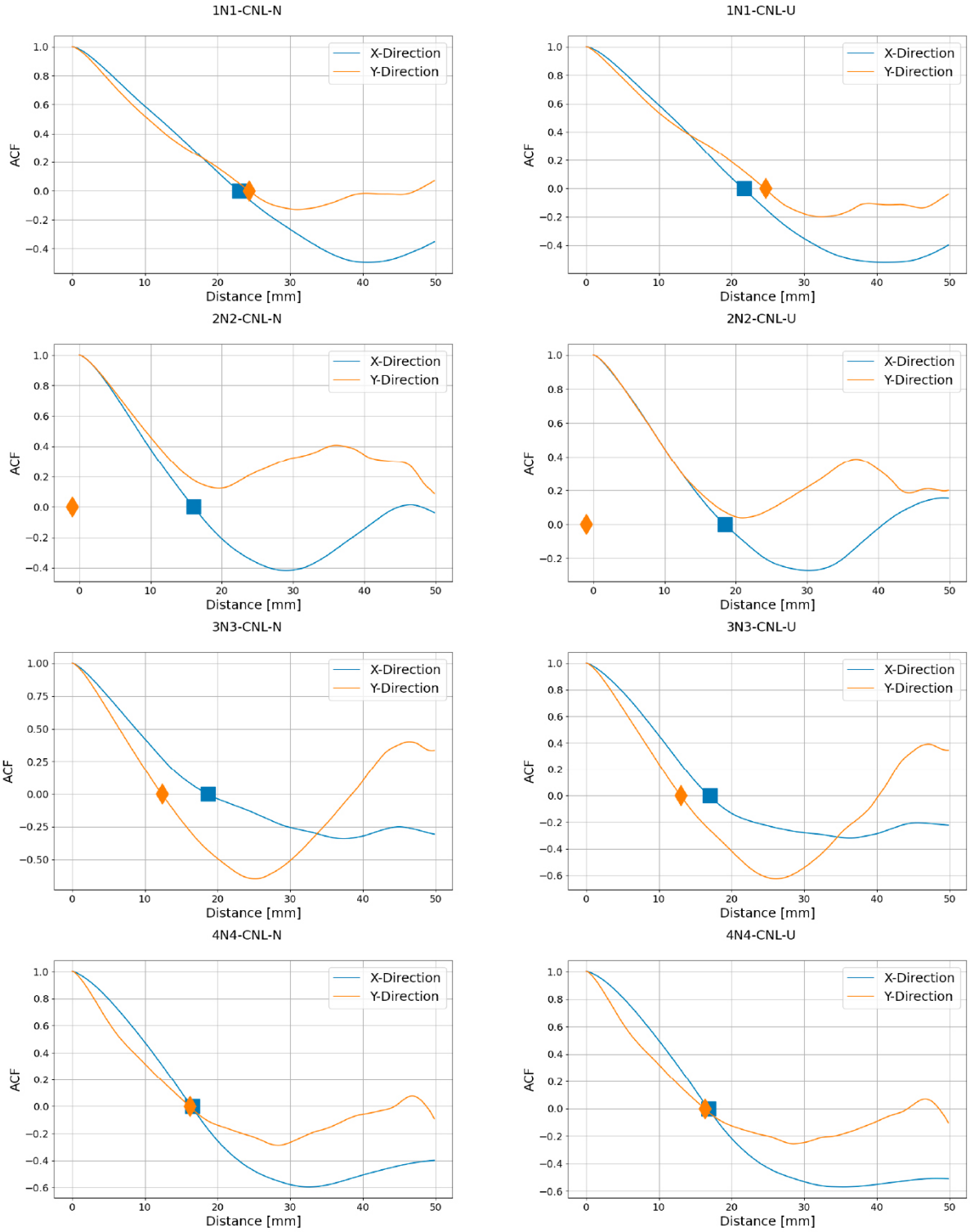

Figure B-6. *Autocorrelation functions for surface samples. The correlation length is assumed to be the first zero crossing of the function.*

Figure B-7 presents the semi-variogram functions for the surfaces. Along with the empirical data, a spherical variogram model is shown. In all cases (except 2N2), the variograms indicate that the surfaces are sufficiently large to have multiple correlation lengths.

Figures B-8 and B-9 show the curvature fields for the surfaces.

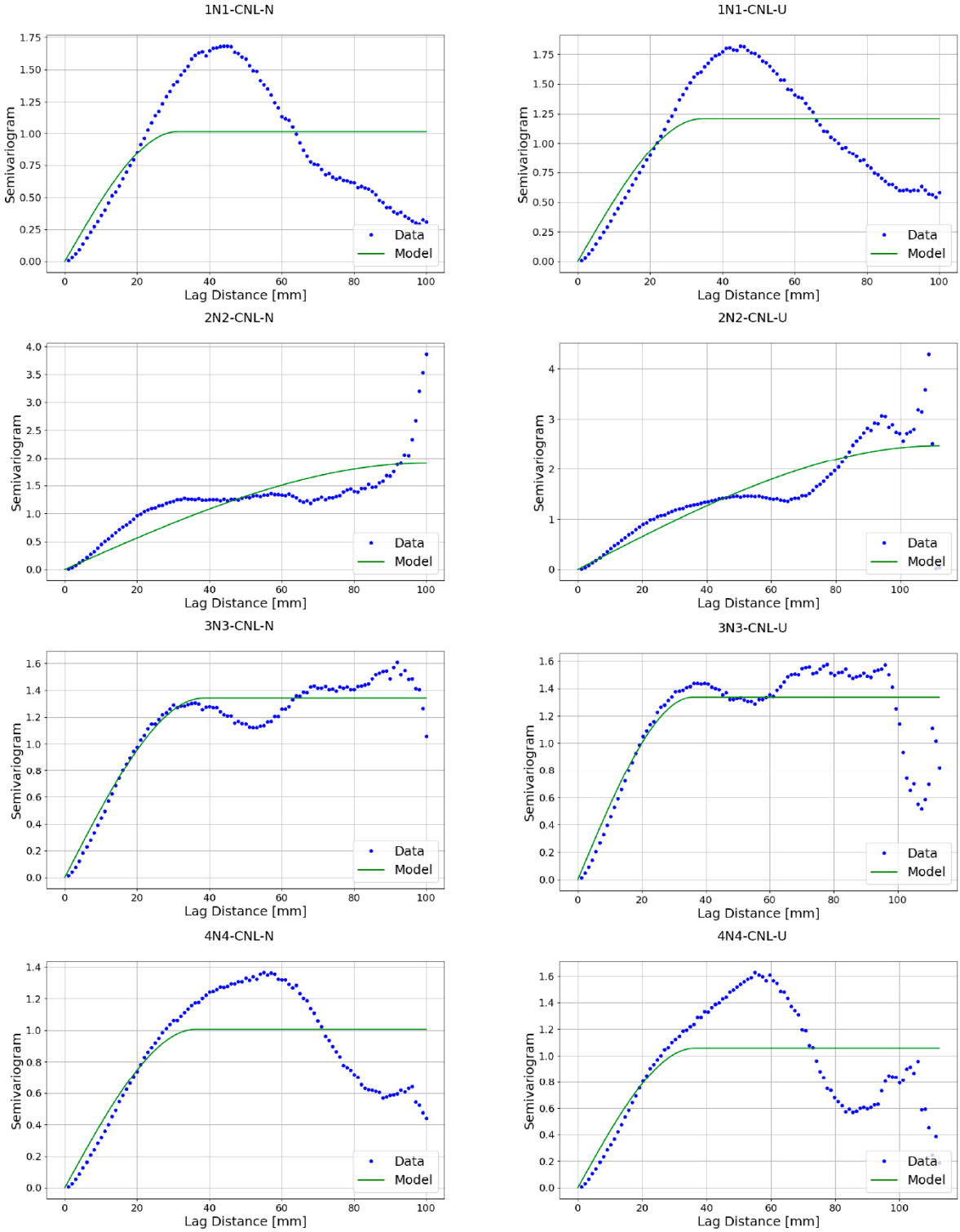

Figure B-7. *Semi-variograms for surfaces. The correlation length is assumed to the value where the semi-variogram is within 80 % of the sill.*

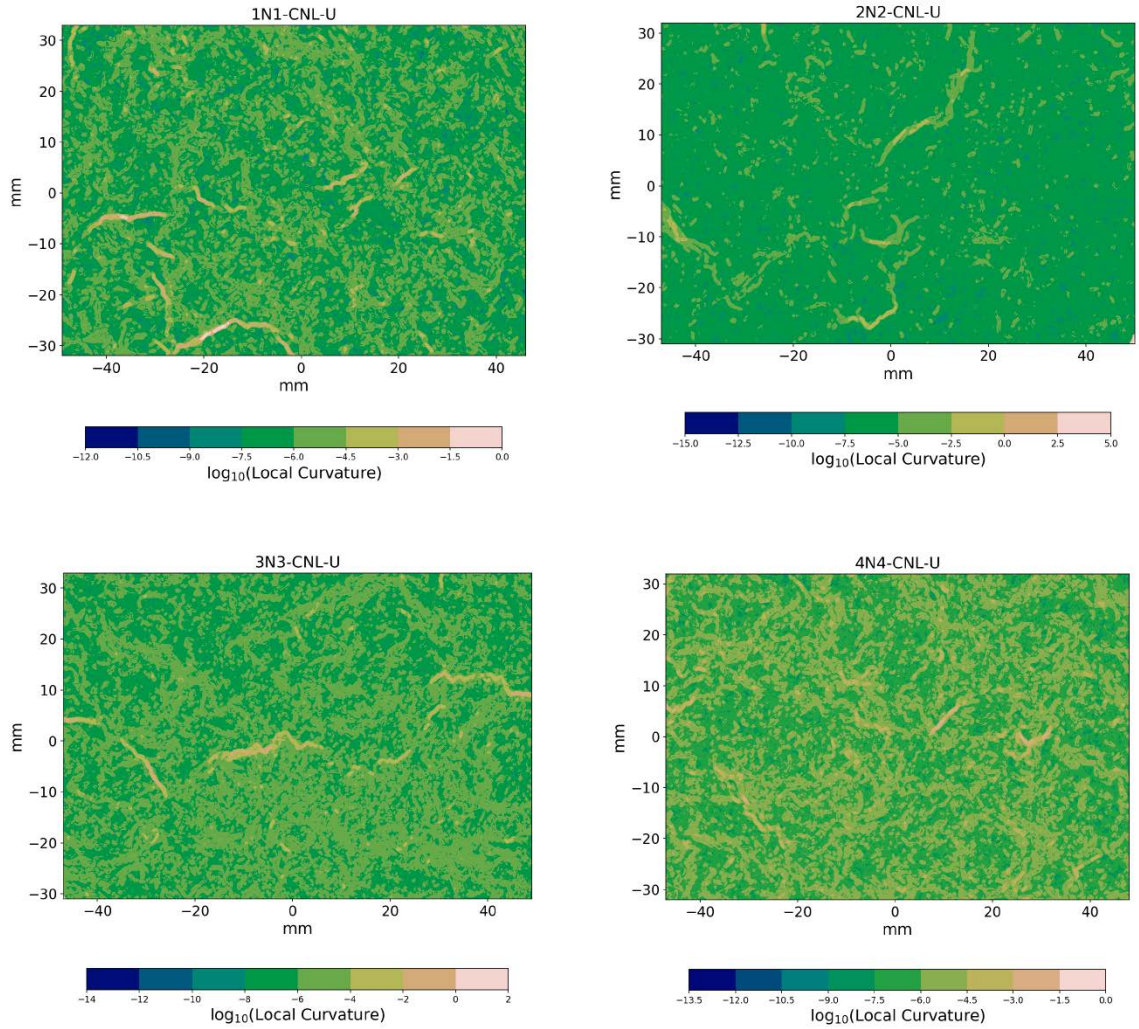

Figure B-8. *Curvature fields of the U surfaces.*

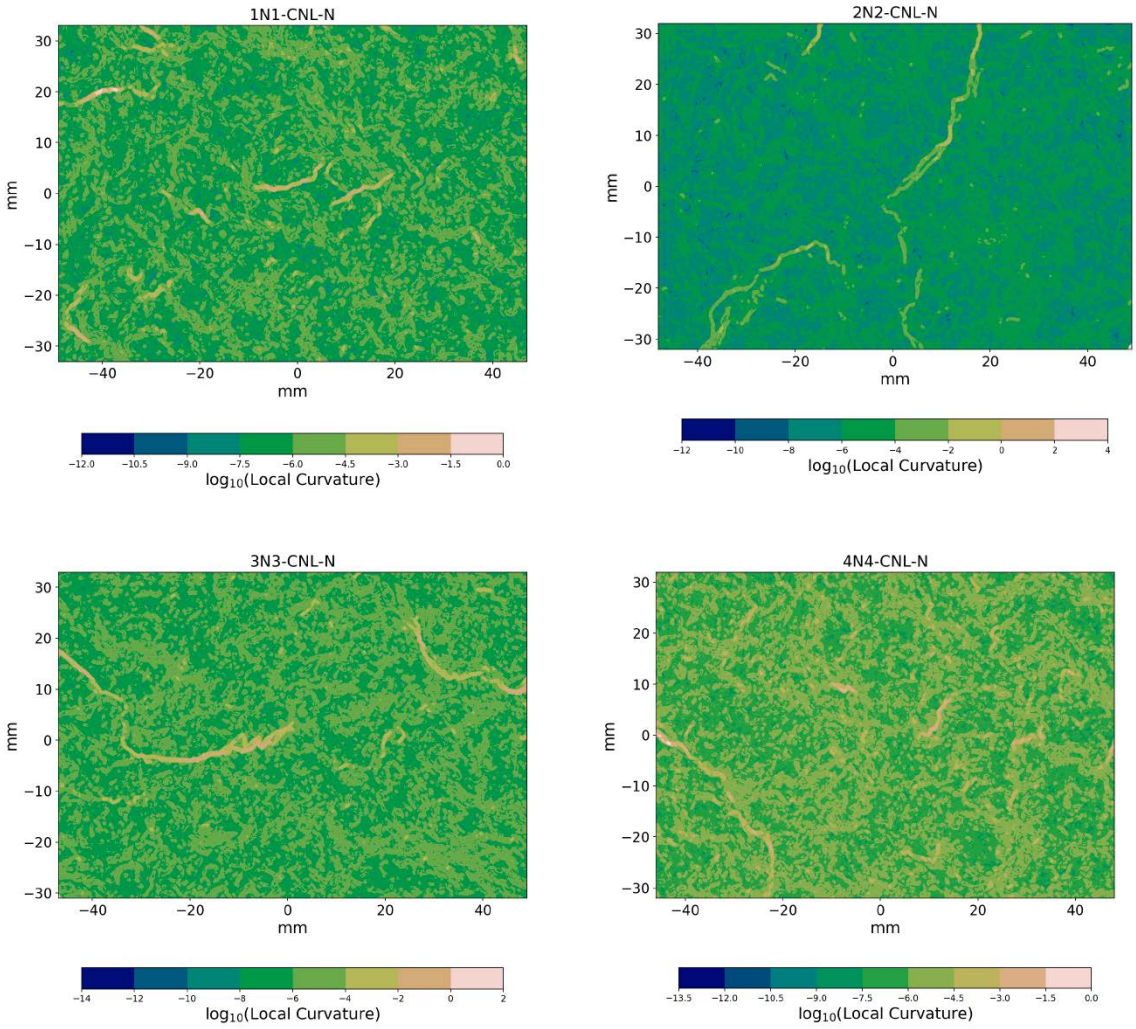

Figure B-9. *Curvature fields of the N surfaces.*

Table B-2 reports the square root of the mean curvature for the surfaces. Sample 2N2 has the highest values.

Table B-2. Curvature.

Sample Name	Square root of mean curvature
1N1-CNL-U	5.12e−02
1N1-CNL-N	4.87e−02
2N2-CNL-U	8.23e−02
2N2-CNL-N	6.95e−02
3N3-CNL-U	5.78e−02
3N3-CNL-N	6.18e−02
4N4-CNL-U	4.78e−02
4N4-CNL-N	5.02e−02

B6.3 Discussion, conclusions, and recommendations

Our modelling goal was the development of the workflow to characterize the scanned fracture surfaces, which was successful. The next steps in this model would be taking the observations obtained here and generating a synthetic fracture surface which matches the properties of the samples in a relative sense, i.e., generated moments within the variance of the observed moments. The exercise was useful in that it helped to create a toolbox fracture surface analysis. This work will be used to produce an open-source python module for the analysis and generation of rough fracture surfaces. All of the metrics and measurements considered here will be part of the toolbox. The data were appropriate to develop the workflow, but likely insufficient to characterize roughness in a manner that could be used to develop synthetic surfaces. For example, in sample 2N2, stabilization of the sample correlation length was not observed. Therefore, the sample ought not be considered in the formulation/informing of a synthetic sample as it does not contain an REV. So, there are only 3 samples which can be considered of satisfactory size to this end. In turn, the statistics of the averages are unreliable. A rule of thumb is 30 samples are required to get within 20 % error of the true mean, this result follows from the central limit theorem. Expanding the number of samples would drastically reduce the uncertainties of the quantities of interest. In turn, this small sample size is the primary cause of uncertainty in the construction of synthetic surfaces.

Appendix C

Modelling Group NTU (Taiwan) – Geometric Evaluation of Fracture Surfaces and Aperture Distributions Under Loading

Tai-Tien Wang, Po-Kai Chen, Chia-Hsiang Tu

National Taiwan University, Department of Civil Engineering, Taipei, Taiwan

C1 Introduction

Task 10 of the SKB Task Force on Modelling of Groundwater Flow and Transport of Solutes (TF GWFTS) is dedicated to building confidence in and "validating" models of flow and transport in fractured rock. The objective is to develop pragmatic approaches to model validation within the Task Force. In addition to Task 10.1 "White Paper", which sets out a possible development approach, Task 10.2 is the first of the Task 10 modelling tasks and focusses on the single fracture scale and channelling. Subsequent tasks will consider networks of fractures at larger scales.

National Taiwan University (abbreviated as NTU hereafter) participated in Task 10 as a modelling group since October 2022 (approximately one and half year later than other modelling groups). With the encouragement of other modelling groups participating in the 41st International Task Force GWFTS meeting held in Seoul, South Korea on April 18–20, 2023, the simulation work of Task 10.2.1 was started and this report was presented.

C1.1 Background

The participation of NTU as a modelling group is under the project entitled "Spent Nuclear Fuel Final Disposal Program: Technical Development Consulting and Parallel Verification of International Cases" supported by Taiwan Power Company (abbreviated as Tai-power hereafter). Major team members of NTU come from the Rock Mechanics Laboratory, Department of Civil Engineering RM/CE NTU. RM/CE NTU has studied characteristics of rock joints since 1990s.

C1.2 Objectives

Per the Task Description, the objectives of Task 10.2 include:

(1) Development of concepts and models for flow and transport at the single fracture scale;

(2) Consideration of the importance of hydro-mechanical coupling (normal loading only) on flow and transport;

(3) Development of modelling approaches for prediction of:

  (i) Flow and transport in single fractures;

  (ii) Upscaled fracture properties from borehole to deposition hole scale.

Task 10.2.1 is the first step in the road map for Task 10.2, focusing on geometric evaluation of fracture surfaces and aperture distribution on a borehole scale and predicting fracture surface topography and aperture distributions on meter scale. The main objectives of Task 10.2.1 are:

(1) Familiarise the modelling groups with the fracture surface datasets and provide the opportunity to develop appropriate tools and concepts.

(2) Develop methods for building a description of the fracture roughness and fracture void space (together with an assessment of relevant uncertainties) for the purpose of flow and transport simulations. This could be in terms of spatially varying aperture, effective aperture or channel dimensions according to the conceptual model.

(3) Investigate scaling of fracture surface properties from borehole to metre scale.

(4) Optionally start to consider the influence of fracture normal closure on this void space description, which will be a topic for Task 10.2.2.

C1.3 Scope and limitations

Geometric data scanned for four fractures are provided by the Task Force. Pre-processing of these data is carried out to incorporate a coordinate system to each fracture first. After that, quantitative evaluation of the roughness of these fractures in terms of joint roughness coefficient (JRC; Barton and Choubey, 1977), Root-mean-square (RMS) of profile slope, Z_2 (Yu and Vayssade, 1991) and Directional roughness metric, $\theta^*_{max}/(C+1)$ (Tatone and Grasselli, 2009) are assessed. Initial distribution of aperture for each fracture and related variation under loading are then calculated. Brief comments regarding this exercise are also given.

C2 Data description

The data to be used in this task is being gathered as part of the second phase of the POST project. The main objective of the POST project is to develop a strategy and guidelines for determining the parameters necessary for assessing fracture stability at the deposition tunnel scale for repository design and post-closure analysis used for the KBS-3 disposal concept.

Per the Task Description, the rock block used for the POST 2 project, which includes a natural fracture, is from the Flivik quarry in Oskarshamn municipality, Sweden. The quarry is located approximately 13 km north of the Äspö Hard Rock Laboratory (Figure C-1(a)). The sampled fracture is from a vertical natural fracture in a medium grained granite. The fracture includes an epidote infill/fracture coating. The vertical fracture is oriented in the "grain" direction and strikes approximately in the direction 040-220 (NE). The current major principal stress is approximately normal to the sampled natural fracture. Figure C-1(b) shows the original location of the samples in the quarry. Figure C-1(c) shows the 15.2-ton rock block that has been used for the POST 2 project. This large block, referred to as Block 15.2, has been cut to more practical dimensions and shipped to RISE's (Research Institutes of Sweden) laboratory in Borås. It is from this rock block that all POST 2 test samples on different scales are cut.

Block 15.2 has been subdivided into many different subsamples. Figure C-2(a) sketches the relation between the different subsamples of Block 15.2. Figure C-2(b) shows the relation of Subsamples 15.2.2.1 to 15.2.2.5 in 3D. A total of 24 samples of the fracture surfaces will be cut from Block 15.2 as part of the POST 2 project. These include:

(1) nine samples with dimension 100 × 70 mm,

(2) twelve samples with dimension 60 × 35 mm, and

(3) three samples with dimension 500 × 300 mm.

3D scans of both surfaces of a total of four samples on the 100 × 70 mm scale form the basis for this subtask (Figure C-3). These four samples have been cut from a slice of rock located behind Sample 15.2.2.5 as show in Figure C-2(a). The four samples (1N1–4N4) come from a set of five adjacent samples. There is an 8 mm gap between the samples, which corresponds to the thickness of the saw used. Unfortunately, the exact location and original orientation of each sample has not been recorded (see Figure C-4). All samples are from the same natural fracture, and larger surfaces can be reconstructed if the original locations of the samples in the fracture are known. Figure C-2(a) shows the approximate location of the different samples of interest in Task 10.2.1. The distributions on approximately a 1 m scale can be reconstructed when the scans of the 500 × 300 mm samples become available (Samples 15.2.2.2 to 15.2.2.4, see Figure C-2 (b) for location and relation to the smaller samples). It should be noted that the 100 × 70 mm samples are located at least 940 mm from the 500 × 300 mm samples.

The POST 2 project has shared with the Task Force the following data for Task 10.2.1:

(1) scanned 3D topography of the upper and lower fracture wall surfaces of four fractures samples, with dimensions 100 × 70 mm determined before shear testing;

(2) contact pressure measurement using pressure sensitive film; and

(3) necessary background information to understand the data.

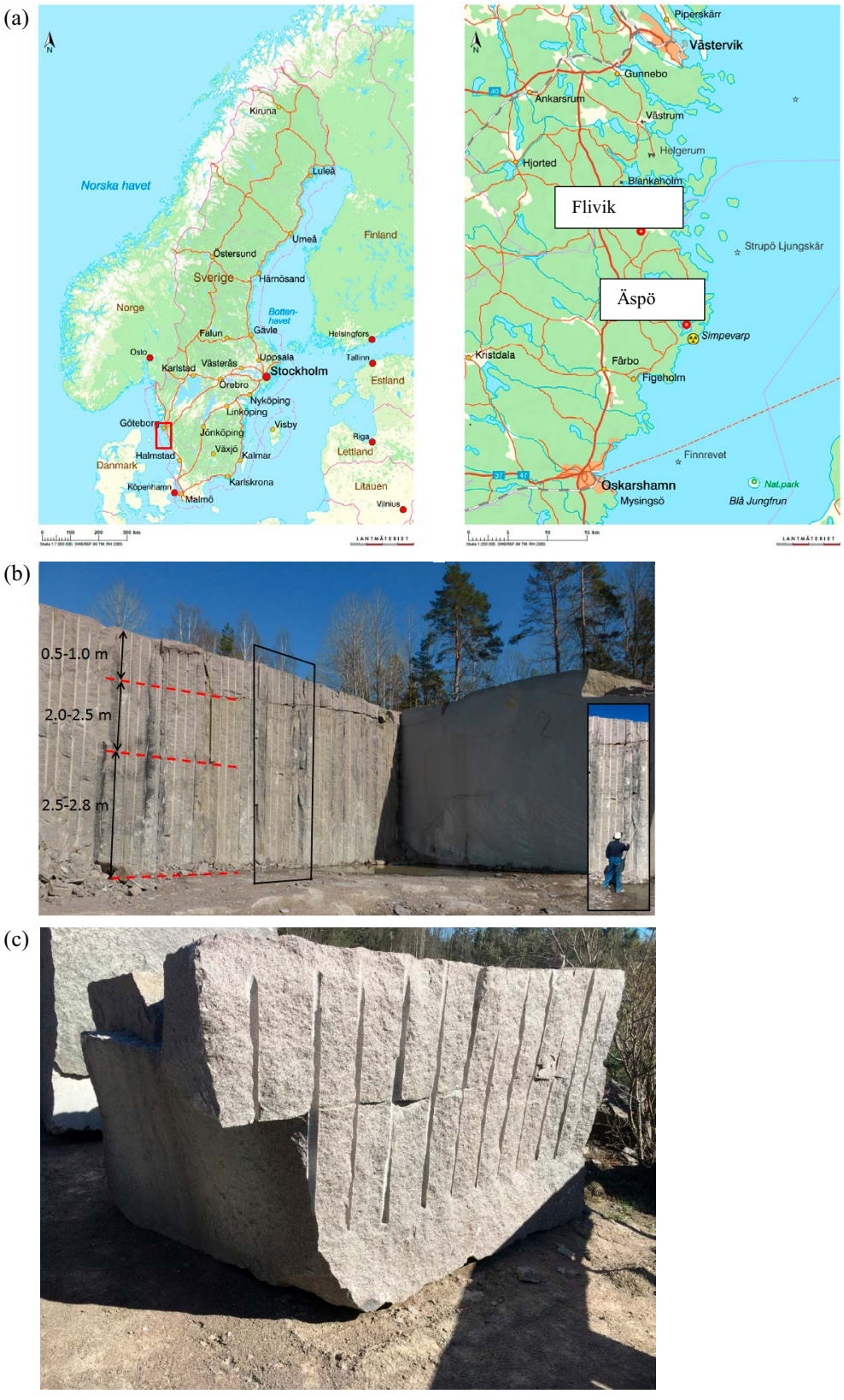

Figure C-1. *(a) Location of the Flivik quarry in relation to the Äspö Hard Rock Laboratory; (b) location of the extracted blocks. The red lines show horizontal exfoliation joints. The small picture insert shows the size of the wall. The vertical wall having drill holes and blasting surface is the hardway plane and the smooth wire cut surface is approximately along the grain plane; (c) the block with a mass of 15.2 tons used in the POST 2 experiments. The fracture indicated is horizontally oriented at the picture but was originally vertically oriented in the rock mass along the grain plane.*

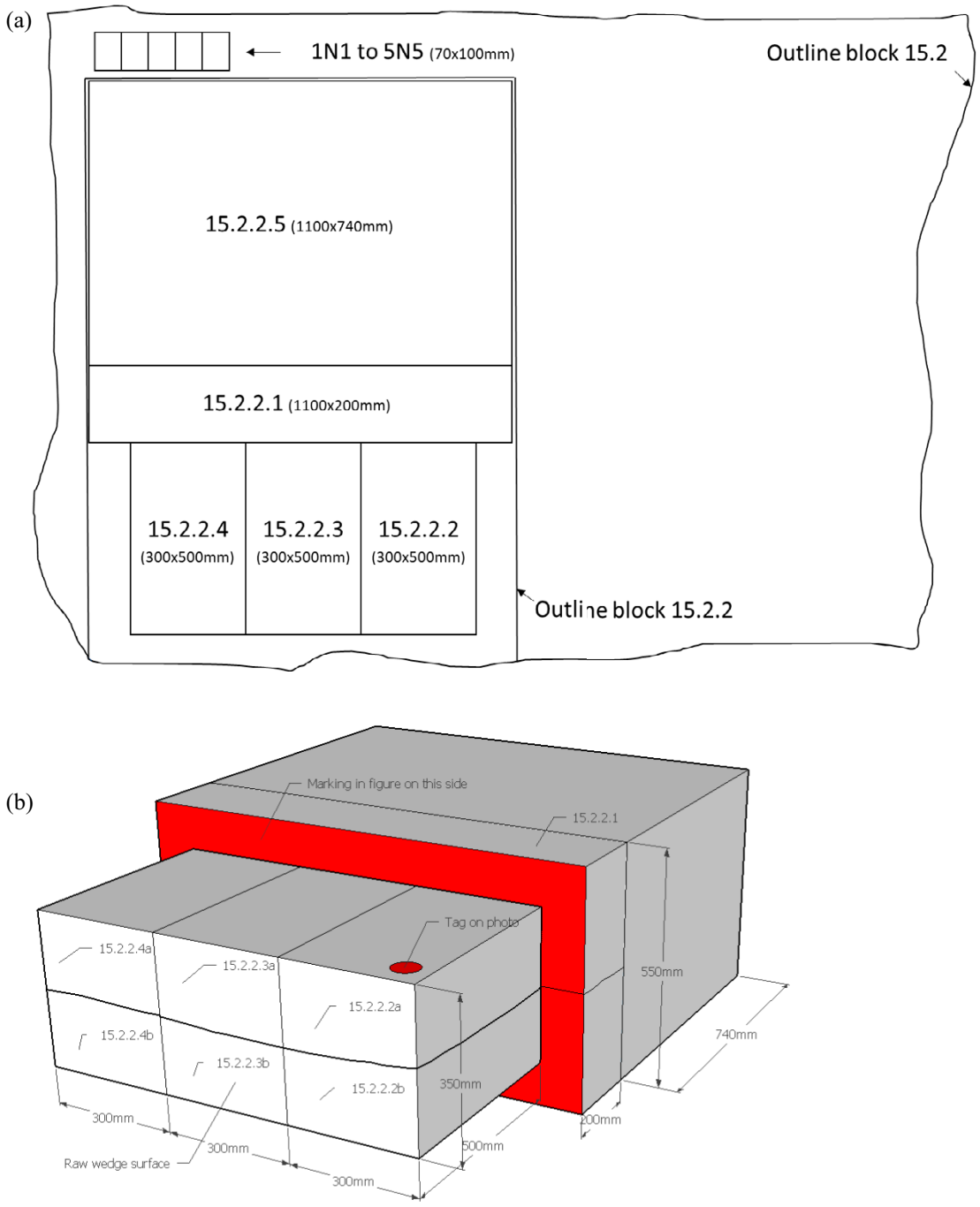

Figure C-2. *(a) Sketch of the fracture plane in block 15.2 showing the approximate location of the different subsamples. The four samples 1N1 to 4N4 are provided as known data representing the borehole scale. Samples 15.2.2.2 to 15.2.2.4 will be provided for verification purposes at a later stage, representing the deposition hole scale. (b)The relation between Samples 15.2.2.1 to 15.2.2.5 cut from Block 15.2.2.*

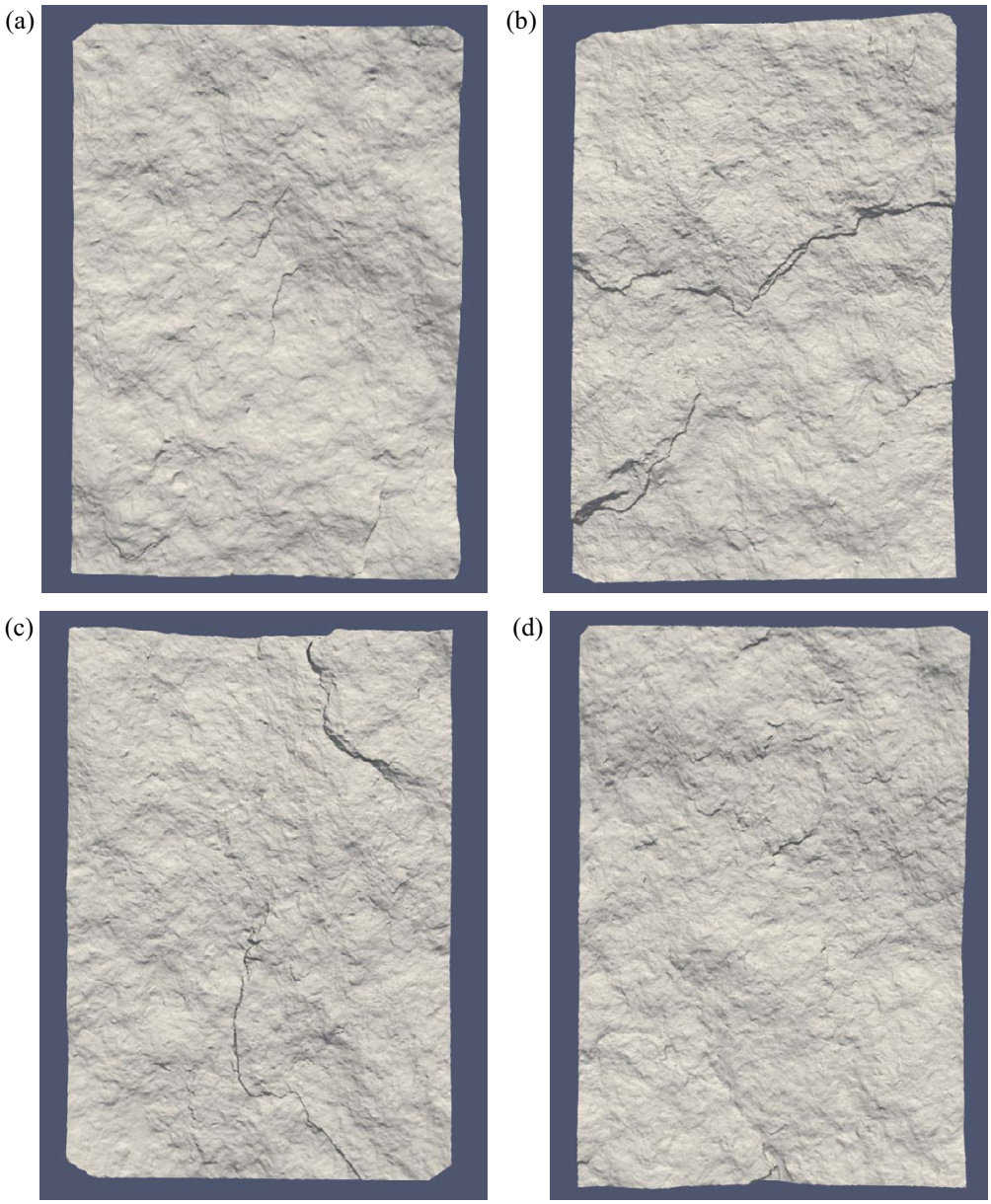

Figure C-3. *Crops of the 3D scans of the lower surfaces of samples a) 1N1-CNL, b) 2N2-CNL, c) 3N3-CNL, and d) 4N4-CNL before shear testing.*

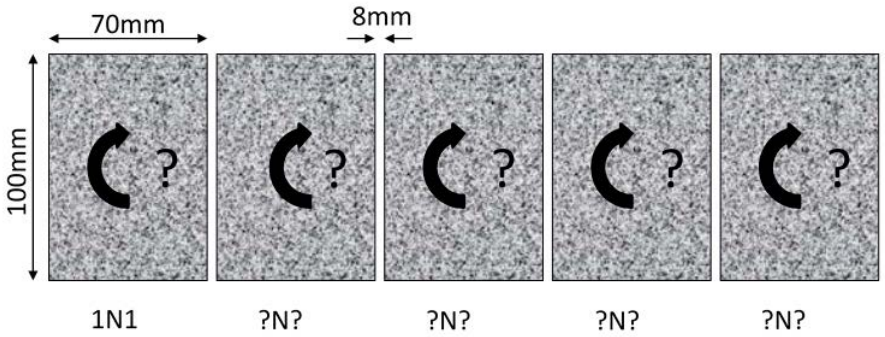

Figure C-4. *The five rock samples with dimensions 100×70 mm were located next to each other as indicated. The gap between the samples corresponds to the thickness of the saw (8 mm). Only the location of Sample 1N1-CNL is known for sure. The order of the other four samples has not been recorded. Furthermore, the orientation of the samples cannot be guaranteed, as samples could have been rotated by 180 degrees around normal of the shown fracture planes or flipped upside down.*

Table C-1 shows the sample name, file name and description of all eight fracture surfaces. The file type used is binary STL (https://en.wikipedia.org/wiki/STL_(file_format)). The STL file describes a set of triangles that constitute a surface and has been generated from the point cloud obtained using the 3D scanner. The unit used in the STL is mm.

The 3D scans have been obtained using a hand-held 3D scanner (Artec Space Spider) employing structured light technology (blue LED). The scanning process is shown in Figure C-5. The best achievable 3D resolution of this technology is 0.1 mm and the best 3D point accuracy is 0.05 mm. Processing of the scanned data has been performed using the Artec Studio software.

Measurement points have been stored approximately every 0.2 mm. Note that this will result in an irregular mesh when looking for instance on the XY coordinate plane. This also means that the nodes of the upper and lower surfaces do not coincide.

A number of uncertainties remain in the scanning of the surfaces and errors in the measurements of the spacer rings that are used for scanned specimen preparation cannot be excluded. The spacer rings used for surface scanning of various fractures have slightly different dimensions and it has not been recorded which spacer ring has been used for which sample. Per the Task Description, the standard deviation of spacer rings is 0.02 mm. Furthermore, the cement in the ring might have moved. For instance, the cement could have shrunk during hardening. Finally, the alignment/fitting of the scanned surfaces was done semi-manually. All of these uncertainties might influence the fit of the surfaces.

Contact pressure measurements have been carried out on the samples with pressure sensitive film. The Fujifilm Pressure Distribution Mapping System for Prescale (FPD-8010E) was used to measure and analyse the contact pressure distributions between the joint surfaces (https://www.fujifilm.com/products/measurement_film/en/prescale/product/). For all four samples a low pressure, two-sheet type film (PRESCALE LW PS) has been used, and an overall normal load of 5 MPa has been applied. The processed localised pressure distribution results are delivered as BMP files and shown in Figure C-6. The lower and upper measurement limits of the pressure film used are 2.5 MPa and 10.0 MPa, respectively. Areas with local pressures below 2.5 MPa are blue, areas with local pressures above 10.0 MPa are red. The different colours are difficult to discern on the figure, but the ten colours used can be extracted from the BMP files for each pixel. Areas where the pressure film has pressure less than 2.5 MPa are shown in blue and white.

Table C-1. 3D scanned fracture surface data files provided to modellers.

Sample name	File names	Description
1N1	1N1-CNL-N.stl	Lower surface of sample 1N1 scanned before shear test
	1N1-CNL-U.stl	Upper surface of sample 1N1 scanned before shear test
2N2	2N2-CNL-N.stl	Lower surface of sample 2N2 scanned before shear test
	2N2-CNL-U.stl	Upper surface of sample 2N2 scanned before shear test
3N3	3N3-CNL-N.stl	Lower surface of sample 3N3 scanned before shear test
	3N3-CNL-U.stl	Upper surface of sample 3N3 scanned before shear test
4N4	4N4-CNL-N.stl	Lower surface of sample 4N4 scanned before shear test
	4N4-CNL-U.stl	Upper surface of sample 4N4 scanned before shear test

Figure C-5. *Scanning a joint surface (not cast in formwork) using a hand-held scanner.*

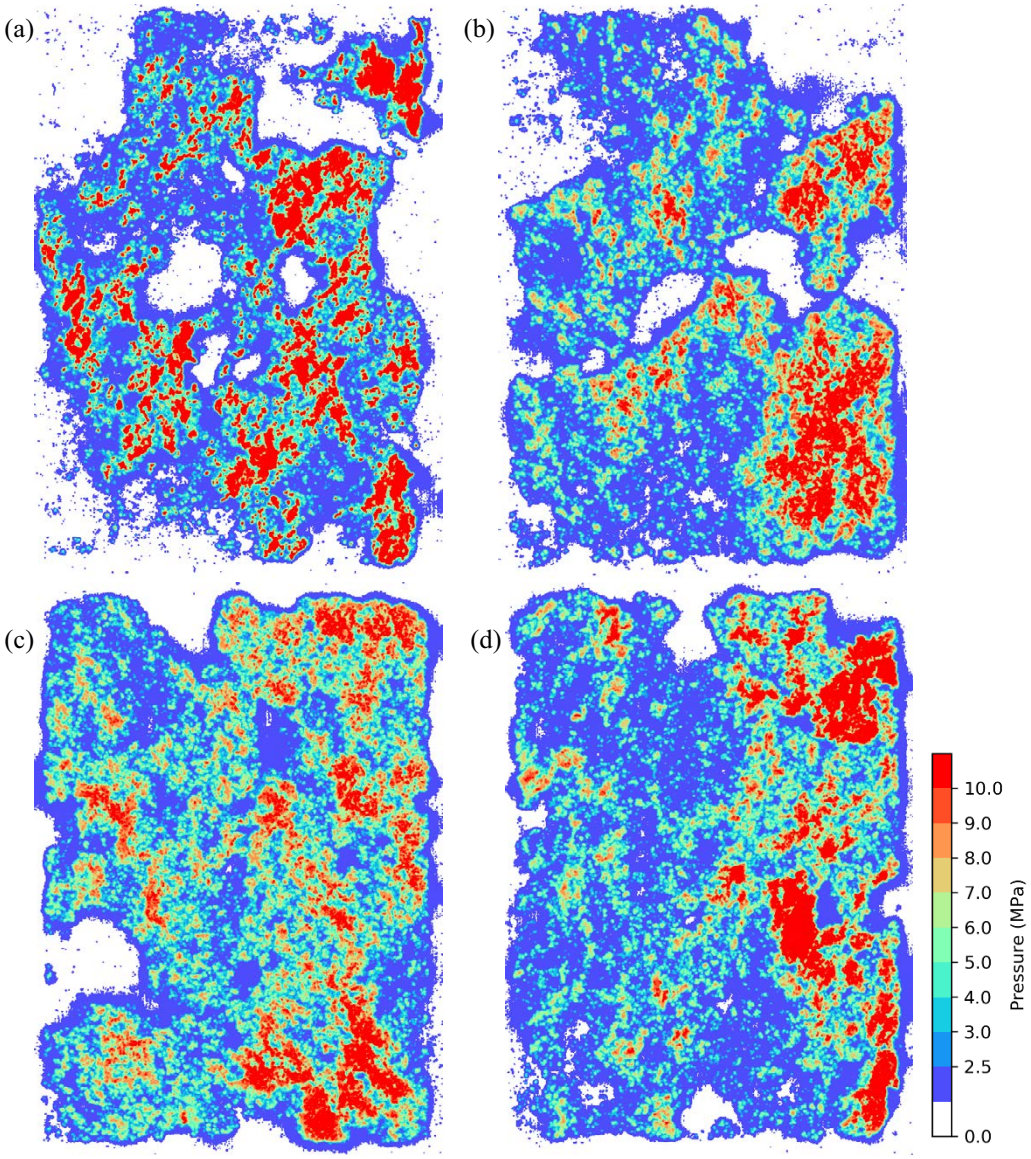

Figure C-6. *Pressure film measurements showing local pressures in MPa for the fracture samples (a) 1N1-CNL, (b) 2N2-CNL, (c) 3N3-CNL, and (d) 4N4-CNL. Note that the colour schemes of the provided bmp files have been changed to better distinguish the different pressure levels.*

C3 Methodology and data pre-processing

C3.1 Workflow and methodology

Before calculating roughness indices and aperture distributions, a local coordinate system is assigned to the upper and lower surfaces for each fracture to better describe the modelling task and related results. The Cartesian coordinate has its origin on the centre of the fracture surface with the *X*-axis along the short side (70 mm) and the *Y*-axis along the long side (100 mm). The geometric data show a curved boundary for each fracture surface (Figure C-3); therefore, some points are trimmed to obtain straight boundaries to facilitate the subsequent usage of the iterative closest point (ICP) algorithm (Wan et al., 2019). The ICP algorithm is applied to obtain a spatial scenario that the upper and lower surfaces of a fracture have minimum aperture with limited overlap of the surfaces.

The roughness indices (JRC, Z2 and $\theta^*_{max}/(C+1)$) describe two-dimensional characteristics of a fracture surface. As such, a referenced coordinate is needed to indicate the locations for the evaluation of these two-dimensional profiles. A local Cartesian coordinate system is assigned to obtain minimum average aperture, defining the data locations used to calculate these indices. In addition, the calculation of these roughness indices follows the suggestion of the literature that introduced these indices.

The spatial aperture distribution is then modelled using corresponding upper and lower surface data. The distance at a specific point between these two surfaces represents the corresponding aperture. The initial aperture is determined using the 1 % contact area criterion suggested by Li et al. (2008). Then the spatial aperture distribution is demonstrated graphically, with corresponding mean, standard deviation, as well as maximum and minimum values.

The aperture change under loading is then modelled using a conceptual contact model which assumes that the aperture at a particular location is constant within the area around each point, i.e., the *Z* value of the area that is half spaced between the could of points in both *X*- and *Y*-axis direction. The aperture will change suddenly if the adjacent location has different magnitude, i.e., the spatial distribution of aperture is discontinuous. Furthermore, the force equilibrium under various normal loading magnitudes is applied to determine the aperture change using the mechanical parameters of the granite.

The statistical theory is then conducted to estimate the roughness indices of a 1-m scale surface (i.e., the 100 × 70 mm fractures) based on the indices mentioned above.

Data pre-processing is introduced in the following subsection, and the modelling results and associated methodology will be explained in the next chapter.

C3.2 Pre-processing of geometric data

Although the geometric data were scanned from the upper and lower surfaces of a fracture, the two surfaces are not matched perfectly, i.e., the aperture change everywhere and the boundaries cannot match each other perfectly. The pre-processing of geometric data aims to select a specific area from both the upper and lower surface of the four fractures to facilitate the subsequent modelling.

First, the point cloud describing the geometric characteristics of the upper and lower surface of each fracture is trimmed to have a rectangular shape (approximately 70 × 100 mm^2). Then the ICP algorithm is applied to determine the best match location of these two surfaces. The point cloud describing the lower surface is selected as the source set **Q**, and the upper surface the target set **P**; these two sets form a correspondence set $\boldsymbol{K} = \{(\boldsymbol{P},\boldsymbol{Q})\}$. **Q** can be transformed to offset horizontally and rotate vertically (not calculated here) using a transformation matrix **T**. The transformation matrix **T** is iteratively updated to obtain the least square function $E(\mathbf{T})$

$$E(\mathbf{T}) = \sum_{(\mathrm{P},\mathrm{Q})\in \mathrm{K}} \|\mathbf{P} - \mathbf{TQ}\|^2$$

$E(\mathbf{T}) \geq 0$. The transformation matrix **T** that minimizes $E(\mathbf{T})$ presents the best match condition of the upper and lower surfaces of the corresponding fracture. After that, a local Cartesian coordinate system is assigned with the *X*-axis along the short side (70 mm) and the *Y*-axis along the long side (100 mm for the use of the subsequent modelling task).

C4 Modelling results

C4.1 Roughness indices

Figure C-7 shows the 2D profiles along the *X*- and *Y*-axis of the scanned upper and lower surface of Fracture 1N1. Using visual inspection with the reference of the so-called standard profile suggested by Barton and Choubey (1977), the joint roughness coefficients (JRCs) of these profiles parallel to the *Y*-axis are estimated to be between 7 and 14, with an average of 10.00/10.20 (upper/lower surface) and standard deviation of 2.79/2.53, and *X*-axis parallel profiles between 6 and 10, with an average of 7.57/7.57 and standard deviation of 1.59/1.59. Notably, the long profile has a length of approximate 100 mm and can be compared with the standard profile directly. The short profiles are moved to fit a certain section with a length of approximate 70 mm in the standard profile for the estimation. Table C-2 lists the results of JRC estimation of Fractures 1N1, 2N2, 3N3 and 4N4.

Table C-2. Summary of JRC estimation for fracture 1N1 to 4N4.

(a) *Y*-axis parallel profiles

Fracture	Surface	*Y*-axis parallel profiles				
		x = −30 mm	x = −15 mm	x = 0.0 mm	x = 15 mm	x = 30 mm
1N1	Upper	7	7	12	11	14
	Lower	7	7	11	12	13
2N2	Upper	11	13	7	7	16
	Lower	15	13	7	7	16
3N3	Upper	6	10	12	9	8
	Lower	6	10	12	10	7
4N4	Upper	11	7	11	10	11
	Lower	11	7	11	10	11

(b) *X*-axis parallel profiles

Fracture	Surface	*X*-axis parallel profiles						
		y = −45 mm	y = −30 mm	y = −15 mm	y = 0.0 mm	y = 15 mm	y = 30 mm	y = 45 mm
1N1	Upper	7	7	7	10	10	6	6
	Lower	6	7	7	10	10	7	6
2N2	Upper	13	8	8	8	9	5	9
	Lower	9	8	7	7	8	5	9
3N3	Upper	12	8	8	8	9	9	14
	Lower	11	8	8	8	9	8	14
4N4	Upper	11	7	12	11	6	7	8
	Lower	12	7	12	11	6	7	8

(c) Mean and standard deviation of JRC

Fracture	Surface	*Y*-axis parallel profiles		*X*-axis parallel profiles	
		Mean	Stdev	Mean	Stdev
1N1	Upper	10.20	2.7857	7.57	1.5908
	Lower	10.00	2.5298	7.57	1.5908
2N2	Upper	10.80	3.4871	8.57	2.1946
	Lower	11.60	3.8781	7.57	1.2936
3N3	Upper	9.00	2.0000	9.71	2.1853
	Lower	9.00	2.1909	9.43	2.1285
4N4	Upper	10.00	1.5492	8.86	2.2315
	Lower	10.00	1.5492	9.00	2.3905

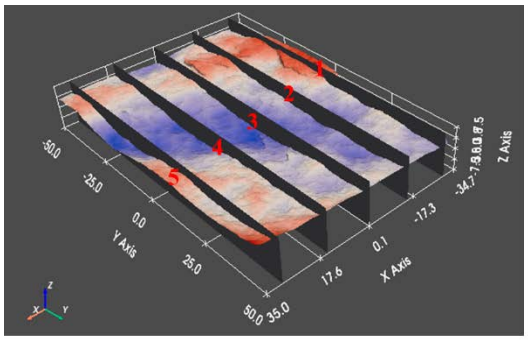

1N1 upper y-axis parallel profiles

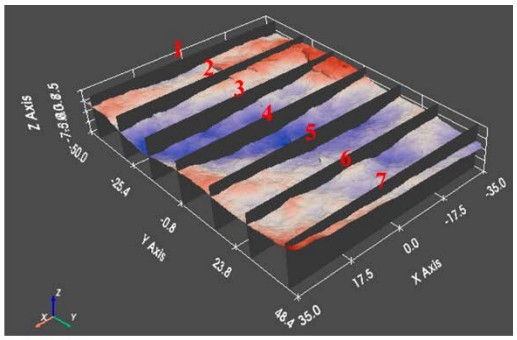

1N1 upper x-axis parallel profiles

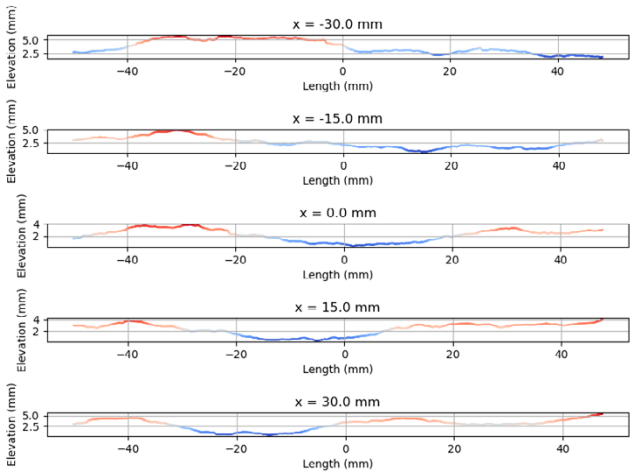

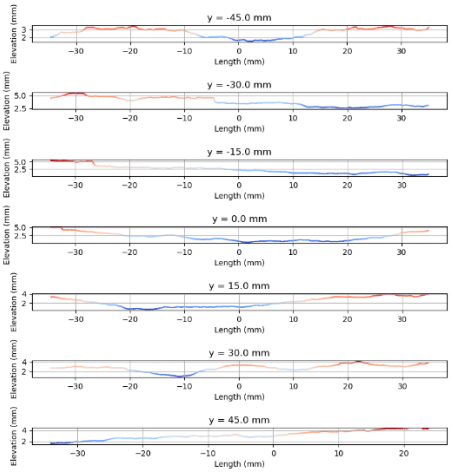

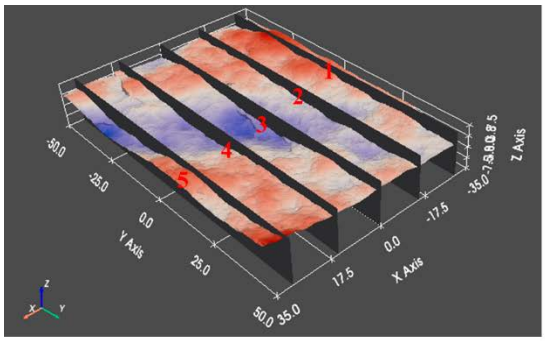

1N1 lower y-axis parallel profiles

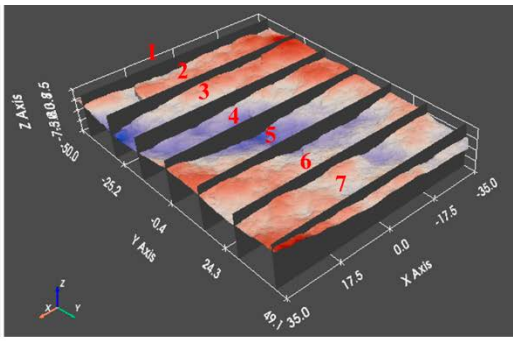

1N1 lower x-axis parallel profiles

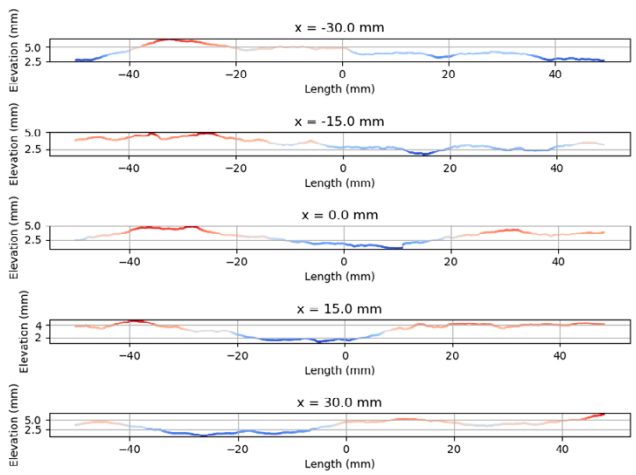

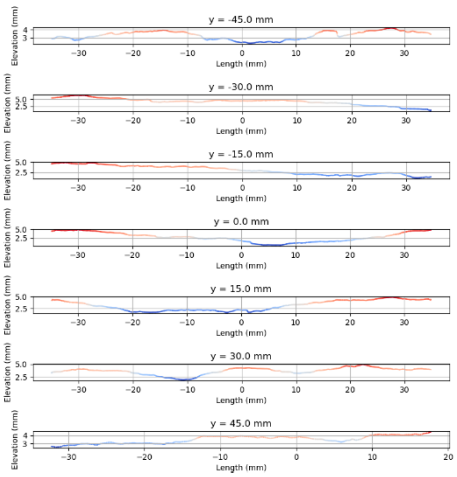

Figure C-7. *2D profiles along x- and y-axis of scanned upper and lower surface of fracture.*

The RMS of profile slope, Z_2 (Yu and Vayssade, 1991), is also calculated using a distance *dx* of 0.05 mm. The Z_2s of the *X*- and *Y*-axis of the upper surface of Fracture 1N1 are, respectively, 0.2465 and 0.2391, with related standard deviations of 0.0630 and 0.0159. Using the JRC-Z_2 relationship equation suggested by Yu and Vayssade (1991), the JRCs are 11.76 and 11.30, respectively. For the lower surface of Fracture 1N1, the Z_2s are 0.2335 (JRC = 10.96) and 0.2236 (JRC = 10.35), with related standard deviations of 0.0290 and 0.0209. Table C-3 lists the Z_2s of fractures 1N1 to 4N4.

Table C-3. Summary of calculated Z_2 for fracture 1N1 to 4N4.

(a) *Y*-axis parallel profiles

Fracture	Surface	*Y*-axis parallel profiles				
		x = −30 mm	x = −15 mm	x = 0.0 mm	x = 15 mm	x = 30 mm
1N1	Upper	0.2646	0.2253	0.2268	0.2277	0.2509
	Lower	0.2066	0.2089	0.2614	0.2097	0.2314
2N2	Upper	0.2063	0.2545	0.2097	0.2548	0.3267
	Lower	0.3571	0.3099	0.2568	0.2917	0.6035
3N3	Upper	0.2301	0.2976	0.3008	0.2388	0.2063
	Lower	0.2457	0.2258	0.4048	0.2866	0.2051
4N4	Upper	0.2518	0.2423	0.2918	0.2336	0.2361
	Lower	0.2331	0.2179	1.8213	0.2329	0.2304

(b) *X*-axis parallel profiles

Fracture	Surface	*X*-axis parallel profiles						
		y = −45 mm	y = −30 mm	y = −15 mm	y = 0.0 mm	y = 15 mm	y = 30 mm	y = 45 mm
1N1	Upper	0.2195	0.2712	0.3706	0.2795	0.1996	0.2237	0.1617
	Lower	0.2374	0.2638	0.198	0.2544	0.2561	0.2431	0.1819
2N2	Upper	0.2794	0.2435	0.2698	1.008	0.2518	0.2067	0.2626
	Lower	0.2028	0.347	0.5651	0.2546	0.915	0.2501	0.2595
3N3	Upper	0.4942	0.2449	0.2913	0.2871	0.2659	0.3138	0.6495
	Lower	0.3609	0.2421	0.7001	0.2825	0.2446	0.3148	0.6962
4N4	Upper	0.2911	0.2373	0.2735	0.2033	0.2113	0.2462	0.2077
	Lower	0.3411	0.2498	0.2336	0.2575	0.2079	0.2896	0.2454

(c) Mean and standard deviation of Z_2

Fracture	Surface	Y-axis parallel profiles		X-axis parallel profiles	
		Mean	Stdev	Mean	Stdev
1N1	Upper	0.2391	0.0159	0.2465	0.0630
	Lower	0.2236	0.0209	0.2335	0.0290
2N2	Upper	0.2504	0.0435	0.3603	0.2653
	Lower	0.3638	0.1241	0.3992	0.2383
3N3	Upper	0.2547	0.0379	0.3638	0.1394
	Lower	0.2736	0.0709	0.4059	0.1887
4N4	Upper	0.2511	0.0213	0.2386	0.0316
	Lower	0.5471	0.6371	0.2607	0.0400

The directional roughness metrics, $\theta^*_{max}/(C+1)$ (Tatone and Grasselli, 2009) are also evaluated. We follow the suggestion of Tatone and Grasselli (2009) to involving the A_0 (normalized area of the surface corresponding to an angular threshold of 0° in the chosen analysis direction. Figure C-8 shows the polar plots of $2A_0\ \theta^*_{max}/(C+1)$ for these four fractures. Table C-4 lists the calculated results of $2A_0\ \theta^*_{max}/(C+1)$ for these four fractures.

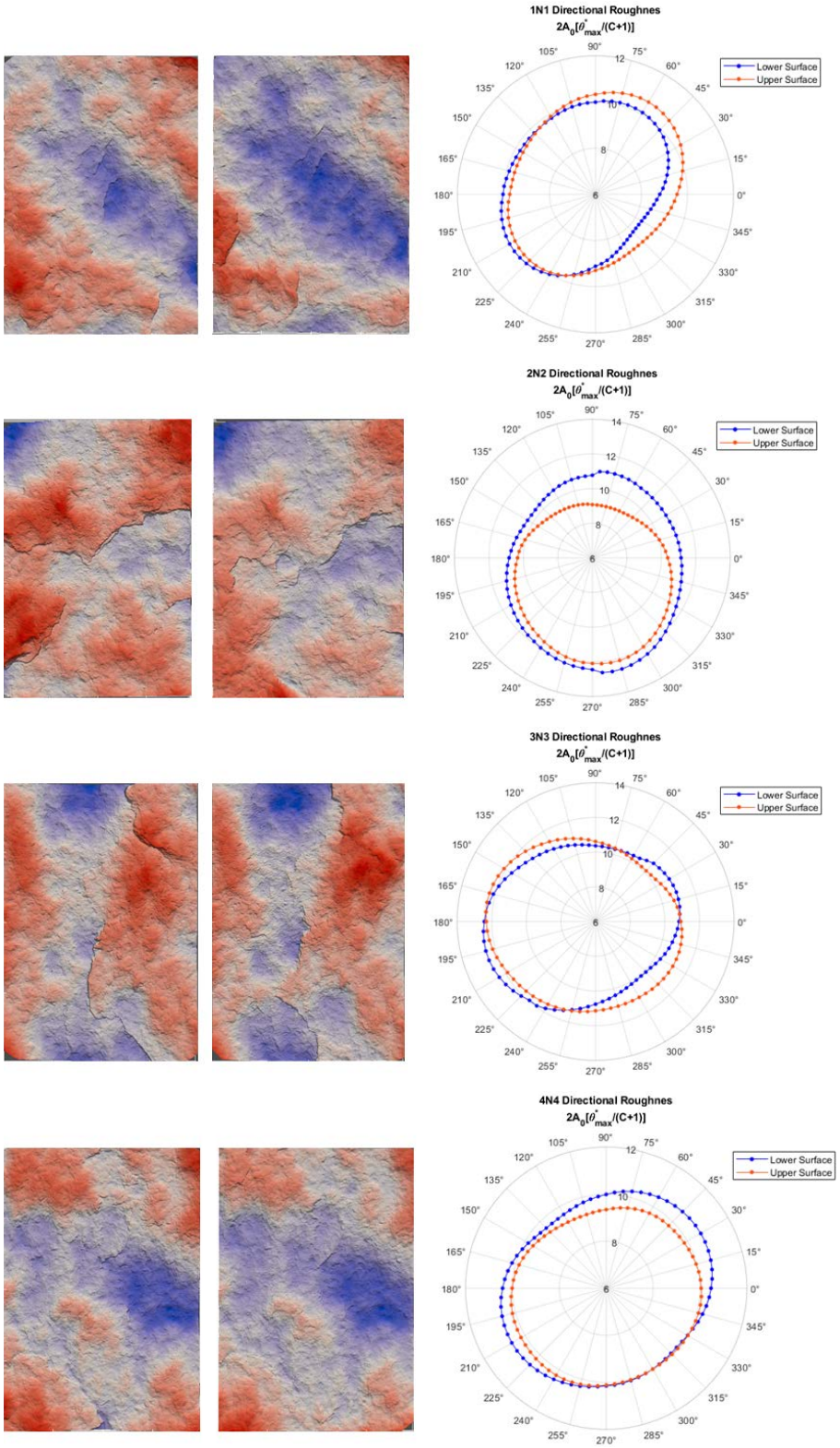

Figure C-8. *Polar plots of calculated* $2A_0\ \theta^*_{max}/(C+1)$ *for fracture 1N1 to 4N4.*

Table C-4. Summary of calculated $2A_0\ \theta^*_{max}/(C+1)$ for fracture 1N1 to 4N4.

Fracture	Surface	$2A_0\ \theta^*_{max}/(C+1)$			Anisotropy
		Max.	min.	Ave.	
1N1	Upper	10.613	8.893	9.772	1.19
	Lower	10.303	8.290	9.534	1.24
2N2	Upper	12.140	9.059	10.432	1.34
	Lower	12.662	10.310	11.296	1.23
3N3	Upper	12.365	10.128	11.214	1.22
	Lower	12.557	10.091	11.067	1.24
4N4	Upper	10.268	9.231	9.866	1.11
	Lower	10.657	9.593	10.227	1.11

C4.2 Spatial distribution of aperture

The pre-processing of geometric data yields two trimmed upper and lower surfaces with straight boundaries for each fracture. However, relative horizontal offsets or even rotation may exist between these two surfaces after their separation. The relative original locations of these two surfaces are unknown, and the void space (i.e., aperture) between these two surfaces can be arbitrary due to free movement along the normal direction of the surface. As such, the ratio of contact area is adopted as a criterion for determining a representative spatial aperture distribution. The 1 % ratio suggested by Li et al. (2008) is referred here.

The K-D tree (k-dimensional tree) method is used to determine the particular condition when the upper and the lower surface have the closest Euclidean distance. The Cartesian coordinate is redefined using this particular condition. The upper surface is gradually moved toward the lower surface, while the spatial aperture distribution is calculated with mean aperture and contact area updated. The representative spatial distribution of the aperture is determined when the contact area of the upper and lower surface is 1 % of the area of these two surfaces, and the mean value and standard deviation of the aperture distribution are obtained, associated with the median and maximum of the aperture. Notably, the contact area has negative aperture using this calculation scheme, and these negative apertures are neglected during the calculation of the mean, standard deviation and median of the aperture.

Figure C-9 shows the initial spatial distribution of each aperture with 1 % contact area ratio in 3D and 2D viewpoint. Figure C-10 shows the histogram of apertures. The apertures of Fractures 1N1 to 4N4 are all lognormally distributed. The aperture of Fracture 1N1 has a mean and standard deviation of 0.3043 and 0.4543 mm, respectively, associated with median 0.1147 and maximum aperture 3.7235 mm. Obviously, most apertures are generally smaller than their mean value, indicating that some area has relatively large apertures.

Table C-5 below summarizes the average apertures and the other statistical parameters for these four fractures. Fracture 2N2 has the largest mean aperture (0.4145 mm), and Fracture 4N4 the smallest (0.1572). The ratio of the mean apertures is 0.4145/0.1572 = 3.5825. The standard deviation of the apertures is always larger than their mean value for each fracture, revealing that the spatial aperture distributions of these fractures are highly heterogeneous.

(a)

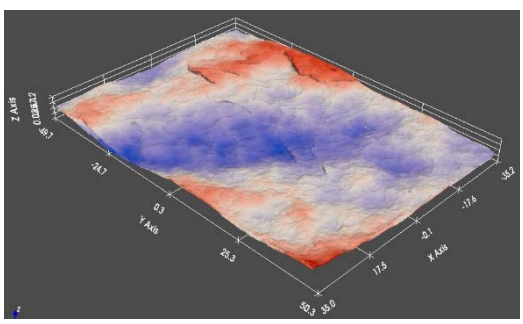

1N1 Fracture Surface

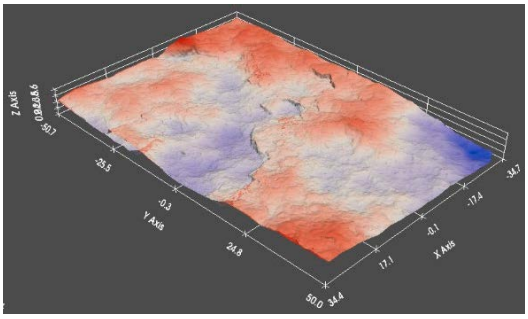

2N2 Fracture Surface

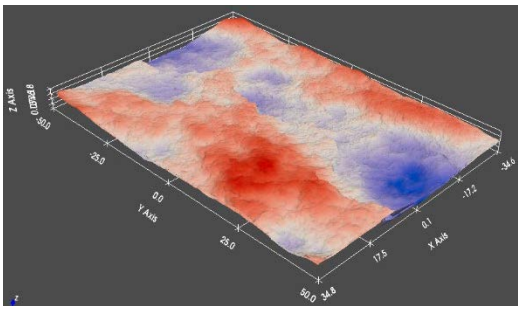

3N3 Fracture Surface

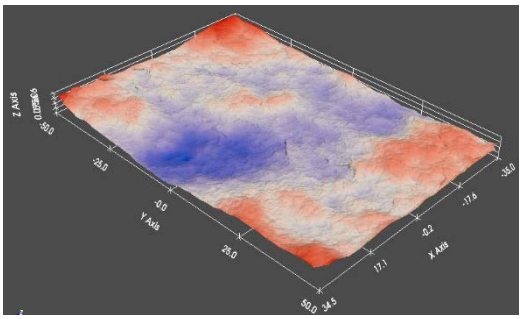

4N4 Fracture Surface

(b)

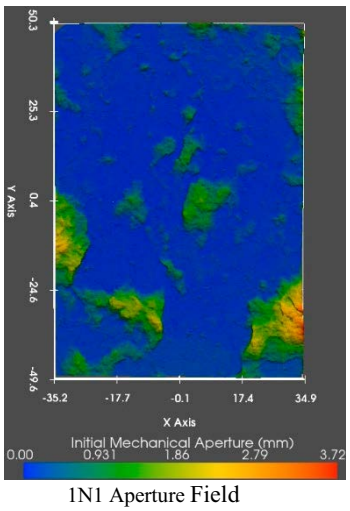

1N1 Aperture Field

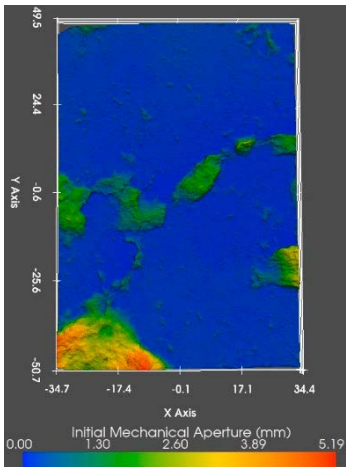

2N2 Aperture Field

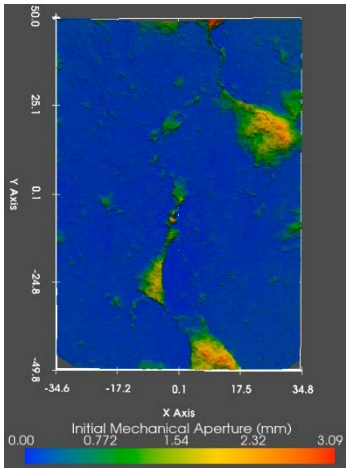

3N3 Aperture Field

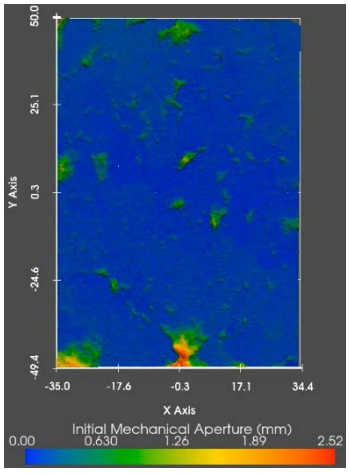

4N4 Aperture Field

Figure C-9. *Initial spatial distribution of each aperture with 1 % contact area ratio for fractures 1N1 to 4N4 in 3D (a) and 2D (b) viewpoint.*

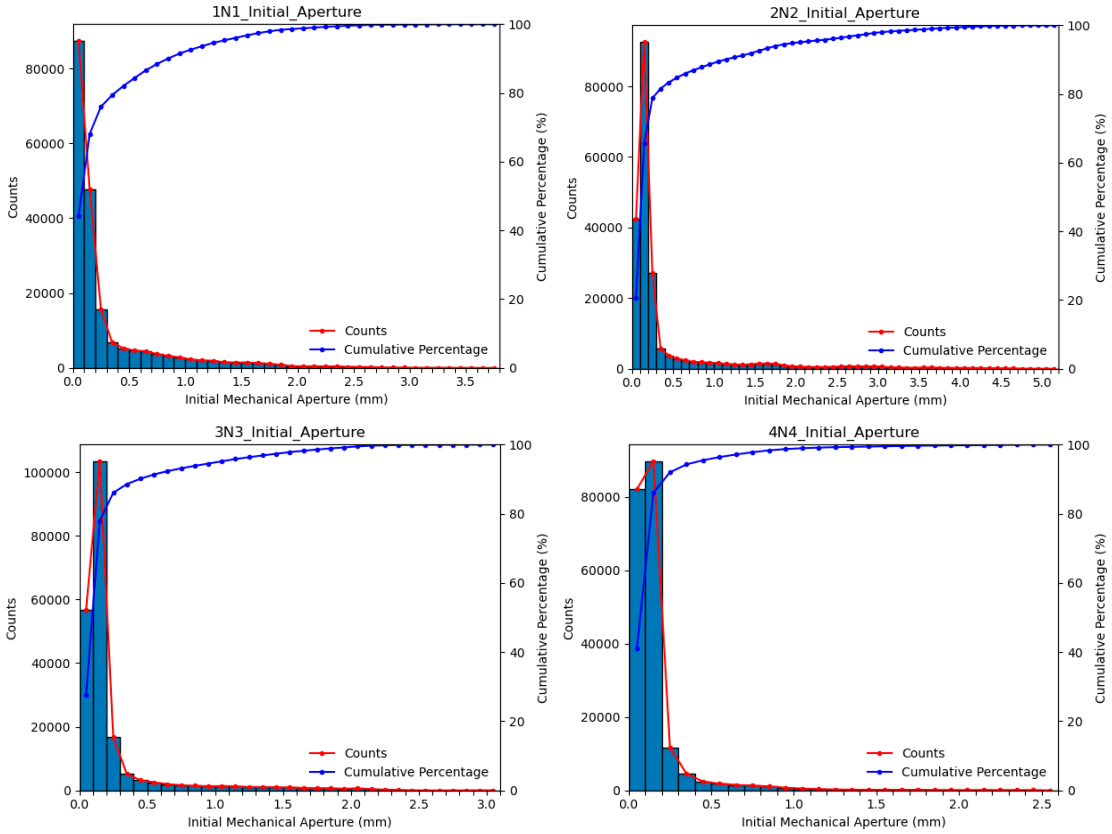

Figure C-10. *Variation of aperture for fractures 1N1 to 4N4.*

C4.3 Variation of aperture under normal loading

The aperture may change under various loading or sedimentary deposition or groundwater scouring. In this section, the variation of aperture under normal loading is modelled considering force equilibrium. The material composes the two sides of the fracture, i.e., the intact granite part is assumed to be elastic during loading. In addition, the conceptual contact model assumes that the aperture, defined by the distance between the upper and lower surface at a particular location, is constant within the area that is centred at the point and composed of half spacing of point cloud in both *X*- and *Y*-axis direction (Figure C-11). The aperture will change suddenly if the adjacent location has different magnitude, i.e., the spatial distribution of aperture is discontinuous.

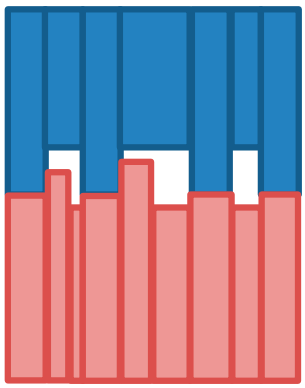

Figure C-11. *Conceptual contact model used for modelling variation of aperture under various loading.*

The Young's modulus, E, of granite is 73 GPa. The fracture has an area of 70×100 mm^2. The aperture has a zero contact pressure at its initial contact condition, and is loaded stepwise with an increment of 0.1 MPa until the normal loading reaches 5.0 MPa. Per mechanics of materials, the axial deformation δ of a structural member with area of A_p and length of L subjected to a normal load P is $\delta = PL/EA_p$. However, the contact area of the fracture A_c should be used instead of the area of the rock block A, and during the loading process, the loading increment at contacted aperture is $P = \sigma A = \sigma_c A_c$, where σ_c is contact stress at the contact area. As such, the deformation increment δ_i caused by each load increment $\Delta\sigma$ can be written as

$$\delta_i = \frac{\Delta\sigma}{A_{c,i}} \times \frac{A_p \times (L - \delta_{t,i-1})}{E}, i = 1, 2 \ldots, n \quad \text{(C-1)}$$

Where $A_{c,i}$ denotes the contact area of the fracture at the i^{th} calculation step. The total deformation $\delta_{t,i}$ at the i^{th} calculation step is

$$\delta_{t,i} = \frac{\Delta\sigma}{A_{c,i}} \times \frac{A_p \times (L - \delta_{t,i-1})}{E} + \delta_{t,i-1}, i = 1, 2 \ldots, n \quad \text{(C-2)}$$

Two scenarios are considered during modelling the aperture change under various loading. One scenario considers vertical force equilibrium only, i.e., the applied force is balanced by the contact area without further consideration of the moment equilibrium. The upper and lower surfaces have their displacement parallel to the loading direction. This modelling approach is simplistic, but may be a viable approach for large fractures where there is no size and shape information. The other scenario considers both vertical force and two horizontal moment equilibria during the loading process. Not only the distribution of contact area, but also the size and shape information of the fracture are needed for the calculation of the moment equilibrium condition. Figure C-12 sketches these two scenarios.

Figure C-13 shows the vertical deformation of the mean aperture for Fractures 1N1 to 4N4 from a contact pressure of 0.1 MPa to 5 MPa. Only vertical force equilibrium is considered in Figure C-13. The deformation of the fracture increases with applied normal loading. Fracture 3N3 has relatively large deformation; however, the difference of these relative deformation is limited.

Figure C-14 shows the spatial aperture distribution under the applied 5 MPa normal loading. Figure C-15 shows the statistical histogram of apertures under the applied 5 MPa normal loading. Only vertical force equilibrium is considered. Table C-5 summarizes the variation of aperture for Fractures 1N1 to 4N4 under 5 MPa normal loading.

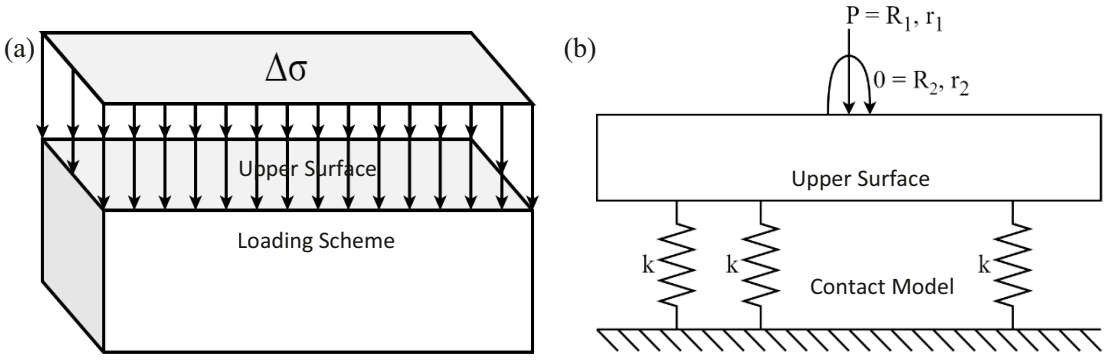

Figure C-12. *Two scenarios considered for modelling variation of aperture under various loading. (a) Vertical force equilibrium only, (b) vertical force and two horizontal moment equilibrium.*

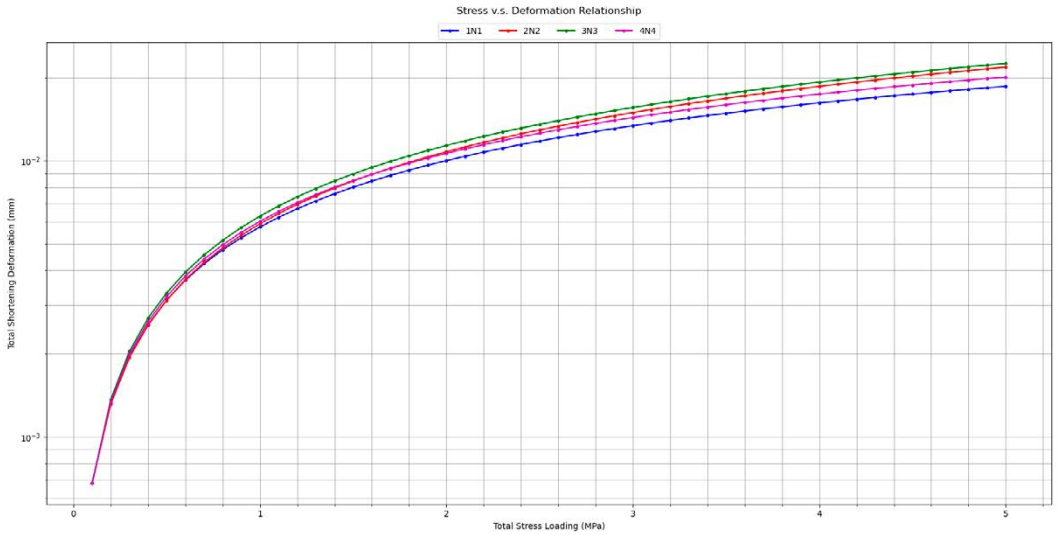

Figure C-13. *Vertical deformation of mean aperture for fractures 1N1 to 4N4 from a contact pressure of 0.1 MPa to 5 MPa loading process.*

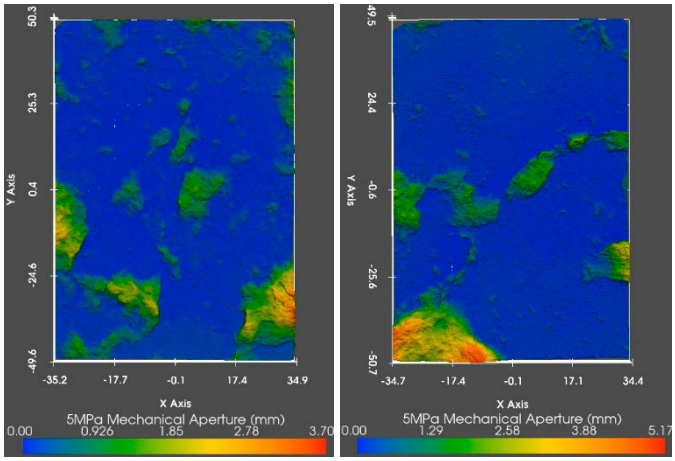

1N1 Aperture Field

2N2 Aperture Field

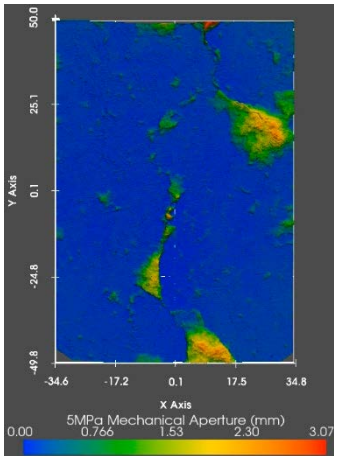

3N3 Aperture Field

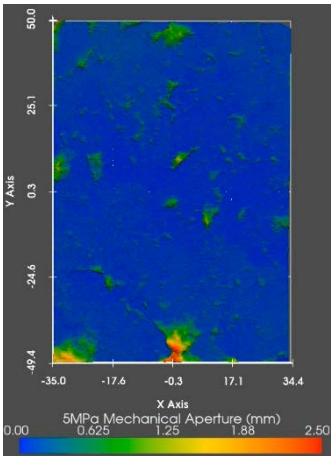

4N4 Aperture Field

Figure C-14. *Spatial distribution of aperture under the applied 5 MPa normal loading. During modelling only vertical force equilibrium considered.*

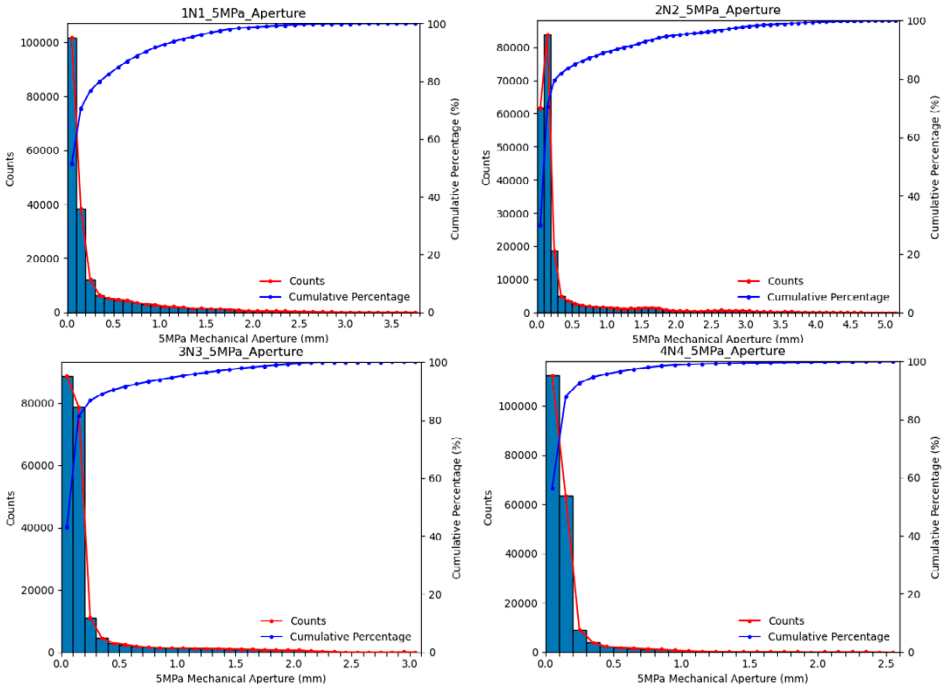

Figure C-15. *Statistical histogram of aperture under the applied 5 MPa normal loading. During modelling only vertical force equilibrium considered.*

Table C-5. Variation of aperture for fractures 1N1 to 4N4 under 5 MPa normal loading. During modelling only vertical force equilibrium considered.

		Initial State		**unit: (mm)**
Specimen	**S.D.**	**Ave.**	**Median**	**Max.**
1N1	0.4543	0.3043	0.1147	3.7235
2N2	0.7226	0.4145	0.1611	5.1909
3N3	0.3578	0.2407	0.1328	3.0883
4N4	0.2061	0.1572	0.1116	2.5212
		5 MPa Loading		**unit: (mm)**
Specimen	**S.D.**	**Ave.**	**Median**	**Max.**
1N1	0.4541	0.286	0.0961	3.7049
2N2	0.7224	0.393	0.1393	5.1691
3N3	0.3576	0.2185	0.1103	3.0658
4N4	0.2059	0.1374	0.0915	2.5011

Figure C-16 shows the spatial aperture distribution under the applied 5 MPa normal loading where both vertical force equilibrium and two horizontal moments are considered. Figure C-17 shows the histogram of aperture under the applied 5 MPa normal loading. Table C-6 summarizes the variation of aperture for Fractures 1N1 to 4N4 under 5 MPa normal loading. The average apertures for these four fractures are always greater than their corresponding medians, revealing the influence of some area with relatively large apertures.

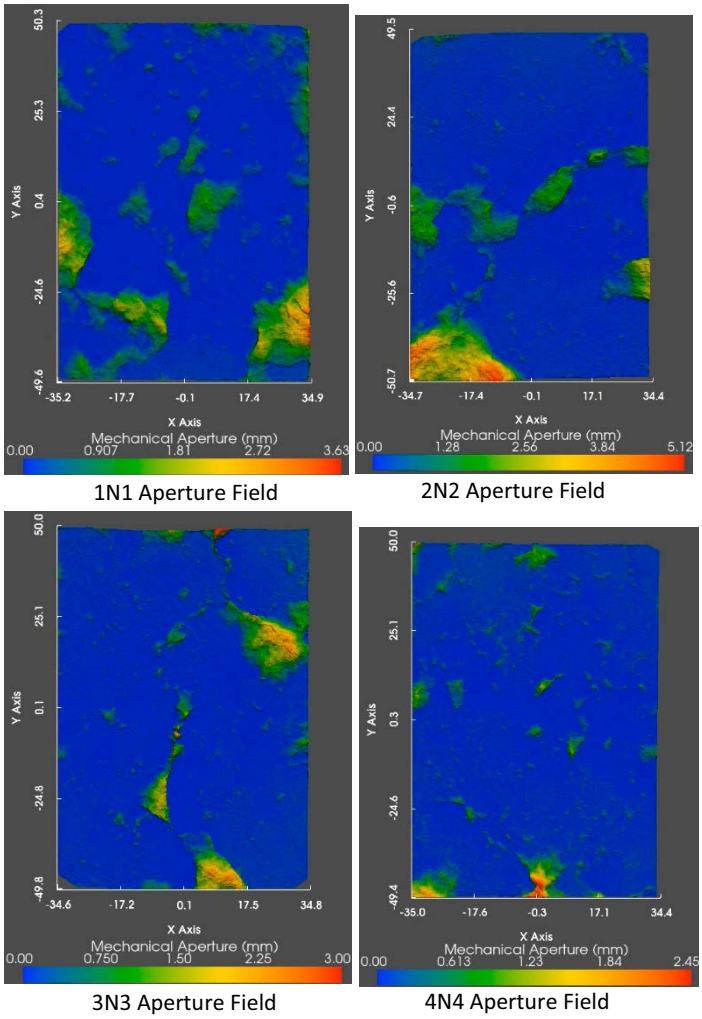

Figure C-16. *Spatial distribution of aperture under the applied 5 MPa normal loading. During modelling both vertical force equilibrium and two horizontal moment equilibrium considered.*

Table C-6. Variation of aperture for fractures 1N1 to 4N4 under 5 MPa normal loading. During modelling both vertical force equilibrium and two horizontal moment equilibrium considered.

		5 MPa		unit: (mm)
Specimen	**S.D.**	**Ave.**	**Median**	**Max.**
1N1	0.4541	0.286	0.0961	3.7049
2N2	0.7224	0.393	0.1393	5.1691
3N3	0.3576	0.2185	0.1103	3.0658
4N4	0.2059	0.1374	0.0915	2.5011
		5 MPa and Moment		**unit: (mm)**
Specimen	**S.D.**	**Ave.**	**Median**	**Max.**
1N1	0.4456	0.224	0.0183	3.6271
2N2	0.721	0.3443	0.0876	5.1174
3N3	0.3549	0.1595	0.046	3.0014
4N4	0.2033	0.092	0.041	2.4507

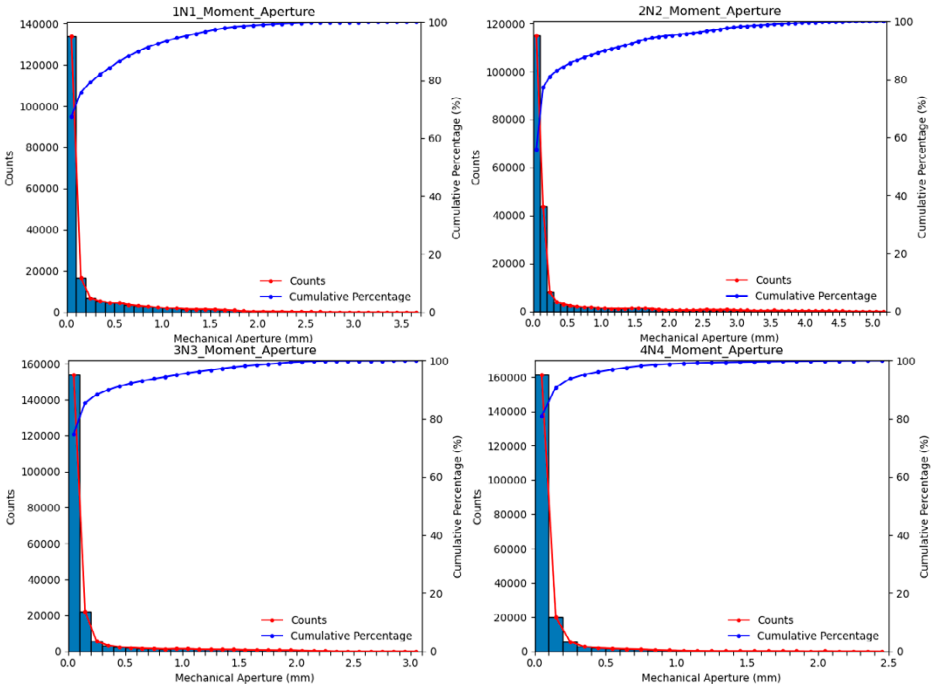

Figure C-17. *Statistical histogram of aperture under the applied 5 MPa normal loading. During modelling both vertical force equilibrium and two horizontal moment equilibrium considered.*

C4.4 Roughness estimation of large surface

The calculated JRCs, Z_2s and the spatial distribution of aperture of the small size fractures 1N1 to 4N4 are used to estimate roughness of a 1 m scale large surface. Numerous publications have concluded that the fracture characteristics are scale-dependent. However, limited quantitative relationships are reported. For the sake of large surface roughness estimation, the amplitude/length method (Barton, 1981) and JRC scale correlation curve (Barton and Bandis, 1982) will be used in this report. The theory of error propagation (or uncertainty propagation) will be conducted to determine the uncertainty.

The amplitude/length method provides estimates of JRC using extrapolation to the desired mean length of a rock block. Based on this method, the relationship between fracture amplitude and the surface scale is linear under log-log coordinates, implying that the aperture will increase with fracture size.

$$JRC = \begin{cases} 400\,a/L \text{ (for } L = 0.1 \text{ m)} \\ 450\,a/L \text{ (for } L = 1.0 \text{ m)} \\ 500\,a/L \text{ (for } L = 10 \text{ m)} \end{cases} \quad \text{(C-3)}$$

where a is the maximum amplitude measured over a fracture sample, and L is the sample length. Accordingly, the mean aperture of 1 m scale fracture estimated from Fractures 1N1 to 4N4 is (0.3043 + 0.4145 +0.2407 + 0.1572)/4 = 0.2792 mm, associated with the standard deviation 0.2370 mm. The standard deviation is determined using the theory of error propagation under the assumption that the apertures of these four fractures are noncorrected and the measurement (and modelling) of each fracture aperture contributes to the roughness estimation of large surface equally. As such, the linear error propagation formula ($Var(aX + bY) = a^2Var(X) + b^2Var(Y) + 2abCov(X, Y)$, where a and b are weighting coefficients, respectively, X and Y are sampling variables, can be applied. The value 0.2370 is obtained using those standard deviation from four modelling, and the weighting coefficients are both ¼, and covariance is 0.

The JRC scale correlation curve suggests

$$JRC_n \approx JRC_0(L_n/L_0)^{-0.02JRC_0} \quad \text{(C-4)}$$

Using Equation (C-4), the $JRC_{1\ m}$ can be estimated to be 7.1 using the Y-axis parallel $JRC_{0.1\ m}$ (12.8), and the standard deviation is 1.47.

C5 Discussion and Conclusion

Roughness and aperture are two important characteristic parameters controlling fluid flow in rock fractures. For fractures with geometric data of compositional surfaces, their roughness parameters, such as JRC, Z_2 and $2A_0\ \theta^*_{max}/(C+1)$, can be estimated based on existing formula. However, the estimation of corresponding aperture needs more information or conditions, such as the ratio of contact area to the total surface area. Geometric data of surfaces on both sides of a fracture is insufficient for the determination of fracture aperture.

In case the geometric data of both surfaces of a fracture are available, the spatial distribution of aperture for this fracture can be estimated under a specific ratio of contact area to the total surface area. If 1 % is adopted as a criterion for determining the aperture, most area of the fracture has smaller aperture than its mean aperture, revealing the influence of some large aperture. Compared to the 3D scanned surfaces with the distribution of contact pressure under MPa of loading stress, the area with large aperture may be caused by spalling during specimen preparation.

The aperture of a fracture decreases as the normal compression applied on the fracture increases. The modelled aperture with consideration of vertical force equilibrium and two horizontal moment equilibrium yields smaller mean and maximum apertures. However, aperture size and shape information is needed for the calculation of these equilibrium conditions.

The amplitude/length method (Barton, 1981) and JRC scale correlation curve (Barton and Bandis, 1982) are used to estimate roughness of a larger surface.

Appendix D

Modelling Group KAERI (Korea) – Evaluation of geometric properties of rock fractures and proposal for upscaling process

Seungbeom Choi, Chae-Soon Choi, Yong-Ki Lee, Kyung-Woo Park, and Sung-Hoon Ji; Korea Atomic Energy Research Institute (KAERI)

D1 Introduction

This task focusses on flow and transport at the single fracture sale, with emphasis on in-fracture channelling, as described in the Task Description (TD). To achieve this, Korea Atomic Energy Research Institute (KAERI) has been conducting studies on joint characterization, upscaling algorithm, and fluid flow simulations. Several rock fracture data distributed to each task force member were used to characterize the geometric properties of the fractures, such as joint roughness, aperture, and spatial correlation. An upscaling algorithm and procedure for the fracture surfaces was developed. Based on the fractal theory, the fractal dimension was obtained and applied to upscale one of the two fracture surfaces. Then, a geostatistical approach was adopted to upscale the other surface, maintaining the matching degree between the corresponding surfaces. However, the upscaling algorithm at this stage requires further validation. Lastly, as an exercise of Task 10.2.2, fluid flow through an aperture space was simulated using numerical modelling. Laminar flow simulations were conducted based on the aperture changes induced by normal stress changes. The simulations did not accurately reflect experimental data, i.e., normal stress – displacement results, so that the models will need to be modified accordingly.

D2 Objectives of Task 10.2.1

The objectives of this report are similar to those outlined in the TD. The first objective is to get familiar with the fracture surface datasets and to provide an opportunity to develop appropriate tools and concepts. The second objective is to develop an upscaling algorithm and procedure. Lastly, we aim to exercise numerical modelling to simulate groundwater flow through rock fracture, as part of Task 10.2.2.

D3 Limitation of Task 10.2.1

As described in the TD, a relatively simple case with a single fracture is used without taking into account conditions such as stress history, temperature, and geochemical evolution. Furthermore, the results in this report, specifically regarding upscaling, require further validation and the numerical modelling also necessitates some modifications at this stage.

D4 Data description

The fracture dataset provided to TF members were used; we tried to use them in their original form as much as possible. Especially, four 100×70 mm^2 specimens, i.e., 1N1, 2N2, 3N3, and 4N4, were mainly used for characterizing geometric properties of the fractures. Additionally, the HM specimen distributed in data delivery 3, sized at 200×200 mm^2, was used to test the upscaling procedure and fluid flow simulations. Furthermore, the input data required for the numerical simulations, such as intact rock properties and hydraulic boundary conditions, were referenced from data delivery (DD) files.

D5 Modelling and methodology

D5.1 Model purpose

According to the Task Description, the model purpose of Task 10.2.1 is to confirm if single fracture observations made on the scale of a pilot borehole can be used to make predictions of single fracture properties on the deposition hole scale. The upscaling modelling process in this report involves two steps. At first, fractal theory is applied to derive the fractal dimension, which is used to upscale

one of the original surfaces. Then, a geostatistical approach is adopted to upscale the other surface, considering the correlations between the corresponding surfaces. In addition, numerical modelling that simulates the fluid flow through the aperture space were conducted, which is related to Task 10.2.2. The simulations were performed using commercial FEM software.

D5.2 Model description

The upscaling modelling adopted in this report consists of two steps. Firstly, the fractal dimension of one surface is determined using FFT, considering the fracture surface as a self-affine object. Candela et al. (2009) reported that the fractal dimension (or Hurst exponent) decided by PSD (power spectral density) remains nearly constant along the direction perpendicular to the slip direction, covering approximately 6 orders of magnitude of length scales for two different fault surfaces. In their study, one fault surface showed consistent results along the shear direction, while the other exhibited some smoothing of the roughness below a length scale of several millimetres. In this report, we assumed that the dimension remains constant within the scale of the distributed data, allowing us to upscale one surface using the FFT procedure. However, if the same procedure were applied to the other surface independently, the correlation between corresponding surfaces could not be guaranteed. Thus, cokriging was adopted as a second step to generate the other surface, taking the correlation into account. Though the approach seems more complex than upscaling the aperture field directly, it was adopted in order to check the applicability and to seek the diversity in the application. In the cokriging procedure, the formerly upscaled surface from the first step is treated as a secondary variable, while the other surface is the primary variable, which is to be upscaled. Additionally, uncertainty analyses can be conducted by multiple realizations, evaluating the prediction results in terms of averages and/or deviations. A flowchart of the upscaling procedure has been generated; however, it requires further validation at this stage and will be subject to further modifications.

Numerical modelling to simulate fluid flow through a single rock fracture was conducted using a commercial FEM software, COMSOL Multiphysics. The numerical model used fracture surface data, i.e., upper and lower surfaces, to generate the void space, i.e., the aperture field. The model solved the Navier-Stokes equation; however, it assumed laminar, incompressible flow so that it became Stokes equation. After building the aperture geometry, appropriate boundary conditions, i.e., inlet and outlet, were applied based on the results of the HM experiment described in the DD. A proper mesh was constructed, which included layer boundaries along the aperture direction to simulate velocity profiles perpendicular to the main flow direction. Then, flow simulations were performed, and the distribution of velocity, pressure, and outlet flux were obtained. It is obvious that the aperture space varies due to normal stress. However, the mechanical behaviour resulting from normal stress changes have not been fully simulated so that the flow simulations will be revisited using a modified aperture space under specific normal stress.

D5.3 Determination of critical aspects

In the upscaling procedure, two separate steps were applied. Firstly, FFT was adopted to evaluate the fractal dimension with the assumption of considering a rock fracture surface as a self-affine object. In addition, we assumed that the fractal dimension remained constant within the range of the database we used, i.e. within the size of 200×200 mm^2 specimen. Therefore, those assumptions and their applicability would be the important aspects that need to be validated. Then, in the second step, cokriging was applied to reflect the spatial correlation between the corresponding surfaces. Cokriging requires variograms of primary and secondary variables as well as a covariogram between the two variables. The precise modelling of the variogram significantly affects the kriging result, making variogram modelling another critical aspect in the upscaling process. In the numerical modelling, the realistic implementation of aperture space is an important factor. Fluid flow occurs through the aperture space so that the variation of the space, such as regional contacts and asperity deformations, become critical factors that should be accurately represented in the model.

D5.4 Definition of performance measures and criteria

Prediction performance can be evaluated by comparing several statistics of the original fracture surface with those of the upscaled surface. It is probably one merit of the applied approach in this study because it provides a complete set of surface coordinates, which makes the comparison easy. As there

certainly exist some discrepancies in terms of overall shape, conducting statistical comparisons seems to be reasonable. When it comes to numerical modelling, comparisons with the experimental results, i.e., outflow flux distribution as provided in the data delivery, would be a good and direct performance measure. This allows for a direct comparison between the simulated fluid flow through the aperture space and the actually observed experimental results. Such comparisons can help validate the accuracy and predictive capability of the model.

D5.5 Identification of influential factors

In the case of the upscaling procedure used in this work, an accurate definition and evaluation of spatial correlations is important because the procedure is based on kriging. At the same time, the aperture distribution and its variation due to loading is influential when it comes to fluid flow simulation.

D5.6 Uncertainty analyses

To conduct uncertainty analyses, multiple realizations of upscaling would be required. These realizations would allow for comparisons between the actual surface and the upscaled surface in terms of various statistics. Additionally, a sensitivity analysis on influential factors would be desired to understand the effects of different input parameters on the upscaling results. This would involve investigating the impact of parameters such as fractal dimension and variogram parameters on the upscaling process to assess their significance in influencing the final results. By performing such sensitivity analyses, we can gain some thoughts into the reliability of the upscaling procedure.

D6 Results, discussion and conclusions

D6.1 Data pre-processing

Before conducting the analyses, the fracture data needed pre-processing in terms of size, point interval, and matching degree between corresponding points. The pre-processing involved several steps, starting with aligning the surfaces. The ICP (Iterative Closest Point) algorithm was adopted to align the upper and lower surfaces. It transforms one point cloud while fixing the other, to minimize an error, which is generally the sum of squared differences between two point cloud sets. After that, detrending was applied to remove any trends present in the dataset. Then, interpolation was performed to ensure an equal point interval, and the interval was set to 0.2 mm. Finally, boundary trimming was carried out to prepare the data for further analysis. Figure D-1 shows the results of the pre-processing procedure, showing the four surfaces (1N1, 2N2, 3N3, and 4N4) with a size of 100×70 mm^2 each. These surfaces are ready for use in the subsequent analyses.

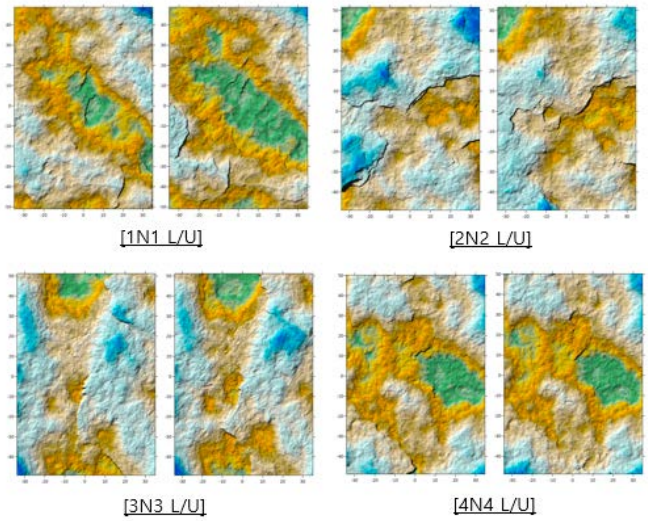

Figure D-1. *Example of pre-processing ; 1N1, 2N2, 3N3, and 4N4 (100×70 mm^2) surfaces.*

D6.2 Characterization of geometric properties

Several geometric fracture properties were investigated using four 100×70 mm^2 size fracture data. The properties were surface elevation, roughness, mechanical aperture, spatial correlation and so on. The distribution of surface elevation showed that most of them were unimodal but somewhat skewed. KS (Kolmogorov-Smirnov) test with 0.05 of significance level rejected normality of all the tested surfaces. Then, spatial correlation of surface elevation was analysed by variogram. The analyses were conducted with proper parameters, including 100 mm of maximum distance, 0.4 mm of radial and 2° of angular division. Anisotropy in correlation was also investigated by drawing directional variogram with 15° of step and tolerance. Both spherical and Gaussian models with nugget effect were examined as experimental variogram models. If there exists remarkable peak, variogram parameters, such as range and sill, were fitted to the first peak. The fitting showed good correlation more than 0.95 of r^2 for both experimental models. Figure D-2 shows an example of a directional variogram, derived from 1N1 case.

Both upper and lower surfaces showed similar results, indicating potential correlations between them. The omni-directional model showed about 40 mm of range and a local drift was observed over a range of 45 mm. In the case where theta equals 0°, the variogram appeared to converge at a larger range. However, for theta of 45° and 90°, a hole effect was observed, which was thought to be the effect of a valley at the central part of the surface. At last, for theta of 135° case, the variogram did not show convergence within the maximal tested lag distance.

The initial mechanical aperture was calculated using the superposition method. It is assumed that 1 % of fracture area is in contact due to its dead weight (Esaki et al., 1998). To calculate the initial mechanical aperture, the surface coordinates were vertically moved until 1 % of total nodes (points) were superimposed. Then, the physical distance between corresponding points, i.e., initial mechanical aperture, was calculated. Because the surface pre-processing made the error between the surfaces minimal, the surfaces were assumed well aligned. The histogram of the aperture showed they followed a negative exponential distribution. Figure D-3 shows spatial distribution of initial mechanical aperture along with pressure film results obtained from uniaxial compression tests. The white part on the pressure film indicates that there existed large apertures, at least larger than the thickness of pressure film, so that no pressure was applied. A comparison of the film with the calculated aperture shows a very similar spatial distribution.

Descriptive statistics of the initial mechanical aperture are shown in Table D-1. 2N2 specimen had the largest aperture on average, however it also had the largest coefficient of variation.

Table D-1. Descriptive statistics of initial mechanical aperture.

	Average	Standard deviation	Median	Max
1N1	0.3843	0.4450	0.2241	3.8981
2N2	0.4060	0.6923	0.1686	4.9458
3N3	0.2284	0.3530	0.1270	3.2889
4N4	0.1486	0.1996	0.1060	2.5059

Various roughness indexes have been proposed, for instance, the joint roughness coefficient (JRC) by Barton and Choubey (1977). Among the indexes, three types of 2D quantitative indexes were grouped in this report and then applied to the 100×70 mm^2 size specimens. The first group is based on the surface shape and amplitude, with Rp (roughness profile index) by Yu and Vayssade (1991) being a typical example of this group. The second one is based on the slope of asperity, and an example of this group is Z2 by Tse and Cruden (1979). The last group, related to fractal and RLM (Roughness Length Method) by Malinverno (1990), is selected as an example. All the indexes mentioned above are two-dimensional, which means they cannot be used to evaluate anisotropy. Therefore, using a 3D index, for example that proposed by Tatone and Grasseslli (2009), could be one option to evaluate the directionality of joint roughness. However, in this report, all the profiles along certain direction were exported and then evaluated by those three indexes. Since multiple profiles were considered, distributions, not just a single value, could be obtained so that it could mitigate the directionality problem. The anisotropy in roughness was investigated by acquiring multiple profiles along different directions from 0° to 165° with an interval of 15°. Figure D-4 shows the roughness indexes and their anisotropy.

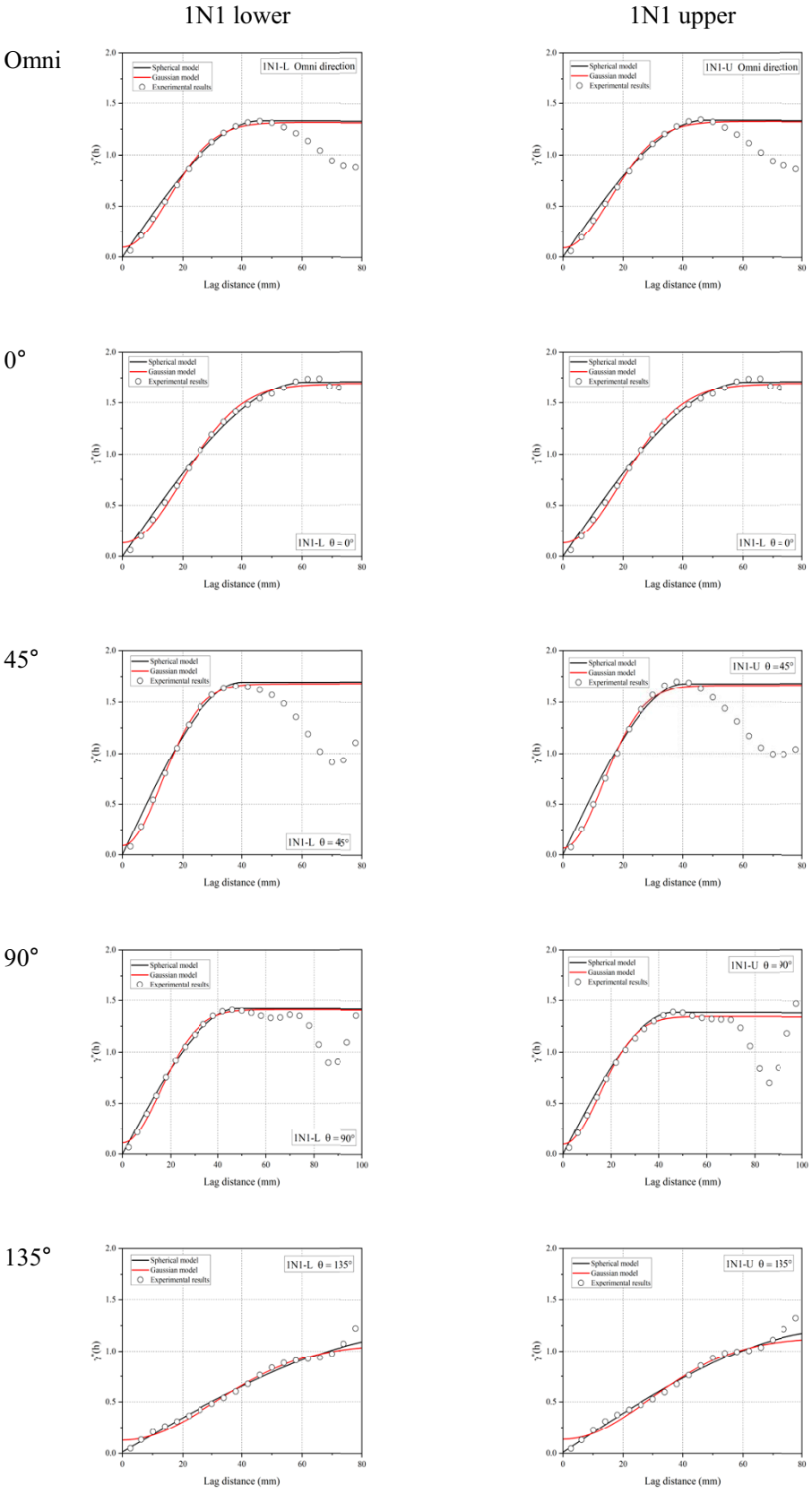

Figure D-2. *Directional variogram of 1N1 specimen.*

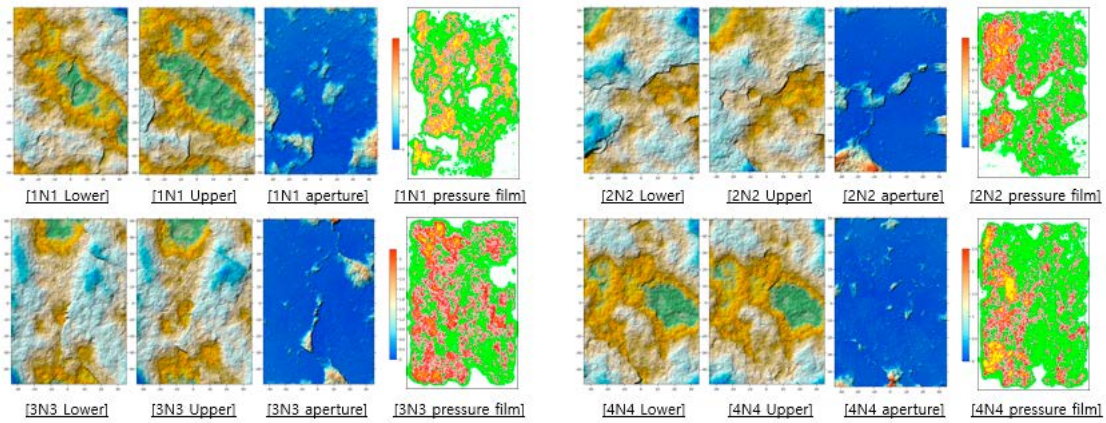

Figure D-3. *Spatial distribution of aperture and comparison with the pressure film data.*

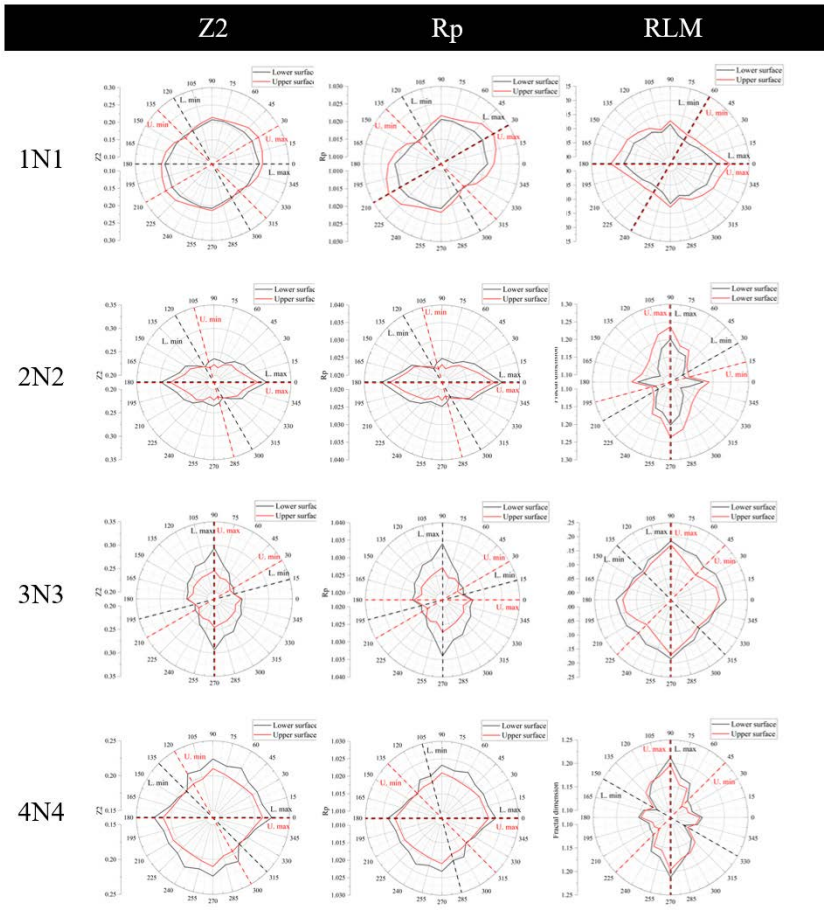

Figure D-4. *Roughness indexes and their directionality.*

In general, the lower and upper surfaces show similar distributions in the roughness indexes. However, the magnitude of Z2 and Rp for 3N3 show a relatively large discrepancy. It indicates that the lower surface of the 3N3 specimen had larger deviations in terms of overall amplitude and asperity height compared to the upper surface. At the same time, distributions obtained from the fractal dimension showed slight difference, while those of Z2 and Rp were similar to each other. The relationships between the indexes require further investigations.

D6.3 Procedure for upscaling

As mentioned before, the upscaling modelling requires further validation at this stage so that in this chapter, we mainly provide an explanation of the methodology. The upscaling procedure consists of two steps. Firstly, one surface of a fracture pair is upscaled by fractal theory. Applying FFT to one fracture surface gives PSD (power spectral density) and fractal dimension, which can be calculated from the slope of PSD curve. Candela et al. (2009) reported that the feature remains almost constant to some extent, so that the upscaling can be performed using inverse FFT, while maintaining the same slope. Figure D-5 shows an example of the procedure.

The procedure allows for easy upscaling of one surface. However, applying the same procedure independently to the other surface does not ensure a proper correlation between the corresponding surfaces. Therefore, it requires some strategy to properly reflect the correlation when upscaling the second surface. In this study, cokriging was adopted as a second step to upscale the other surface. Cokriging is a kriging algorithm that incorporates correlations between primary and secondary variables. In this case, the upscaled surface in the first step corresponds to the secondary variable. Then the other surface, as a primary variable, is upscaled by kriging, taking into account the variogram of primary and secondary variable as well as covariogram between the variables. Figure D-6 shows the upscaling procedure. In this example, a 200×200 mm^2 specimen, which was distributed in data delivery 3, was used to explain the procedure.

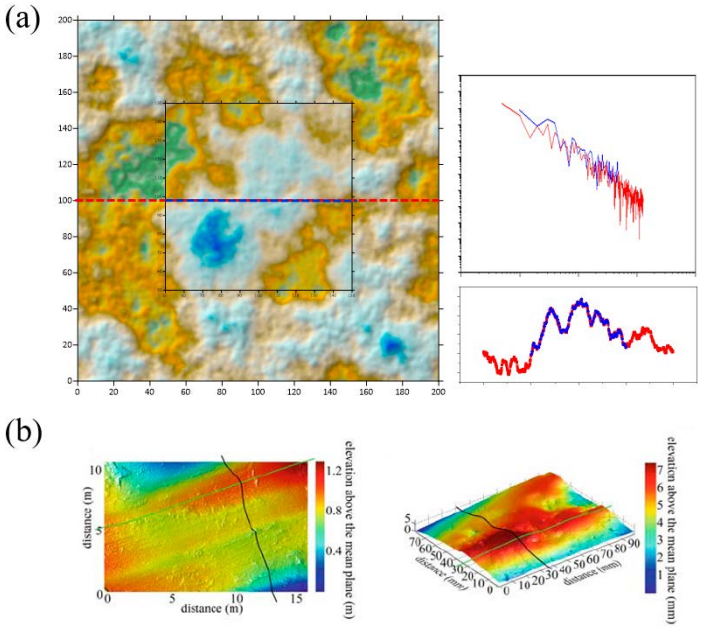

Figure D-5. *Upscaling procedure step 1; (a) PSD analysis, (b) example from Candela et al. (2009).*

Firstly, let us assume that the central part of the lower surface (100×100 mm^2 size) in Figure D-6 is upscaled properly to 200×200 mm^2 by PSD analyses. The upscaled lower surface provides the secondary variables for cokriging. Then, the central part of the upper surface, as a primary variable, is upscaled by cokriging considering the correlation between the surfaces.

Since the original surface data is available, a comparison between the original and the predicted data can be conducted to assess the performance of the procedure. Figure D-7 shows the prediction results and the comparison. The prediction result is the average of 10 realizations.

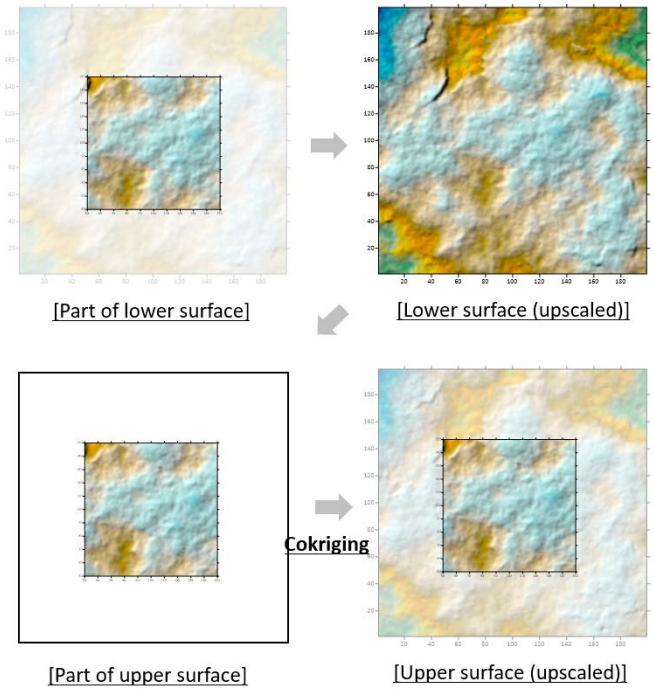

Figure D-6. *Upscaling procedure.*

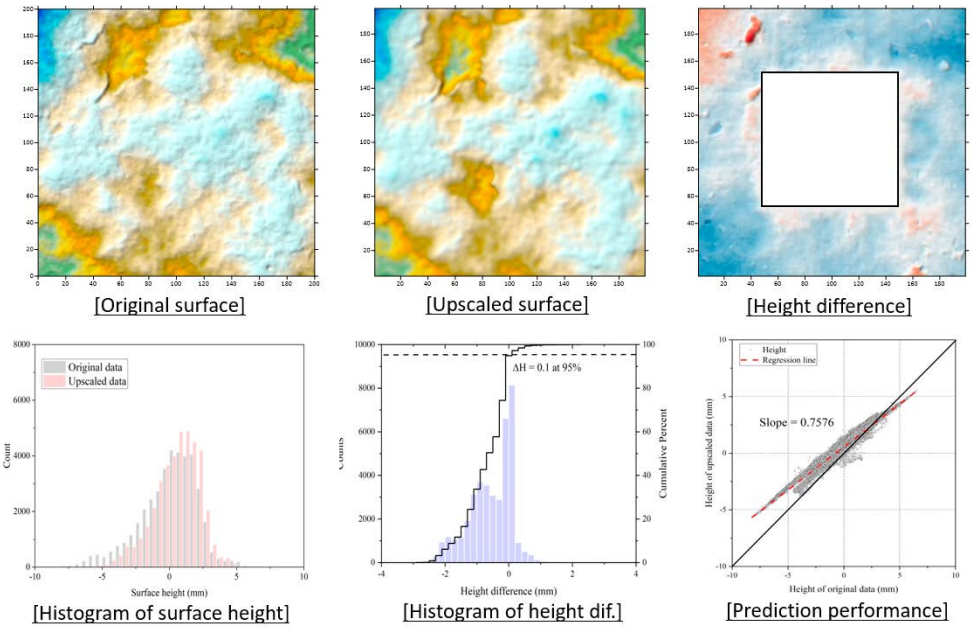

Figure D-7. *Upscaling result and its comparison.*

Histogram of both surface heights, from a reference (mean) plane, seems to be similar, however, some discrepancies between original and upscaled surfaces exist. The prediction performance indicates that the prediction underestimates the surface height, with a slope of 0.7576. Two surfaces were vertically translated until the mean height (z coordinates) became zero. Then descriptive statistics were calculated and listed in Table D-2.

Table D-2. Descriptive statistics of original and upscaled surface heights and their discrepancy.

	Original	Upscaled	ΔH
Average	0.0000	0.0000	0.0000
Standard deviation	2.1523	1.6812	0.6634
Median	0.3011	0.2044	0.1326
Min	−8.2128	−6.1643	−2.3547
Max	6.5756	5.0141	2.7393

Clearly, the procedure developed in this study underestimates the surface heights. However, the reason for the underestimation needs more deducing at this stage. It may originate from the algorithm itself or from variogram modelling so that further investigation as well as uncertainty analyses are essential.

D6.4 Numerical simulation for fluid flow

In order to conduct numerical simulations, a dataset of the 200×200 mm^2 fracture from the HM experiment was used. Before making numerical models, geometric properties were investigated. As mentioned in the previous section, surface height, spatial correlation, and mechanical aperture were evaluated. Especially, fluid flow occurs mainly through the aperture so that its quantitative evaluation is of importance. As descripted in A6.1, two surfaces were properly processed, then the upper surface were translated vertically so as to estimate initial mechanical aperture. The aperture was estimated as 0.4616 mm on average.

Both normal and shear stress acting on the rock fracture can lead to variations in aperture. In case of normal stress changes, it compresses the aperture space, which interrupts fluid flow through it. However, the amount of compression is difficult to estimate since various factors affect it. Therefore, aperture variations that fit the data delivery (DD), i.e., normal stress and displacement data, should be investigated first.

A commercial FEM software, COMSOL Multiphysics, was used to conduct both mechanical and hydromechanical simulations. The coordinates of both upper and lower surfaces were imported into the software, and they were converted to solid objects that represent the fracture specimens. Elastic properties of intact rock were assigned to these solid objects and a contact pair was designated between the upper and lower surfaces to simulate contact mechanics. Then, appropriate boundary conditions, such as prescribed displacement and fixed conditions, were applied to simulate uniaxial compression on the fracture specimens. However, the process of assigning properties to the contact pair is complex, and it requires further tuning at this stage to accurately simulate the macroscopic behaviour of the fracture specimen, specifically the normal stress – displacement behaviour. Given this complexity, an approximation of the variation of the aperture space was assumed to approximately follow the normal displacement, as referenced from the experimental results provided in the data delivery (DD).

Figure D-8 shows the numerical modelling procedure used to construct an aperture domain space. Suppose that fracture surfaces were deformed by normal load. Then, those deformed surfaces were imported into the software and the superimposed parts, which represent contact areas, were removed. Finally, in order to create a three-dimensional aperture space, four sidewalls were added to enclose the aperture domain.

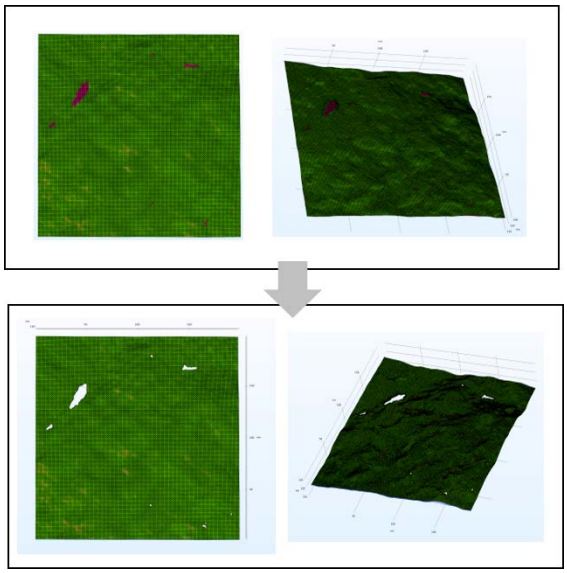

Figure D-8. *Numerical modelling procedure of an aperture space.*

In the numerical modelling process, the fluid flow was assumed to be laminar and the fluid itself was treated as incompressible. As a result, the Navier-Stokes equation was simplified to Stokes equation. Then, the boundary conditions for the simulation, specifically the pressure at the inlet and outlet boundary faces, which were specified as in DD file. To discretize the domain and solve the equations numerically, a mesh was generated, including boundary layers perpendicular to the fluid flow direction. The mesh with boundary layers aimed to simulate the parabolic velocity profile typically observed in laminar flow regime. Figure D-9 shows an example of fluid simulation, which present pressure field and velocity profile. Central figure in D-9 shows the fluid flow from top to bottom while the right most figure shows the flow from right to left. The two figures used the same geometry, indicating pressure field and fluid velocity(arrows).

In addition to the previous simulations, the effects of flow direction and normal stress were investigated, as shown in Figure D-10. As the normal stress increased, the aperture decreased due to the compression, also leading to outlet flux decrease. Variation of contact area and asperity deformation should be investigated further, however, at this stage, they were not included. Hydraulic aperture is a calculated value from flow experiments, based on the assumption of cubic law. Rock fractures are neither flat nor parallel so the hydraulic aperture can never exceed the mechanical aperture in real cases. Deviation from the 1:1 line was affected by several factors, such as surface roughness, tortuosity, contact conditions, and it indicates the importance of realistic simulation of fracture surface. As described, an approximation of the variation of the aperture space was assumed to approximately follow the normal displacement of the results provided in the data delivery. Though it used assumed an aperture space, the methodology of building a numerical model was established so that simulations will be conducted again after obtaining the proper aperture variation results. These simulations will consider the actual aperture variations resulting from the deformation due to normal stress, which will provide more accurate and realistic representations of the fluid flow behaviour through the fracture.

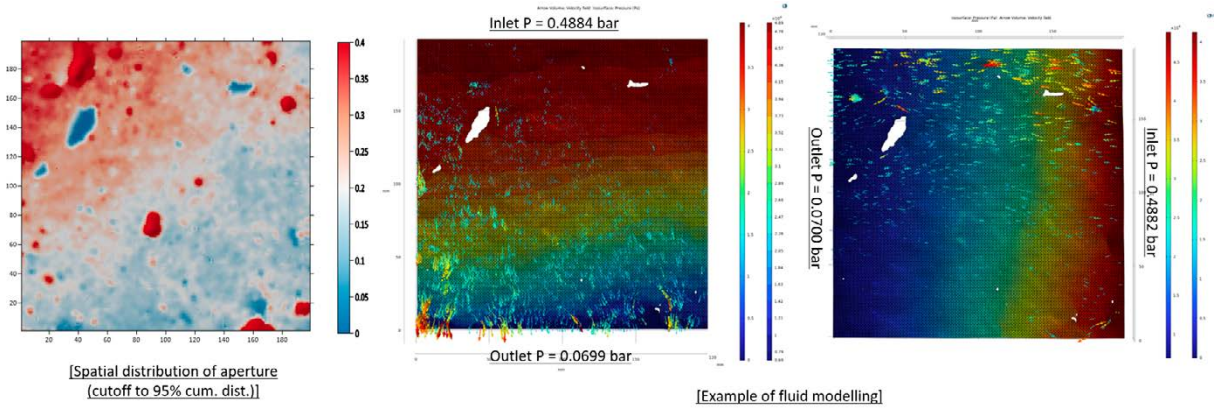

Figure D-9. *Example of fluid flow simulation.*

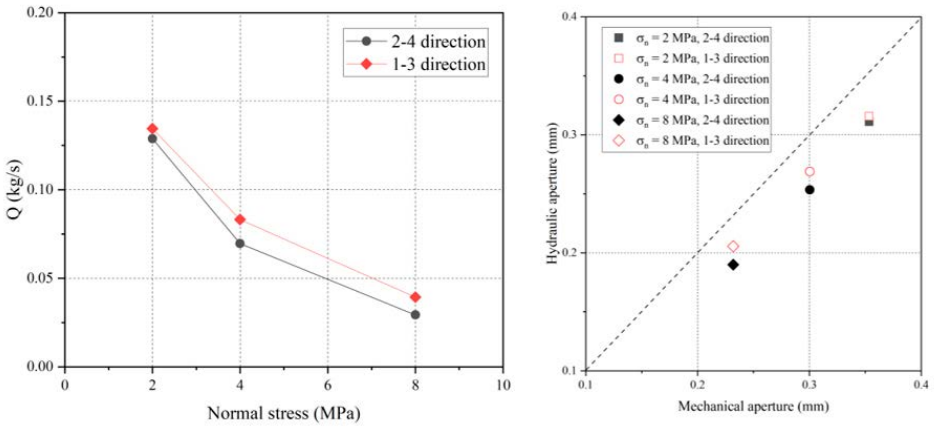

Figure D-10. *Variation of simulation results according to flow direction and normal stress.*

D6.5 Summary

As mentioned in the previous sections, this report still has many aspects for further improvement. In particular, the upscaling modelling requires additional validation work to ensure its reliability. The numerical modelling also needs further tuning of input parameters to correctly reflect the aperture variation resulting from normal stress. Despite these limitations, the objectives of this task have been partially achieved, which is to get accustomed to the dataset and overall workflow. Furthermore, the data and description provided to each task member are thought to be sufficient in terms of quantity and type for achieving the task objectives.

Appendix E

Modelling Group Stockholm University (SKB/Sweden) – Methodology for pre-processing surface scan data and presentation of an updated method for generating rough surfaced aperture

Stock, B. and Frampton, A., Department of Physical Geography, Stockholm University, Sweden

E1 Introduction

According to the Task Description, Task 10 of the GWFTS is dedicated to building confidence in, and pragmatic validation of, models of flow and transport in fractured rock. Understanding fluid flow through natural fractured rock systems is important for several applications and can have a range of safety related implications. It is known that aperture variability exhibits significant control over the flow field through a fracture network. However, its inclusion in models is often hampered due to lack of measurements and numerical representation. For example, to investigate the suitability of a deposition hole on the meter scale, most likely a single pilot borehole will be drilled, yielding information on intersected fracture on the centimetre scale. The aim of this study was to develop and evaluate a method for reproducing rough surfaced fractures with variable apertures using information obtained from 3D scans of a natural rock fracture surfaces. This also includes a description of the pre processing that the surface scans must undergo in order to be used for this method, and increase the accuracy of the final measured deterministic apertures. A model for the stochastic fracture aperture generation is further developed based on previous work using self-affine fractal concepts, which includes a refined method for representing correlation between the upper and lower surfaces of the fracture.

E2 Objectives of Task 10.2.1

Our main objectives of this subtask are based on the Task Description, which are as follows:

- To gain insight to the fracture surface datasets provided by the Task Force.
- To develop appropriate tools and concepts for analysing the data provided.
- To develop methods for building a description of fracture roughness and fracture void space (together with an assessment of relevant uncertainties) for the purpose of flow and transport simulations, focussing on including spatially varying aperture.
- Investigate scaling of fracture surface properties from borehole- to metre-scale, based on the data provided.
- To start to consider the influence of fracture normal closure on this void space description, which will be a topic of Task 10.2.2.
- Evaluate applicability of self-affine theory for describing aperture distributions, based on the assumption that fracture roughness is scale dependent.
- Evaluate the fracture roughness generation procedure and rescaling against data provided by the Task Force.

E3 Limitation of Task 10.2.1

In addition to limitations identified by the Task Description Document, the method we have employed is based on self-affine theory, which assumes the rough surfaces of fractures can be described by fractal theory/concepts. Another assumption is that correlation between the fracture surfaces is scale independent, and hence this method can be used for upscaling.

E4 Description of data pre-processing

First, we describe all the pre-processing steps we performed in order to create an accurate data set for use in the modelling.

As described in the Task Description, rock samples were taken from a medium grained granite block from the Flivik quarry in Oskarshamn municipality, Sweden and included a natural vertical fracture running through it. During the sampling campaign a block weighing 15.2 tonnes was extracted and subsequently divided into 24 rock block samples, of which four with the smallest dimensions are used in this study. The four fracture samples are denoted as 1N1, 2N2, 3N3 and 4N4 with XYZ dimensions of 70 × 100 × 100 mm and have been cut from the rock block. For each sample, the fracture runs through the centre of the block, approximately parallel to the top of the sample. The dimensions of the samples are representative of the borehole scale.

Scans of the fracture surface as well as pressure film data were used to obtain the data that will be used for modelling. Details of the methods used to obtain this data can be seen in the Task Description, Section 3.3.3. However, due to the methods used, pre-processing must be completed on the provided data to create an accurate aperture from the scans.

Measurement points are stored approximately every 0.2 mm. This results in an irregular mesh when observing the XY coordinate plane, which means the nodes between upper and lower surface do not necessarily align. This can be seen in Figure E-1 which shows a cropped section of the upper and lower point-cloud of the 1N1 fracture surfaces. Points from the upper surface do not align with those of the lower surface, which becomes more apparent as the point density increases, for example around x = 2.5 mm, y = 1.0 mm. Note the point density increases at locations where the surface gradient rapidly changes, creating a cluster of data points.

Fujifilm Pressure Distribution Mapping System for Prescale (FPD-8010E) was used to measure and analyse the distributions of pressure between the contact of the upper and lower surface of the fracture under a load of 5 MPa. The data was delivered in a raster bitmap format (Figure E-2). These files contain 10 discrete colours which represent different pressures. The pressure film measurements have an upper and lower limit of 10 MPa and 2.5 MPa, respectively, which are represented by red and blue (Figure E-2). White areas represent areas of no pressure data, meaning the upper and lower surface of the fracture have not compressed the pressure film.

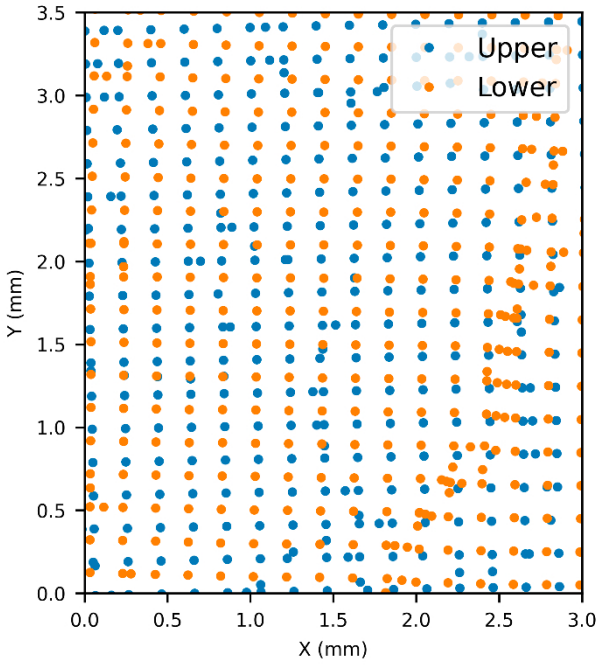

Figure E-1. *Point-cloud data of a cropped section of the upper and lower surface from sample 1N1 obtained from a 3D scan of the surface.*

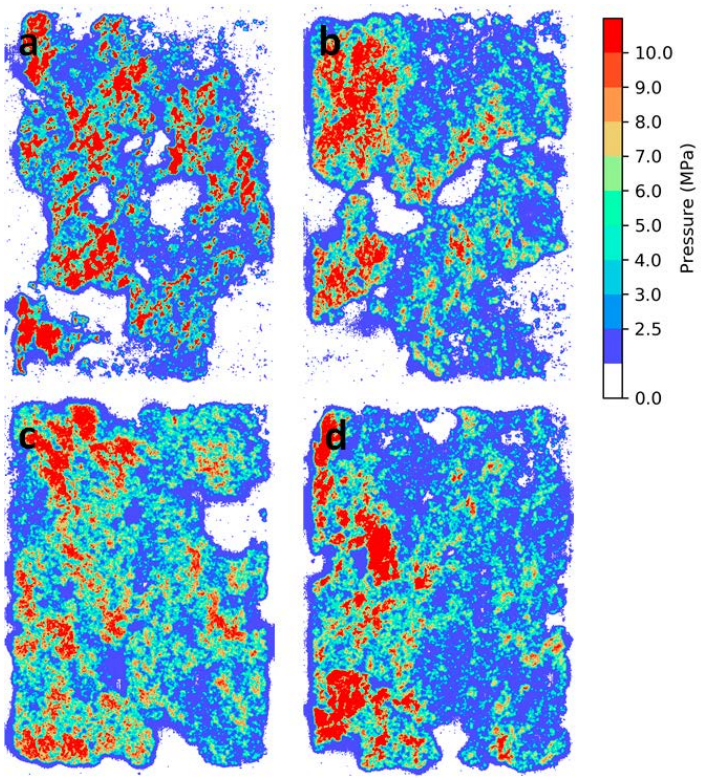

Figure E-2. *Contact pressure films for samples 1N1 (a), 2N2 (b), 3N3 (c) and 4N4 (d) under 5 MPa of normal load.*

In order to create an aperture from the raw data, several steps must be taken. The first is to interpolate the point cloud surface data of each scan onto a regular grid of the same dimensions. By doing this, the nodes on the upper and lower surface of the same sample now align on the XY coordinate plane. Once both surfaces of the sample are represented on a regular grid, the upper surface must be shifted vertically by 9.92 mm, the dimension of the spacer ring, in order to properly reference both surfaces. Subtraction of the lower surface from the shifted upper surface, which is now possible due to node alignment, provides the aperture field for that sample as a 2D array.

E4.1 Interpolation

The interpolation of the point cloud data onto a regular grid requires adopting an interpolation method. Here we evaluate three approaches, a linear, nearest neighbour and cubic spline interpolation, using the *SciPy griddata* package within Python. For each case, a grid resolution of 0.5 mm is adopted.

The two-sided Kolmogorov Smirnov (KS) test was systematically applied on the aperture distributions obtained from the interpolated surfaces to evaluate whether they statistically originate from the same distribution. The result shows that for linear against nearest neighbour interpolation, the null hypothesis that the two samples come from the same distribution must be rejected. The null hypothesis must also be rejected when cubic interpolation is tested against nearest neighbour. However, for linear interpolation against cubic interpolation, both samples are statistically likely to come from the same distribution with a significance level of 0.05.

Due to the surface scans not being perfectly rectangular, there are sections without data around the edges of the grid when using linear and cubic interpolation. However, nearest neighbour interpolates all the way to the grid edges. Using methods that only interpolate to the spatial limit of the data and not the grid retains more accuracy from the raw data, hence nearest neighbour is excluded for this reason. Also, as mentioned above, it is not statistically similar to the other interpolation methods.

Therefore, either linear or cubic interpolation are determined to be more robust. Linear was selected for the following reasons. As previously mentioned, the scans are not perfectly rectangular hence interpolation using both these methods results in areas with no data along the edge of the scans. However, cubic

spline interpolation is very sensitive to edges, typically causing unrealistic values due to truncation at boundaries. This is not the case with linear interpolation, hence retaining as much accuracy from the raw data as possible. The surfaces have been cropped to remove areas of no data along the edges of the grid, as well areas of obviously erroneous data where the edge of the sample has been included in the scan, causing a sudden sharp increase in the surface height. Thereby, the final dimension of the surfaces after cropping is 95×65 mm

E4.2 Resolution

The point cloud data obtained from scanning the fracture surface is unstructured, typically with a high density of closely spaced points around areas where there is a sharp change in gradient on the surface. Therefore, it is important that during interpolation onto a regular grid a resolution that does not exclude relevant information from the point cloud is selected. To determine the best resolution, the point-cloud data was analysed as follows.

First, the data was converted into an STL format using a combination of MeshLab (https://github.com/cnr-istivclab/meshlab) and the Open3D Python package (https://github.com/isl-org/Open3D). It is important to note that although the upper and lower surface can be quite easily converted to an STL file, the two surfaces are still independent, and directly obtaining an aperture field from these surfaces is not possible. However, creation of the STL allows for the mean, maximum and minimum distances between points on each surface to be obtained.

The maximum distance between points, in 3D space, is approximately 0.25 mm with a minimum distance of 1.5×10^{-5} mm. The mean distance between points is approximately 0.15 mm with a standard deviation of 0.06 mm. Therefore, a resolution of 0.1 mm was selected when interpolating onto a regular grid as it is within the standard deviation of the mean distance between points and should be sufficient to retain most of the data. In order to check that this resolution did not exclude relevant data during linear interpolation, such as along steep gradients, a resolution of 0.01 mm was created. By subtracting the upper and lower surfaces, aperture fields were obtained at the respective resolutions of 0.1 mm and 0.01 mm, and then compared.

The resulting normalised cumulative frequency of the aperture distributions obtained from the two resolutions can be seen in Figure E-3, from which no obvious differences can be observed. It should also be noted that each aperture is calculated at this point by referencing the upper surface by the spacer ring and then subtracting the lower surface, which can yield negative apertures.

Changing the resolution increases the range of values, meaning more data from the surfaces are preserved after interpolation (Table E-1). The increase in range equated to an average across all samples of 0.0149 mm, which is an average percentage increase of 0.44 %. The apertures of each case using different resolutions were statistically tested against each other using a Kolmogorov Smirnov test to determine whether they come from the same distribution. There was no significant difference between the samples using 0.1 mm and those having a resolution of 0.01 mm, with p values for all cases above the significance level of 0.05.

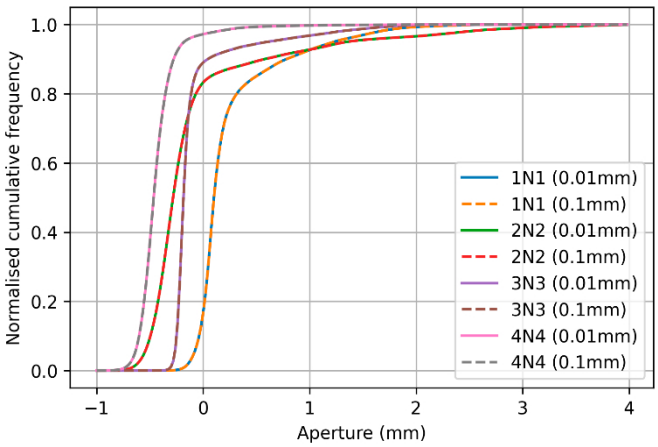

Figure E-3. *Normalised cumulative frequency of the apertures for all four samples, comparing the use of a resolution of 0.01 mm and 0.1 mm during interpolation.*

Table E-1. Minimum and maximum aperture values (mm) for each sample using a resolution of 0.1 mm and 0.01 mm during interpolation.

	1N1	2N2	3N3	4N4
Minimum Res 0.1 mm	−0.337	−0.892	−0.997	−1.004
Maximum Res 0.1 mm	2.734	4.460	2.344	2.015
Minimum Res 0.01 mm	−0.339	−0.899	−1.015	−1.020
Maximum Res 0.01 mm	2.735	4.460	2.357	2.018

Therefore, using a resolution of 0.1 mm captures sufficient surface data, and allows for the data to be processed much faster than higher resolution cases while remaining statistically similar to a resolution of 0.01 mm. Increasing the resolution does not improve the aperture distribution either, as the minimum value decreases further with higher resolution, moving it further away from the expected reality of no negative apertures.

As Table E-1 and Figure E-3 highlight that there are many negative apertures present in all the samples when the upper surface has been correctly referenced and shifted for the spacer ring dimensions. Sample 1N1 shows the least negative values with 13 % of the aperture being below zero. However, cases 2N2, 3N3 and 4N4 have 82 %, 88 % and 97 % of the aperture below zero, respectively. If the negative values are assumed as contact area, then the spatial distribution is not consistent with observations of the pressure films (Figure E-4). Therefore, it is clear that the number of negative values present in the aperture field distribution is due to a processing error.

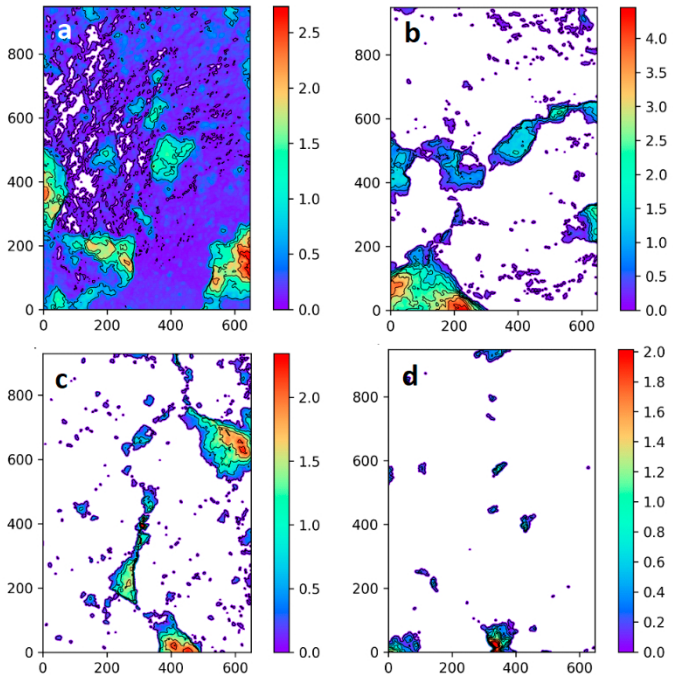

Figure E-4. *Aperture field (mm) for 1N1 (a), 2N2 (b), 3N3 (c) and 4N4 (d) with dimensions 95 mm by 65 mm. Negative apertures are assumed as contact points and represented by the white areas. These are based on the stated spacer ring dimension used for separating the upper and lower surfaces.*

E4.3 Translation

During the scanning process it was not possible to align the surfaces perfectly, and after interpolation the upper and lower surface may be offset from the original fracture which could lead to the negative values present. To address any misalignment, the lower surface was translated relative to the upper surface to increase the minimum aperture value with the rationale that negative apertures should not occur. This method did not consider the area of the negatives, only the minimum value, and the translations were done in 0.1 mm steps so the nodes of the upper and lower surface are always aligned. Only small translations were required in order to reduce the negative values, with the largest translation in the X direction of 0.4 mm for cases 1N1 and 4N4. The greatest Y translation of 0.4 mm was required for 2N2 and 4N4; however, reduction of the minimum aperture still produced an aperture distribution with many values below zero.

The effect of translations on the normalised cumulative frequency of the samples can be seen in Figure E-5. For all cases the number of negative values below 20 % of the distribution increased, bringing the values closer to zero. However, this only resulted in a reduction in negative areas for 1N1, were the percentage contact area decreased from 13 % to 6 % after translation. Samples 3N3 and 4N4 remained the same with 88 % and 97 % negative values respectively. Sample 2N2 was the only case in which increasing the minimum value resulted in negative apertures actually increasing from 82 % to 84 % after translation. This is not sufficient to account for all the negative apertures seen within the samples, so it is apparent that further corrections are needed.

E4.4 Vertical adjustment using pressure film

The basis for this analysis is the fact that the spacer ring dimension is a potentially significant source of error, because the measurements were not made at the time of the experiment, due to an error in protocol. When the spacer ring measurements were made at a later date, it was by then uncertain which rings had actually been used in the experiment. Therefore, we treat this as an uncertain parameter, albeit based on the mean value provided (9.92 mm). Also, we adopt the previously discussed translation of the surfaces combined with the use of the pressure film data as a starting point for increasing the vertical shift.

In order to use the data from the pressure film, the bitmap data set was interpolated, using nearest neighbour, onto a regular grid of the same dimensions as the surfaces and same resolution. Each cell has one of 11 colours, where white represents no pressure data and red represents pressure above 10 MPa. Using nearest neighbour interpolation ensures that the 11 colours remain constant and new colours are not introduced as a result of interpolation between cells. According to the manufacturer, the thickness of the film is 200 ± 10 microns, so areas of white are assumed to be greater than the thickness of the pressure film, and not in contact.

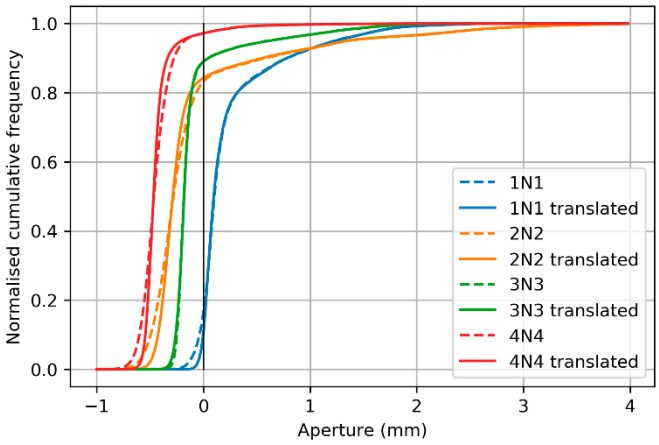

Figure E-5. *Normalised cumulative frequency of original and translated aperture fields showing reduction in minimum aperture after translation.*

As a first comparison, calculated apertures greater than 200 microns were removed and only areas of white (corresponding to 200 microns and greater) were selected from the pressure film. An overlay of the pressure film containing only white areas and the calculated aperture field only containing values less than 200 microns was then compared. Therefore if the pressure film and aperture perfectly aligned the two overlays should fit together, as two jigsaw pieces would (Figure E-6c,d). By increasing the vertical shift of the upper surface, the number of calculated aperture values above 200 increases and hence the boundary of this cut-off changes. In this way the shift can be increased systematically until a visual best fit is achieved between the pressure film and calculated aperture field.

With this approach, it was found that only using white areas (Figure E-6c) from the pressure film made it hard to visually match up areas of the aperture field. Therefore, it was concluded to be insufficient to only consider white areas (> 200 microns) in the pressure film data. Next, a combination of white and dark blue areas was used, where dark blue on the pressure film represents the lower limit of pressures, at or less than 2.5 MPa. This represents small pressures where the film is just in contact. Hence it is assumed that a combination of blue and white can still be assumed as approximately 200 microns or greater. Using this combination yielded significantly better qualitative results as it was easier to visually match the pressure film and areas of the aperture removed (greater than 200).

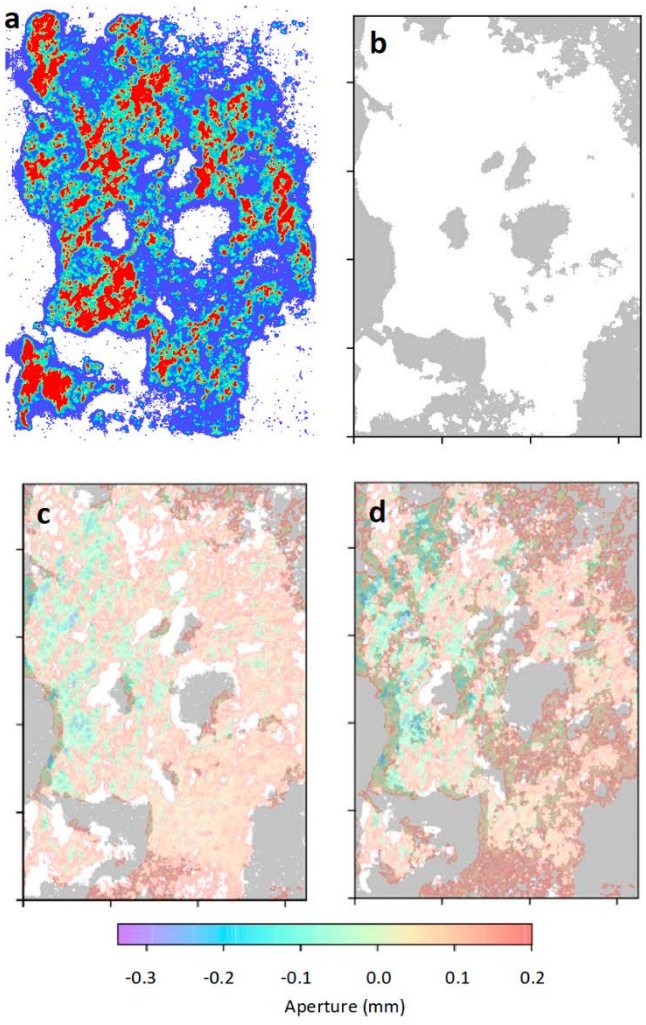

Figure E-6. *a) Pressure film data for 1N1, b) pressure film interpolated onto grid with grey representing white areas from the pressure film, c) aperture field with upper surface shift of 9.92 mm overlay, with pressure film data representing white areas, d) overlay with blue and white areas included in pressure data.*

Assuming no negative apertures should exist in a fracture under no load, it would be reasonable to shift the upper surface by the minimum negative value, so that the smallest aperture is set to zero and all other apertures become positive. For all cases this produced an aperture field that did not correspond with the pressure film with most of the aperture values being above 200 microns and the largest aperture being unrealistically large (> 6 mm).

Instead, the aperture field was calculated, based on using a shift of 9.92 mm. The shift was then systematically increased until the aperture and pressure film showed good visual correspondence. Decreasing the shift did not improve the alignment of the aperture with pressure film for any case. Once good correspondence was achieved all remaining negative values were assumed to represent contact areas, and were therefore removed from the aperture field (i.e., set to zero). Sample 1N1 required the least additional shift, of 9.96 mm instead of 9.92 mm, although it was still 0.02 mm above the standard deviation of the spacer rings. For all other cases, the required shift was significantly greater, with 2N2, 3N3 and 4N4 upper surfaces being vertically shifted by 10.37, 10.22 and 10.47 mm, respectively. For 4N4, this is a shift of 0.55 mm above the stated spacer ring dimension and significantly greater than the standard deviation.

E4.5 Corrected apertures

The resulting corrected apertures can be seen in Figure E-7, and the corresponding distributions are shown in Figure E-8. Each surface has been interpolated onto a regular grid with a spatial resolution of 0.1 mm, the upper surface translated relative to the lower to increase the minimum negative value and finally the upper surface vertically shifted so that the resulting aperture corresponds with the pressure film data. Negative values are still present in all cases which equate to 4 % of the aperture for samples 2N2 and 4N4, and 1.5 % for 1N1 and 3N3. Negative values are set to zero and assumed to be contact areas between the upper and lower surface. This method provides a realistic aperture resulting from data used from a natural fracture. This methodology serves to make significant corrections to the scanned surfaces, so that the resulting calculated and processed aperture field more closely resembles the (unknown) natural fracture aperture field.

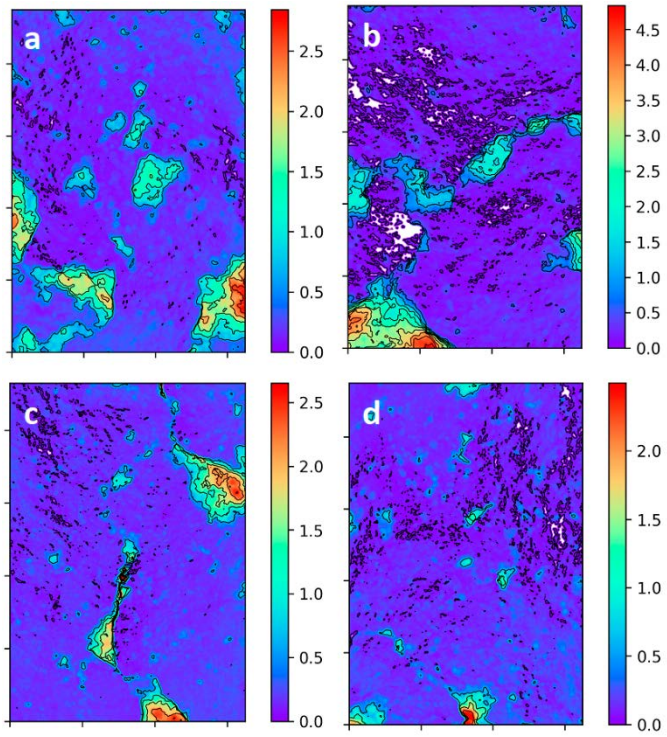

Figure E-7. *Corrected aperture fields (mm) for 1N1 (a), 2N2 (b), 3N3 (c) and 4N4 (d) with dimensions of 65 × 95 mm.*

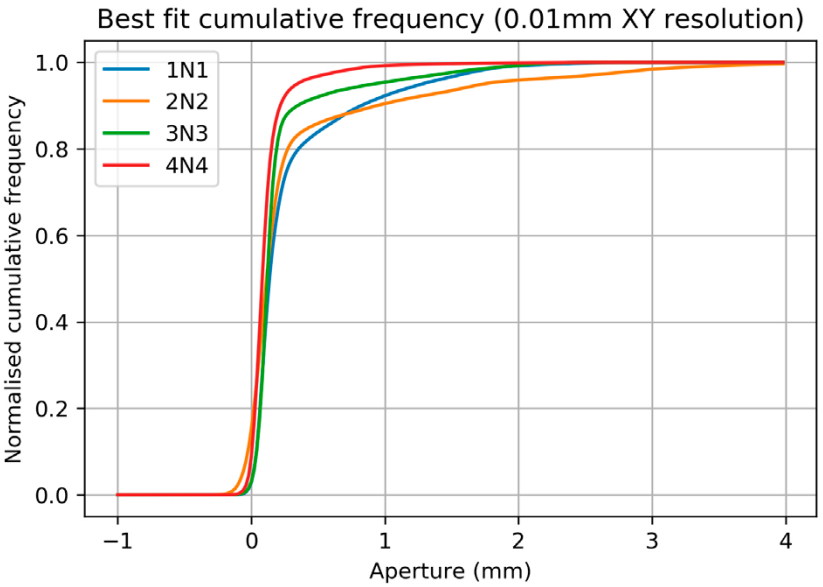

Figure E-8. *Normalised cumulative frequency for the corrected aperture distributions of all samples.*

E5 Modelling and methodology

E5.1 Model purpose

The model purpose in Task 10.2.1 as outlined by the Task Description is to confirm if single fracture observations made on the scale of a pilot borehole can be used to make predictions of single fracture properties on the deposition hole scale. Our initial focus has been on analysing and re-creating fracture surface roughness, which is a relatively easy task with the methods we have used. However, using the rough surfaces to obtain a variable aperture field with a distribution consistent with measurements of aperture is a more difficult task. Therefore, most of our efforts have been placed on the latter, i.e., on developing methods and workflows for obtaining variable aperture fields, and such that practical model validation on the basis of both fracture surface roughness and fracture apertures is attainable.

Thus, the main aim of our work is to develop and evaluate a method for reproducing rough-surfaced fractures with variable aperture using information obtained from 3D scans of natural rock fracture surfaces. A model for stochastic fracture aperture generation is developed based on previous work using self-affine fractal concepts, which includes a refined method for representing correlation between the upper and lower surfaces of the fracture. The model is used to generate an ensemble of realisations of fracture apertures, which is evaluated against the measured natural fracture aperture. Furthermore, a detailed sensitivity analysis is conducted on the variability of the Hurst and scaling parameters and the correlation obtained from the surface scans of the fracture in terms of their impact on model performance. Finally, the model is used for spatial upscaling, where a subsection of the measurements are used to predict the full extent of a fracture length scale of 1 meter.

E5.2 Model description

Fracture surface roughness has been shown to exhibit self-affine fractal properties (Brown 1987; Power and Tullis 1991; Renard et al. 2006). The underlying concept of our approach is to generate two self-affine fractal surfaces, representing the upper and lower surfaces of a fracture, using fractal scaling information derived from measurements of natural fractures. The two generated surfaces will have partial correlation so that the resulting void space distribution is consistent with the measured aperture distribution, and such that there is high correlation between the surfaces for large-range roughness and lower correlation at smaller scales.

A spectral synthesis approach is used to numerically produce fractals that represent two surfaces which when combined form a fracture with variable aperture. To do this a symmetric matrix containing Fourier components must be defined, where the Fourier components can be obtained from measurements to obey the various desired properties of the fracture. Each component is comprised of an amplitude and a phase. Fractal dimension and any information about relative anisotropy is contained within the amplitude component that scales with a power law. Thus, the topography of the fracture surfaces are controlled by the phase of the Fourier components. If the phase is identical for the upper and lower surfaces, the resulting fracture aperture is constant, representing a perfectly mated fracture. In order to create a variable aperture field, the topography of the two surfaces need to be uncorrelated or partially correlated at different wave lengths. When random numbers are used to describe the phase of the Fourier components, the degree of matedness between the surfaces can be controlled by the degree of correlation between the random numbers used.

Natural rock surfaces can be described by a power spectral density function *G(k)* as follows (Brown 1995):

$$G(k) = Ck^{-\alpha} \quad \text{(E-1)}$$

where $k = 2\pi/\lambda$ is wavenumber, λ is the wavelength which corresponds to distance along the profile, C is a proportionality constant which varies among surfaces and corresponds to the intercept of the logarithm of the power spectrum, and α is the fractal dimension in the range of $2 < \alpha < 3$ which corresponds to the slope of the logarithm of the power spectrum. To obtain the correlation between the upper and lower surfaces of the fracture scans, the power spectral density of each surface and the resulting aperture needs to be obtained, which can readily be calculated using Fast Fourier Transforms (FFT).

In principle the Fourier decomposition can be done for an infinite number of k values, however in practice there is a clear limit. The limit is defined by the resolution of the surface scans, and any pre-processing interpolation that has been done before calculating the power spectral density (PSD) of the fracture surface. When the period of the sine waves are equal to the number of mesh cells in one dimension, then each oscillation of the sine wave exactly covers one cell. Increasing the resolution beyond this point so more sine waves cover a single cell would have no effect on the amplitude. The maximum frequency that is useful for the surface is therefore $k = 1/N$, where N is the maximum number of cells along one edge length of the fracture scan. Also, when $k = 1$, this corresponds to a sine wave that fits exactly once within the surface.

– Correlation analysis

The correlation of the upper and lower fracture surfaces as a function of wave number k can be calculated by using the ratio of the PSD from the aperture over the sum of the PSDs of the two surfaces. Ogilvie, Isakov, and Glover (2006) called this the PSD Ratio (PSDR, $\xi(k)$), where

$$\xi(k) = \frac{G(k)_{aperture}}{G(k)_{upper\ surface} + G(k)_{lower\ surface}} \quad \text{(E-2)}$$

If the PSDR tends towards unity then the surfaces are completely independent (Glover et al. 1998b; 1998a). If the PSDR is less than unity, then some correlation is occurring between the upper and lower fracture surfaces at that specific wavenumber. The correlation at each wavenumber is obtained by subtracting the values of the PSDR polynomial regression from 1, i.e., $\mathrm{Corr}(k) = 1 - \xi(k)$. Here we introduce a polynomial regression over the PSDR obtained from measurements of a rock fracture from the smallest to largest PSDR(k) value as a convenient approach to remove the fluctuations and obtain values for the general trend as a function of wavenumber (or wavelength). Fluctuations in the PSDR inevitably occur when calculating the PSD from measurements of fracture surfaces due to natural variability in the upper and lower surface as well as measurement precision.

During aperture generation, different quantities of wavenumbers may be required and will not necessarily match the amount obtained from the analysis of the real fracture. Therefore, the correlation values are typically re-scaled along the length direction of a profile to the correct number of values that are needed for the generation method. Due to the method of generating a self-affine fractal surface, the dimensions are limited to $2 \times 2^n + 1$ in X and Y, so the correlation values are scaled in length to 2^n, which is half of the desired edge length of which the aperture will be generated at. This is important as it will maintain the desired correlation and structure regardless of the resolution used to generate the aperture.

Fractures typically have high correlation at small wavenumbers (large wavelengths), indicating there is large-scale correlation across the fracture. As the wavenumber increases (and wavelength decreases) the matching between the surfaces typically decreases. Once the correlation function ξ(k) is obtained, a number swapping algorithm is used to create several arrays of different correlations which represent the different wavenumbers. We adopted a method similar to Ogilvie et al. (2006), and developed a number swapping algorithm that swaps the positions of numbers within one random normally distributed array until a set correlation, defined by the matching analysis, is reached between the other random normally distributed array. The algorithm is executed several times such that two correlated arrays are created for every wavenumber that is needed. Correlated pairs of values are selected from the arrays and are placed in two grids that represent the upper and lower surface in the corrected position depending on the wavenumber. This creates a partial correlation between the upper and lower surface that changes with scale. To create different realisations, different pairs are randomly selected from the arrays, and the phase of the Fourier components is defined by these random number sets.

– Scaling properties

The other parameters needed to generate a self-affine fractal surface are representations of the Hurst exponent and scaling parameter. For a self-affine profile to appear similar at different scales, it must be scaled anisotropically in two principle directions, which for fractures corresponds to length versus topographical height of the rough surface. If the abscissa (length) is scaled by a factor of λ, the ordinate (height) needs to be scaled by λ^H. The RMS-COR method applies this relationship and is used to analyse the standard deviation of height difference at different length intervals (Malinverno 1990; Renard et al. 2006; Candela et al. 2009). At vertices Δv apart, the standard deviation σ of the height differences δh can be calculated as follows:

$$\sigma[\delta h(\Delta v)] = \sqrt{\frac{\sum_{v=0}^{N-\Delta v}(h(v+\Delta v)-h(v))^2}{N+1-\Delta v} - \left(\frac{\sum_{v=0}^{N-\Delta v}(h(v+\Delta v)-h(v))}{N+1-\Delta v}\right)^2} \quad \text{(E-3)}$$

where Δv is the number of vertices between the height values being analysed, $h(v)$ is the height value at vertex v, and N is the number of vertices within the line. When the standard deviations are plotted as a function of the distance between the vertices in logarithmic space, a straight line will be produced. The slope of the line represents the Hurst exponent and the intercept equals the standard deviation of adjacent vertices, the value of which is used to scale generated surfaces.

The method is relatively easy to implement but affected by the finite length of trace profiles. Therefore, Δv must be small compared to N; for this reason, if Δv is above approximately 10 % of maximum trace length it is not considered reliable (Marsch and Fernandez-Steeger 2021). The Hurst exponent can also be underestimated due to the finite trace length. However, the RMS-COR method is considered to underestimate the Hurst exponent when $H > 0.5$ (Stigsson and Mas Ivars 2019). Therefore, we implement the following correction as suggested by Marsch and Fernandez-Steeger (2021); if $H_{RMS,cal} > 0.5$ then $H_{RMS} = \ln(H_{RMS,cal}) + 1.18$.

– Fracture surface and aperture generation

Here, we take trace profiles across each surface in the X and Y directions along every mesh cell, so the total number of profiles in one direction is the same as the total number of cells along one edge length. This results in 1 970 trace profiles in each direction, with a length resolution of each trace profile of 0.1 mm. The RMS-COR function is then executed on every profile, providing a Hurst and scaling parameter for each profile, where a combination of parameters that most represents the surface must be selected. The relative anisotropy is calculated by using the median $H(X)/H(Y)$. The Hurst exponent and anisotropy are used to define the amplitude of the Fourier components.

When all the Fourier components are known and arranged in a 2D complex and symmetric matrix in the correct position regarding wavenumber, a 2D Fast Fourier Transformation is executed over the measurements, the real part of which represents the fracture surface with a mean value of zero. The last steps are to scale the surface to the required size, and scale the asperities to that defined by the scaling parameter obtained from the RMS-COR function and vertically shift the mean level of the fracture surface such that no negative values occur in the aperture field. It is important to account for different trace resolution between the real data and generated aperture, so the scaling value can be corrected to represent the same resolution, and hence produce an accurate re-scaling of the surface and aperture.

Note that the topography of each pair of surfaces will depend on the random numbers used to define the Fourier shifts as well as the sequence used to select the correlation arrays. Therefore, due to this stochastic nature of sampling, an ensemble of aperture realisations must be generated for a given set of input parameters in order to compare against the measured fracture aperture. However, each generated sample is an equally probably realisation based on a given set of input values. Therefore, this can enable a convenient approach for generating multiple fractures based on a limited number of fracture measurements. Furthermore, since the scaling behaviour of the surface and relative positions of different size asperities is controlled by the Hurst exponent, it enables a convenient approach to up-scaling fracture surfaces, based on the assumption of the properties of the rough surfaces being self-affine for the spatial scales considered and the correlation between surfaces being scale independent.

E5.3 Determination of critical aspects

The key model aspects and assumptions of the method are listed as follows:

- Assumes fracture surfaces are self-affine.
- Assumes that the vertical alignment of the upper and lower scanned surface is correct; this is important because incorrect alignment will change the correlation between the surfaces and the resulting aperture field.
- Assumes that the correlation between the two surfaces is scale independent; this is necessary for up-scaling fractures.
- Assumes that rock debris and fall out during opening the fracture does not significantly perturb the fractal nature of the surface; that is, that the Hurst exponent and scaling parameters obtained are representative of the natural surface even after opening.
- It is necessary to study multiple trace profiles along the fracture surfaces in order to obtain parameter combinations that produces aperture distributions that correspond with the measured aperture distribution.
- The stochastic nature requires sufficient realisations of fractures to be used to ensure stable results when comparing distributions of generated fractures against a measured fracture.

Model parameters

Model parameters are described in the Model Description Section A5.2 above.

To obtain the Hurst exponent, H, and the scaling parameter from the measurements of the fracture surface roughness measurements of each fracture 1N1, 2N2, 3N3 and 4N4, profiles are taken along the X and Y directions of the upper and lower surfaces of the mesh, which is linearly interpolated from the surface scans. This produces a large number of H and scaling parameter pairs, spanning a large range in values. Based on the analysis of Stock and Frampton (2023), we simply select the 75^{th} percentile of H and the scaling parameter, under the assumption that this acts a sufficiently accurate representation for fracture generation. It should be noted that the 75^{th} percentiles work well for the 200×200 mm fracture that was analysed, and we assume these fractures 1N1, 2N2, 3N3 and 4N4 to behave similarly, although other fractures may behave differently.

E5.4 Definition of performance measures and criteria

The performance measures considered to characterise fracture roughness are the Hurst exponent H, scaling parameter, standard deviation of the asperities and the El-Soudani metric. The El-Soudani is the ratio of the true length of a profile to the nominal length of the profile.

The performance measures considered to characterise fracture aperture are the aperture distribution of the sample ensemble compared to the measured aperture, where the Kolmogorov-Smirnov test is used to quantify the maximum deviation between them. The median and inter quartile range of the distributions will be used as a comparison to validate the effectiveness of the aperture generation method in terms of distribution.

E5.5 Identification of influential factors

The influential factors that affect the actual and modelled fracture aperture roughness distribution are identified in the following.

The method used is not directly process based, as it does not attempt to represent the physical mechanisms causing fracture generation; however, it is based on observations. The essential idea of self-affine fractals is that large scale behaviour can be predicted based on establish qualitative similarity with behaviour on the smaller scale. Thereby, the method is based on an assumption that the physical mechanisms responsible for causing fracture roughness is the same at all scales. In practice, there is of course a limited range of scales on which this can be valid; however, such spatial length limits have not been studied within the scope of this work.

Influential factors included the method by which the surfaces are modelled, which assume that the natural rock surfaces are self-affine. Any process that has altered the surface, making it no longer self-affine, cannot be accounted for. This also applies for any sharp changes in gradient on the surface or ridges which cannot be reproduced using this method. It is important to choose a Hurst exponent and scaling parameter that is representative of the surface to generate the aperture realisations. A range of Hurst and scaling parameter values are obtained when trace profiles are taken across the surface, which makes it non-trivial to select. An analysis has been conducted which found that the 75th percentiles of the Hurst exponent and scaling parameter produce an ensemble that best corresponds with the measured aperture distribution (Stock and Frampton 2023). Other factors include the correlation between the upper and lower surface, which is understood to be affected by rock fall out. These have been accounted for by introducing a polynomial regression which removes fluctuations within the PSDR. Assuming that the correlation is scale-independent, then the surfaces can be up-scaled to any dimension with the same correlation structure.

It may also be possible to account for normal loading and generate aperture distributions that represent different stress states by altering the input parameters. However, it is currently unknown how the Hurst exponent and scaling parameter change under loading, so further analysis needs to be done on this.

E5.6 Uncertainty analyses

The uncertainties in measurements and in the method used, as well as model parameter sensitivity is discussed in the following.

During opening of the fracture, some rock was broken off, and although the volume of debris is unknown, it could be the cause of isolated and abnormally large apertures seen in the aperture fields. For this reason, the largest 5 % of apertures have been filtered from each case, removing these anomalies. If there was no rock break-outs or other debris, the corresponding aperture field would have been significantly smaller. However, it is difficult to predict how exactly adding rock pieces would affect the aperture field. By filtering we aim to obtain an aperture distribution that better represents the unopened fracture aperture by removing the largest apertures. Excessive filtering increases the risk of unintentional removal of large apertures. Therefore, we determine a threshold of 5 % to be a reasonable balance without excessively impacting the overall shape of the aperture distributions.

After the surfaces have been vertically aligned with the pressure film, not only large apertures are present, but also negative apertures. These have been corrected to zero aperture, i.e., are assumed to correspond to contact areas. This highlights that uncertainties in the scanned surfaces and their alignment is not only present for large apertures, but also leads to negative void space, which must be corrected.

Trace profiles taken across the measured surfaces result in a range of Hurst exponents and scaling parameters. This shows that no single value represents the surface, and selecting which value best represents that full surface is another uncertainty. Stock and Frampton (2023) show that the Hurst exponent and scaling parameter that follow the upper bound of this parameter space results in aperture distributions that best fit the measured data. However, the range in in Hurst exponent and scaling parameter is highly influenced by the method which is used to calculate the parameters. We used to RMS-COR function, which is affected by the maximum step length. Reducing the step length reduces

the likelihood of the regression line curving in log-log space in the method (Marsch and Fernandez-Steeger 2021). Changing the step length has no effect on the number of values obtained as the same number of trace profiles are used. Increasing the step length can increase the spread of Hurst exponents and scaling parameters obtained, which leads to greater uncertainties in the data. Because a trace profile is taken along every possible mesh profile in *X* and *Y*, there are some profiles that will go across areas where rock has fallen off the surface, leading to outliers. This may violate the assumption of the fractal nature of the fracture surfaces, and give values that are not representative of the total fracture surface. Reducing the step length reduces the spread in data, which reduces the error present when larger step lengths are used. It was found that the 75th percentiles for Hurst exponent and scaling parameter produce an aperture ensemble that best represents the measured aperture distribution (Stock and Frampton 2023). However, note that this study is based on the 200 × 200 mm fracture sample retrieved for the subsequent Task 10.2.2.

The correlation between the upper and lower surface can also potentially increase the uncertainty of the resulting fracture aperture generation procedure. We use the PSDR with a third-order polynomial regression to obtain the increasing correlation between the upper and lower surfaces with increasing length scale. Small fluctuations are not included with a lower order polynomial regression. However, this has little effect on the generated aperture realisations. It was found that it is more critical to obtain the end points of the PSDR accurately to reproduce measured apertures. However, as there is currently no method to digitally replace rock fall out, this can have a major effect on the measured aperture distribution. If a significant area of the surface has been altered, the correlation of the whole structure will not be accurately represented using this method. This could lead to large apertures generated that are not naturally present in the measured aperture field. Due to the number of uncertainties in the provided data, the correlation between the surfaces represents a significant source of uncertainty.

The method used, which relies on the assumption that the fracture surfaces are self-affine, cannot recreate any sharp steps within the surface. These could be natural or an artifact of opening and scanning the surface, but sharp changes in surface height are difficult to capture. These types of features are omitted, which may also lead to uncertainties in the generated fracture realisations.

E5.7 Prediction-outcome exercise

Fracture roughness

The method described in Section A5.2 has been implemented on the facture surface data from 1N1, 2N2, 3N3 and 4N4. For each case, 50 realisations of the upper surface, lower surface and the resulting aperture field are generated at the same scale. Out of the ensemble of 50 realisations, 5 are selected and converted to an STL file that can be used with the Surface Roughness Calculator (Magsipoc, Zhao, and Grasselli 2020) to obtain parameters from the full 3D surface. The El-Soudani Roughness coefficient is calculated, which is the ratio of the true surface area to the nominal surface area, and the standard deviation of the asperities is calculated to compare the measured surface with the generated surfaces. The same five surfaces are also used to calculate the Hurst exponent and scaling parameter along each possible profile in *X* and *Y* directions which are plotted on a scatter plot for comparison. All 50 realisations of the upper and lower surface are then used to calculate the Hurst exponents for the whole ensemble, and compared with the range in Hurst exponents from the measured surfaces.

The surfaces are then upscaled to the meter scale and used to calculate the aperture distribution for the up-scaled aperture fields. This does not require generating the surfaces again as they are, by design, self-affine fractal surfaces; it is a relatively trivial matter to rescale them to the appropriate size desired (Section A5.2, scaling properties).

1N1 surface

Table E-2 shows the calculations of El-Soudani roughness coefficient and standard deviation of the asperities across the upper and lower surface of 1N1, as well as for the 5 selected realisations of the upper and lower surface. As can be seen, the El-Soudani value is underpredicted for the generated surfaces for both the upper and the lower surfaces. However, the values for one surface remain consistent and only show a small variation. The opposite is seen for the standard deviation, with the generated surfaces having values greater than the measured 1N1 surface. However, the difference between each realisation also remains similar, with the largest difference between realisations being 0.08.

Table E-2. The El-Soudani roughness coefficient and standard deviation of asperities calculated for the lower and upper surface and generated realisations of both surfaces for 1N1.

1N1	El-Soudani	Std of asperities
Lower surface	1.041	2.13
Gen lower realisation 1	1.013	2.17
Gen lower realisation 2	1.013	2.25
Gen lower realisation 3	1.014	2.16
Gen lower realisation 4	1.013	2.15
Gen lower realisation 5	1.013	2.21
Upper surface	1.044	2.17
Gen upper realisation 1	1.022	2.25
Gen upper realisation 2	1.023	2.24
Gen upper realisation 3	1.023	2.25
Gen upper realisation 4	1.024	2.18
Gen upper realisation 5	1.024	2.21

As can be seen from Figure E-9 the range of Hurst exponents and scaling parameters obtained from the measured surface and the generated surfaces have significant overlap. However, the Hurst exponents from the generated surfaces do not generally have the large values seen from those obtained from measurements. This can be seen from both the scatter plot and the boxplots. The underprediction can also be seen in the boxplots of Hurst exponent for the five realisations.

The underprediction of Hurst exponent is not only in the 5 realisations, but is also present when the Hurst exponent is calculated from trace profiles across all the 50 realisations (Figure E-10). The H values for generating the lower and upper surfaces are 0.976 and 0.952, respectively, which represent the 75th percentile of the values obtained from the measured surface scans. However, the generated ensemble produces values of 0.897 and 0.874 for the 75th percentile, with median of 0.85 and 0.825 for the lower and upper surfaces. The total range in Hurst exponents is also larger than that of the measured surfaces, with values on the boxplot as low as 0.612, approximately 0.1 lower for the generated surface ensemble.

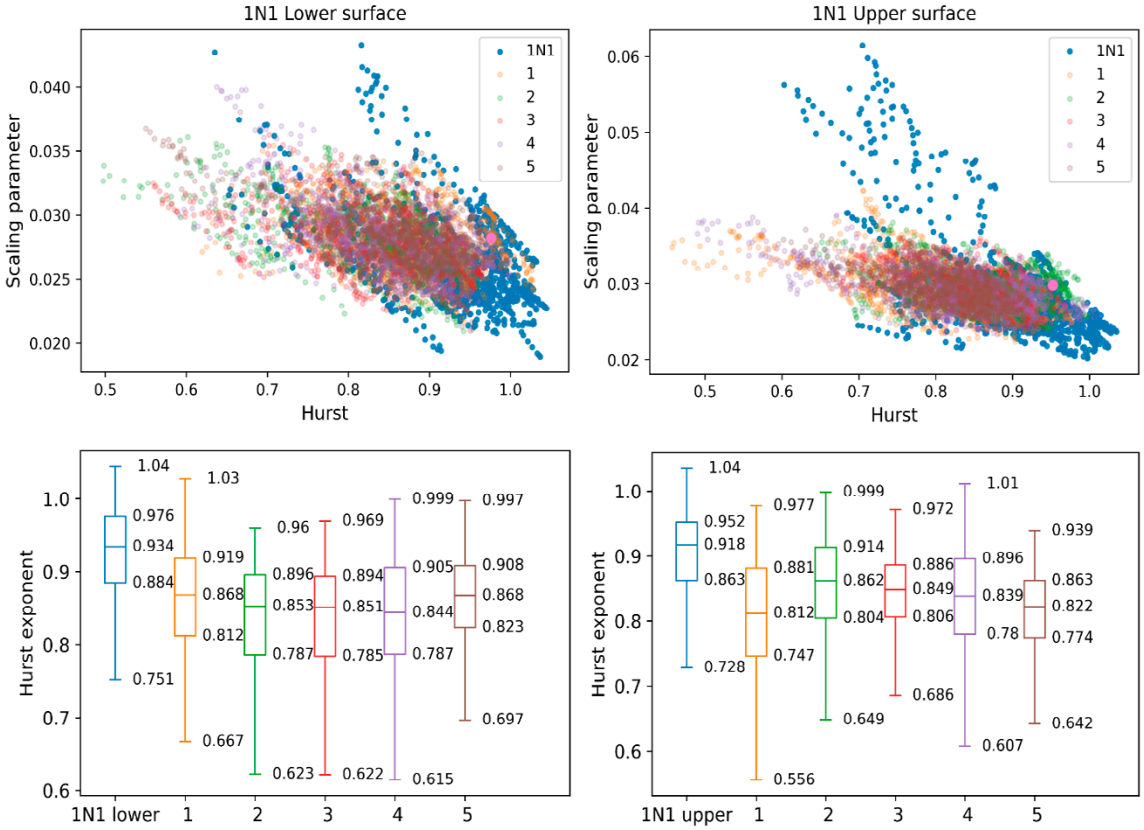

Figure E-9. *(Upper panels) Hurst exponent versus scaling parameter for the measured surface scans of 1N1 (blue) and five realisations of the generated surfaces. (Lower panels) Boxplot statistics of the Hurst exponent for the scans and five realisations.*

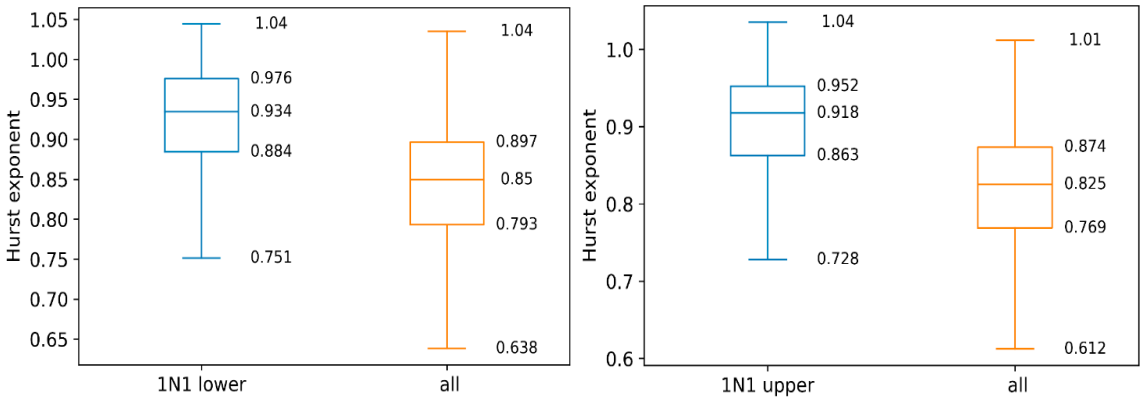

Figure E-10. *Boxplot of the measured Hurst exponent and the ensemble of 50 realisations for 1N1.*

2N2 surfaces

Values for El-Soudani are larger than that of the five selected surfaces, with a difference of approximately 0.04 for the lower and 0.02 for the upper surface. This shows that the measured surface scans are rougher than the generated surfaces. The values for the generated surfaces remain similar for all the generated surfaces; however, they show that the roughness is maintained, as expected. The standard deviation of the asperities for the measured 2N2 surfaces is lower than the generated surface (Table E-3). The smallest difference is 0.02, with the biggest difference of 0.09 mm.

Table E-3. The El-Soudani roughness coefficient and standard deviation of asperities calculated for the lower and upper surface and generated realisations of both surfaces for 2N2.

2N2	El-Soudani	Std of asperities
Lower surface	1.066	2.21
Gen lower realisation 1	1.026	2.27
Gen lower realisation 2	1.027	2.26
Gen lower realisation 3	1.027	2.25
Gen lower realisation 4	1.027	2.23
Gen lower realisation 5	1.026	2.25
Upper surface	1.054	2.19
Gen upper realisation 1	1.032	2.28
Gen upper realisation 2	1.032	2.26
Gen upper realisation 3	1.033	2.22
Gen upper realisation 4	1.034	2.23
Gen upper realisation 5	1.033	2.25

Scatter plots of the Hurst exponent and scaling parameters for the generated realisations and 2N2 surfaces show a larger spread in scaling parameter than the generated surfaces (Figure E-11). However, the generated surfaces produce smaller Hurst exponents across the surface. This is highlighted by box-plots that show each realisation underpredicting the Hurst exponent. The general trend of the generated realisations is also less steep than the apparent trend of the measured surfaces, and also shows a more compact scattering of the pairwise parameters.

The Hurst exponent obtained when all the generated realisations are used is still underpredicted, but the overall range in values is similar (Figure E-12). For the lower surfaces, the difference in minimum values is 0.026 and 0.01 for the maximum Hurst exponent. For the upper surfaces, the difference in the lowest value is greater at 0.056, with the maximum values being very similar again with a difference of 0.01. Differences between the median is approximately 0.07, and approximately a 0.2 difference between the 75th percentile of the Hurst exponent used to generate the surfaces and the median value of the generated realisations.

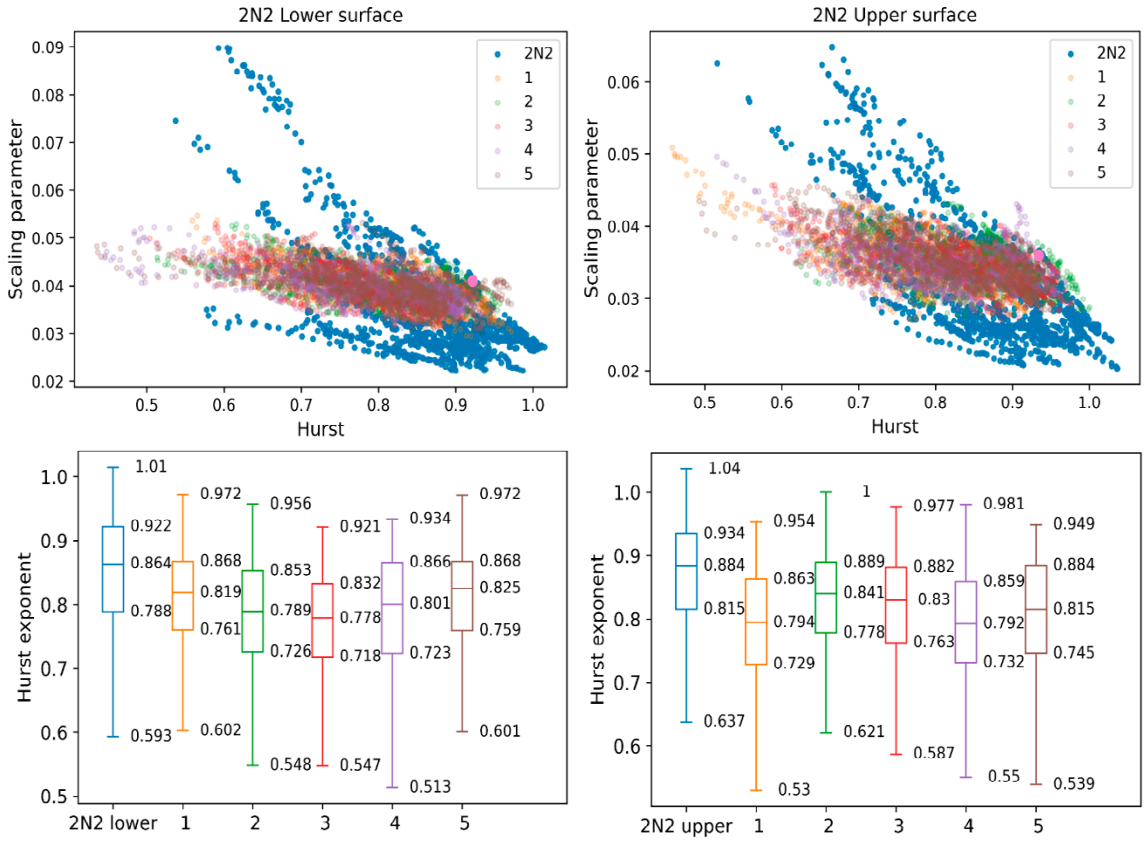

Figure E-11. *(Upper panels) Hurst exponent versus scaling parameter for the measured surface scans of 2N2 (blue) and five realisations of the generated surfaces. (Lower panels) Boxplot statistics of the Hurst exponent for the scans and five realisations.*

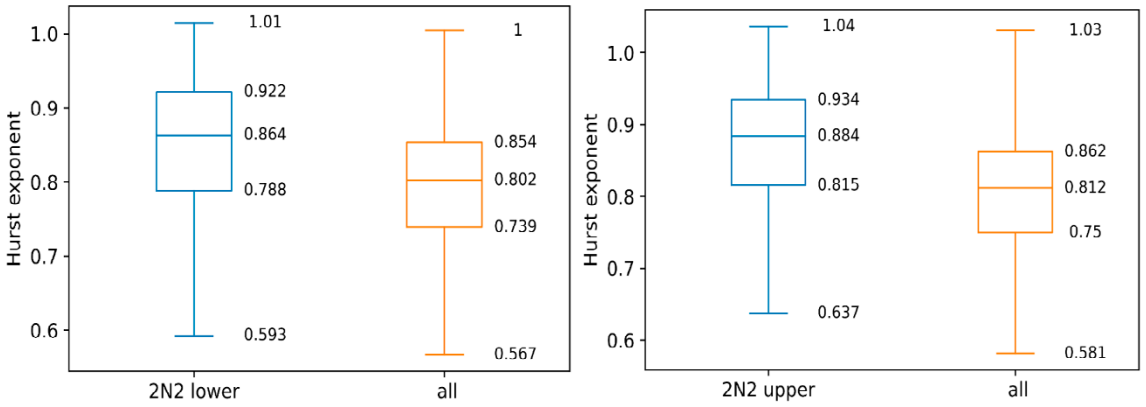

Figure E-12. *Boxplot of the measured Hurst exponent and the ensemble of 50 realisations for 2N2.*

3N3 Surface

The generated lower and upper surfaces (see Table E-4) show a consistent, but smaller value for the El-Soundani roughness coefficient with a difference of approximately 0.04 and 0.03, respectively. The measured lower surface standard deviation of the asperities is approximately 0.04 smaller than the generated realisations. However, for the upper surface, there are two realisations that only have a difference of 0.01 for the standard deviation. This shows that the generation method has generated a surface that is very similar to the measured 3N3 upper surface.

Table E-4. The El-Soudani roughness coefficient and standard deviation of asperities calculated for the lower and upper surface and generated realisations of both surfaces for 3N3.

3N3	El-Soudani	Std of asperities
Lower surface	1.064	2.21
Gen lower realisation 1	1.026	2.28
Gen lower realisation 2	1.026	2.25
Gen lower realisation 3	1.027	2.25
Gen lower realisation 4	1.027	2.23
Gen lower realisation 5	1.026	2.25
Upper surface	1.063	2.20
Gen upper realisation 1	1.034	2.21
Gen upper realisation 2	1.034	2.26
Gen upper realisation 3	1.035	2.24
Gen upper realisation 4	1.036	2.21
Gen upper realisation 5	1.035	2.25

The 3N3 lower surface has a significant range in scaling parameters (see Figure E-13), ranging from approximately 0.02 and 0.14 which is much greater than the variation seen from the generated lower surfaces. For the upper surface, the range isn't as large but is still greater than that calculated from surface realisations. For both 3N3 surfaces, the Hurst exponents exceed 1, whereas the generated realisations are limited to 1, as values greater than 1 are not possible in self-affine fractal theory. This is also the case for the measured surfaces but can happen due to uncertainties on the surface producing profiles that are no longer fractal. This is further highlighted with the boxplots of each realisation where the values are lower than the measured surfaces, and where the median of 3N3 surfaces is similar to the 75^{th} percentile of the generated surfaces. Both of the measured surfaces seem to have two trends, one steeper linear regression and another lower gradient, where most of the Hurst and scaling parameters from the surface realisations are located.

When all 50 realisations are measured, the median Hurst exponent of the measured lower and upper surfaces is approximately 0.01 higher than the 75^{th} percentile of the generated ensemble (Figure E-14). For the lower surface, the total range between minimum and maximum is similar at approximately 0.4 for both the generated ensemble and measured surface. However, for the upper surface, the range is greater for the measured surface, at 0.47 compared to 0.4 for the generated surface.

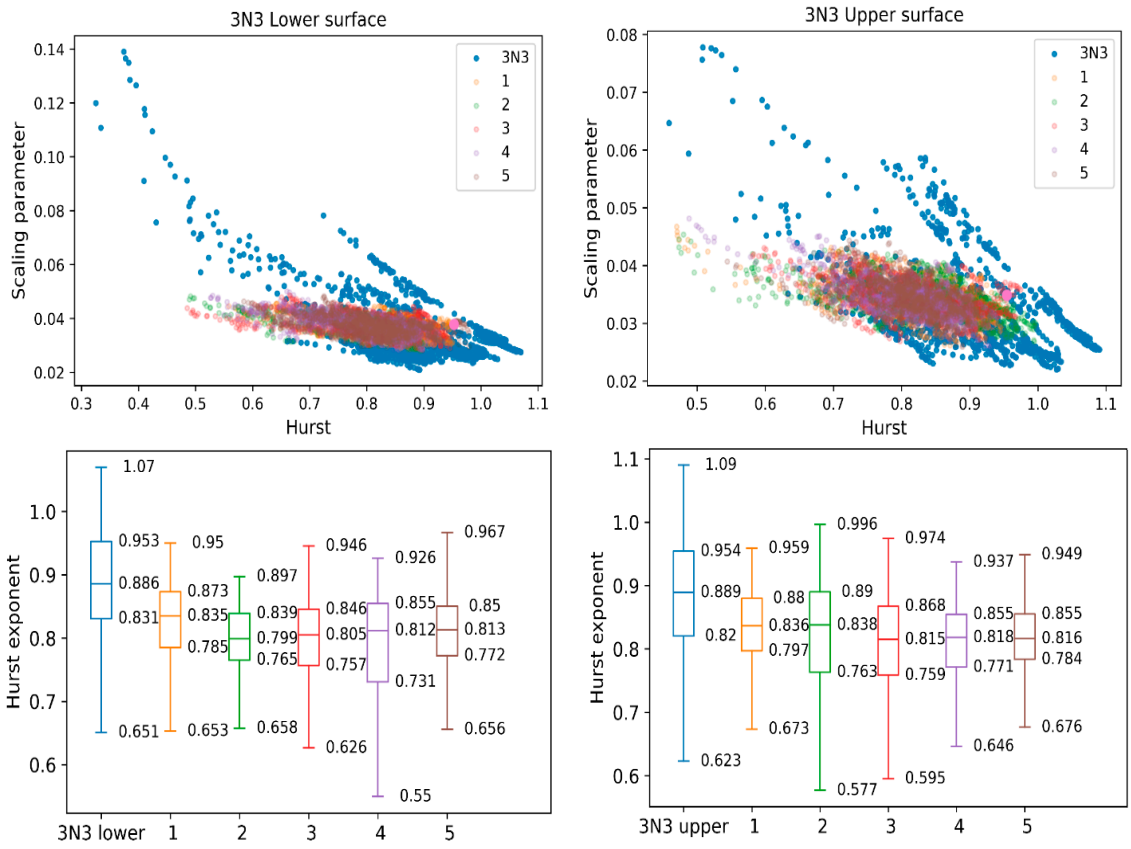

Figure E-13. *(Upper panels) Hurst exponent versus scaling parameter for the measured surface scans of 3N3 (blue) and five realisations of the generated surfaces. (Lower panels) Boxplot statistics of the Hurst exponent for the scans and five realisations.*

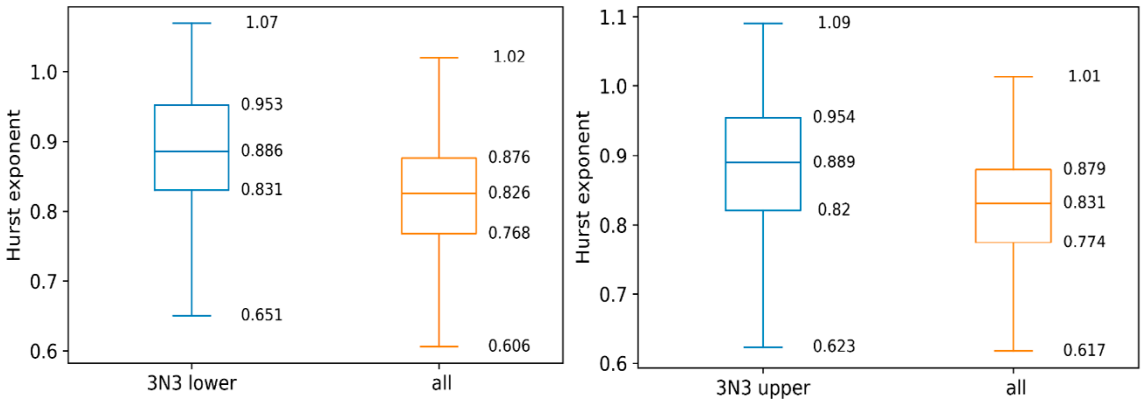

Figure E-14. *Boxplot of the measured Hurst exponent and the ensemble of 50 realisations for 3N3.*

4N4 Surfaces

Table E-5 shows calculated values for the El-Soudani and standard deviation of asperities calculated for the surface, which show a similar pattern to that seen on all the other surfaces. The roughness coefficient is larger for the measured surface than the generated surfaces for both the upper and lower, with a difference of approximately 0.02 and 0.03 respectively. The standard deviation of asperities for the measured surface is smaller for both the measured surfaces compared to the generated surfaces. This difference between the measured and the generated ranges from a minimum of 0.04 to a maximum difference of 0.09.

Table E-5. The El-Soudani roughness coefficient and standard deviation of asperities calculated for the lower and upper surface and generated realisations of both surfaces for 4N4.

4N4	El-Soudani	Std of asperities
Lower surface	1.048	2.16
Gen lower realisation 1	1.014	2.20
Gen lower realisation 2	1.013	2.23
Gen lower realisation 3	1.014	2.18
Gen lower realisation 4	1.013	2.18
Gen lower realisation 5	1.014	2.24
Upper surface	1.044	2.15
Gen upper realisation 1	1.020	2.24
Gen upper realisation 2	1.019	2.23
Gen upper realisation 3	1.020	2.20
Gen upper realisation 4	1.019	2.23
Gen upper realisation 5	1.020	2.21

A scatter plot for the Hurst exponent and scaling parameter for the lower and upper surfaces, and the generated realisations of those surfaces, can be seen in Figure E-15. The values from the generated surfaces overlap those of the measured surfaces significantly; however, they produce smaller Hurst exponents than obtained from the measured surfaces. The scaling parameter from the measured upper and lower surface also goes higher than is generated in the realisations.

When the ensemble of all 50 realisations is used to obtain the Hurst exponent (Figure E-16), the values are underpredicted compared to the 4N4 lower and upper surfaces. The difference observed between the minimum and maximum is also greater for the generated surfaces, with all the values (except for the top cap) are smaller than the measured surfaces.

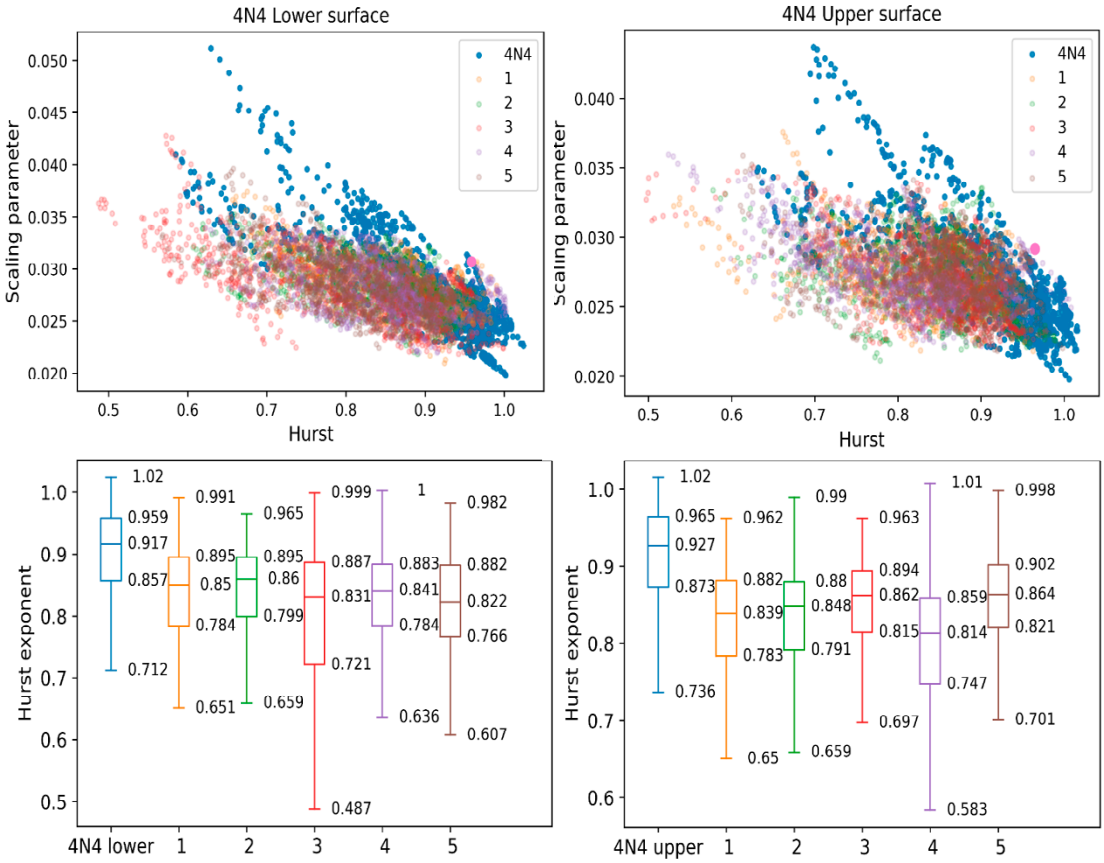

Figure E-15. *(Upper panels) Hurst exponent versus scaling parameter for the measured surface scans of 4N4 (blue) and five realisations of the generated surfaces. (Lower panels) Boxplot statistics of the Hurst exponent for the scans and five realisations.*

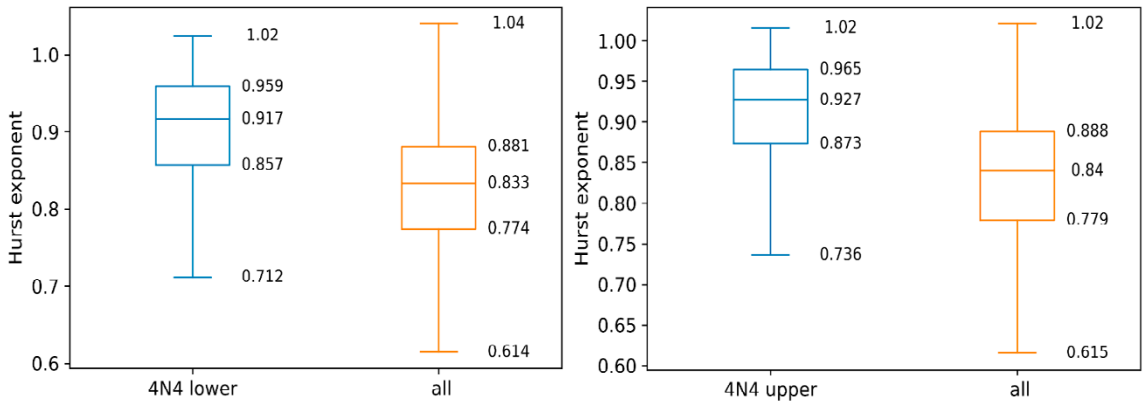

Figure E-16. *Boxplot of the measured Hurst exponent and the ensemble of 50 realisations for 4N4.*

Fracture aperture

The aperture distributions have been predicted at the same scale as the measured aperture distributions as well as upscaled to the 1-meter scale. Both the generated ensembles comprise of 50 realisations of the aperture field. To get an ensemble for the meter scale, the surfaces have been up-scaled according to the methodology based on self-affine theory described above, so the surface parameters will remain consistent.

Figure E-17 through Figure E-20 show the aperture distribution of the measured data, with the largest 5 % of apertures filtered from the data, compared against the ensemble generated at the same scale, as well as boxplots for additional comparison of the measurements with generated data. For 1N1 and 2N2 the aperture generation method underpredicts the aperture distribution for intermediate to large apertures, and for 3N3 and 4N4, the distributions are only slightly underpredicted for the largest apertures. 4N4 shows an overall very good fit, with the generated ensemble being extremely close to the measured aperture distribution. A Kolmogorov Smirnov test was used to quantify the goodness-of-fit between generated ensemble and measured distribution for 1N1, 2N2, 3N3 and 4N4 with KS test static values of 0.158, 0.162, 0.133 and 0.038, respectively. A perfect fit would have a value of zero, so calculated KS values closer to zero represent a better fit, which confirms 4N4 has the best correspondence between generated and measured apertures.

Figure E-21 shows the aperture ensemble distributions generated at the 1-meter scale. Up-scaling yields significantly smaller apertures, which is expected from the methodology used, if the mesh resolution remains the same. This is because as the mesh is upscaled, one cell represents a larger area, and due to the scaling behaviour of self-affine fractals, the surface topography is reduced, leading to a smaller aperture. The ensembles with the smallest median aperture do not necessarily generate upscaled apertures with the smallest values as the Hurst exponent is also used in rescaling the surfaces. This is the reason for 1N1 having the smallest median in the upscaled ensemble but second largest when generated at the same scale compared to 2N2, 3N3 and 4N4.

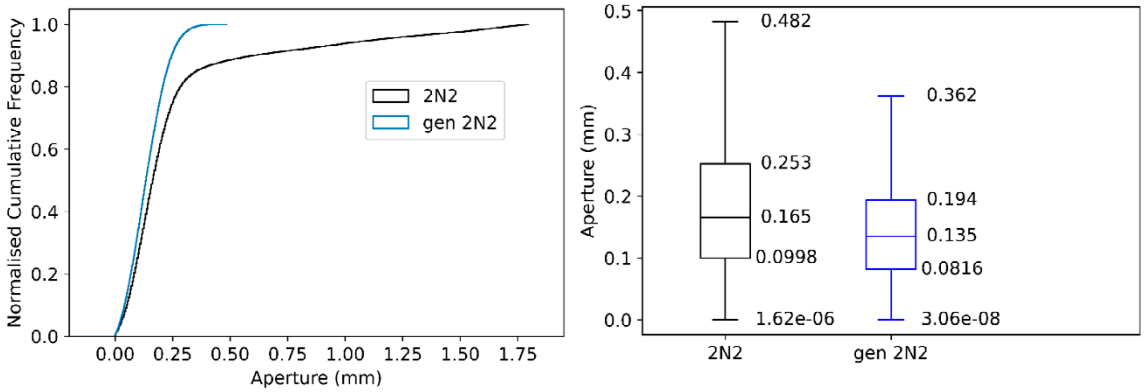

Figure E-17. *Distributions of the ensemble of 50 realisations of 2N2 generated at the same scale compared with the measured distribution and box plot of the data.*

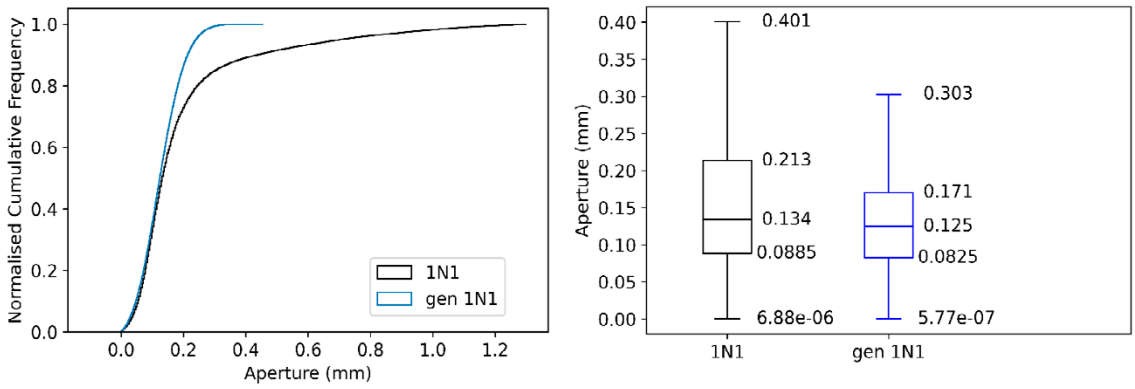

Figure E-18. *Distributions of the ensemble of 50 realisations of 1N1 generated at the same scale compared with the measured distribution and box plot of the data.*

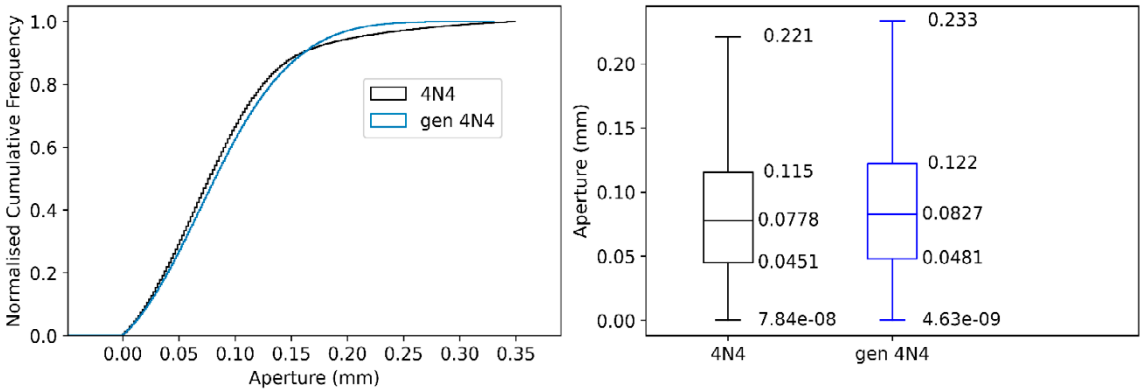

Figure E-19. *Distributions of the ensemble of 50 realisations of 4N4 generated at the same scale compared with the measured distribution and box plot of the data.*

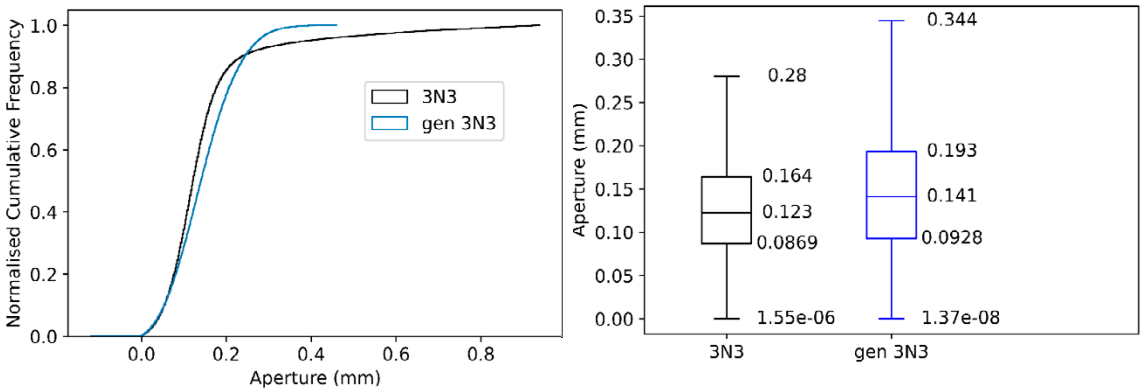

Figure E-20. *Distributions of the ensemble of 50 realisations of 3N3 generated at the same scale compared with the measured distribution and box plot of the data*

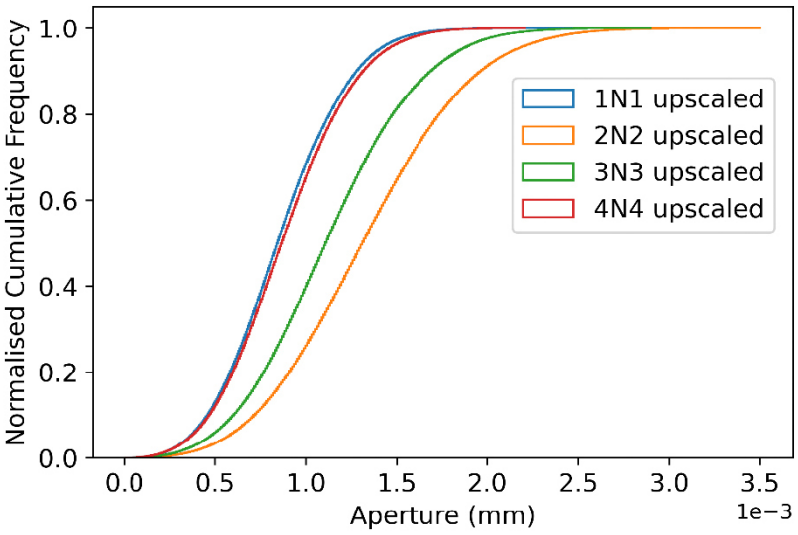

Figure E-21. *Ensemble distributions for 1N1, 2N2, 3N3 and 4N4 upscaled to one meter.*

E6 Results, discussion, recommendations and conclusions

E6.1 Outcomes and deliverables

The goal was to develop a method for reproducing naturally occurring rough surfaced fractures with variable apertures using information obtained from 3D scans of natural rock fractures. We could generate realisations of the fracture surfaces based on the parameters obtained from the surface scans that had similar El-Soudani roughness coefficients and standard deviations of asperities. However, the method tended to underpredict the Hurst exponents of the surface when trace lines are taken in X and Y directions across the surface. This could be the reason for the generated surfaces and the measured surfaces not having precisely the same values for the roughness metrics. Although the surfaces can be accurately reproduced, the resulting aperture ensemble distributions of the generated fractures tend to deviate from the measured distributions to a varying extent for the four fracture cases.

However, the method used here has been shown to produce much more accurate fracture aperture distributions for the 200 × 200 mm fracture sample using in the subsequent Task 10.2.2, which is reported in Stock and Frampton (2023). Therefore, it is relevant to investigate the reason for the same method not performing as well in the four 1N1, 2N2, 3N3 and 4N4 fracture samples. One reason could be the correlation between the upper and lower surface not being accurately represented. This could be the result of the rock fall out affecting the power spectral densities across the surface, and hence changing the correlation structure obtained from the fracture (Figure E-22).

As can be seen from Figure E-21 each fracture has a different correlation structure even though they are cut from the same fracture at locations next to each other. This suggests that the size of the fracture samples are not large enough to get a correlation structure that is representative of the fracture as a whole. For both cases 1N1 and 2N2, the lowest correlation is approximately 0.5 and 0.4, respectively, significantly lower than for the other two cases. The generated ensembles for 1N1 and 2N2 also have the highest Kolmogorov Smirnov statistic score, showing the largest dissimilarities from the measured distributions. The generated ensemble from samples with a higher correlation at larger wavenumbers show better correspondence with the measured data, with 4N4 fitting well.

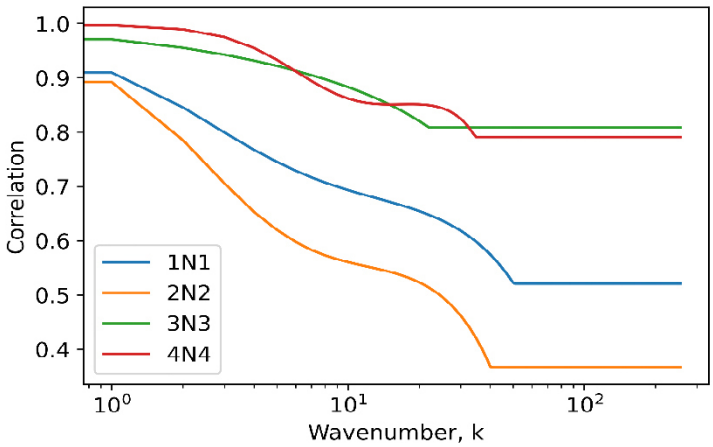

Figure E-22. *Correlation with scale between the upper and lower surface of 1N1, 2N2, 3N3 and 4N4.*

Improvements to the method could be made by developing a robust methodology to correct for any rock fall out. This not only affects the correlation analysis between the upper and lower surface but also affects the Hurst exponent and scaling parameters that are obtained from the surface. Achieving this would remove the main uncertainties of this method, which lie in the delivered data.

Another reason for the mismatches in aperture distribution could be the use of a single pair of values for the Hurt exponent and the scaling parameter. In this work, we select the 75th percentile value of Hurst and scaling parameter for each fracture, based on the assumption that this captures the roughness of the surfaces. This assumption stems from the analysis of the 200 × 200 mm fracture sample (Stock and Frampton 2023), where a more thorough analysis of the fracture parameter values is performed, and correspondence between the generated and measured aperture distributions are evaluated with Kolmogorov Smirnov tests. The study shows that a linear range of values for H and scaling parameter along the pairwise upper bound of the correlation between them produces the most accurate correspondence in terms of aperture distributions, which includes the 75th percentiles, but also indicates that it is only one possible choice from a range of values. It is, however, not yet known if this behaviour is similar for other fractures in addition to the 200 × 200 mm fracture sample considered in that study. Hence, a similar analysis for the four fracture samples 1N1, 2N2, 3N3 and 4N4 could be performed to determine their respective upper bounds, and could help determine whether the choice of 75th percentile is adequate or not for these fracture samples.

In terms of aperture distributions, the medians for all the cases are moderately similar, and differences can be due to large uncertainties within the provided surface data. It is known that the large apertures, that cause the aperture distributions from the measured aperture and generated aperture ensemble to deviate, are highly isolated and hence less likely to be affect flow through the fracture. The provided surface data is vital though, and this method would not work without any information on the fractal parameters of the surfaces and correlation between them. The generated apertures may also be more representative of the unopened fracture, which would explain why for 1N1 and 2N2 the generated aperture ensemble has a smaller median value.

E6.2 Comments on value of task and data and further recommendations

This exercise was useful as it resulted in an improved variable aperture generation method using data obtained from natural rock surfaces which can be implemented in further modelling, such as for representing realistic internal fracture variability in discrete fracture network models. Surface roughness data is useful as it can be used to generate aperture distributions that correspond to measured aperture fields. However, further work is needed to see whether predicting aperture distributions also improves predictions of flow through the fracture.

The amount of data provided was sufficient to develop the aperture generation model; however, more data would be useful in exploring the link between Hurst exponent and scaling parameter across several different fractures. The uncertainties with the measurements caused notable uncertainties in the resulting aperture field, even with the addition of pressure films for vertical alignment. The correlation is affected by debris and rock fall out, which makes the correlation used for this method highly dependent on the data provided. Although it was found that any fluctuations in the PSDR do not have a major effect on the generated aperture field, if the overall correlation is for low wavenumbers then this can significantly affect the generated aperture ensemble. The RMS-COR function used to calculate the Hurst exponent and scaling parameter can also be affected by rock fall out as it may create areas that are none fractal. This is hard to correct for though and has potential to lead to greater uncertainties.

Lower quality data would also have an effect on the generation method. Decreasing the resolution changes the PSDR of the data which is the method used to find the correlation between the surfaces. The scans of the natural surfaces should be done in the highest possible resolution. This also improves the accuracy of the RMS-COR method as the trace profiles will more accurately represent the true profile of the surface.

The main lessons learnt is the importance of the accuracy of the 3D scans, not only the resolution of the data but the vertical alignment of the surfaces. To generate an aperture field that is representative of reality, the correlation between the upper and lower surface is important. It is known that fluctuations in the PSDR have little effect on the aperture ensemble, but the minimum correlation value can affect

the overall aperture ensemble. Lower correlation would generate a larger median aperture and place the surfaces further apart. Even with pressure film data available to align the surfaces, it still comes with a large uncertainty.

Recommendations for further work would be to focus on aperture distribution rather than solely on surface roughness of individual surfaces. Without the correlation structure, and the ability to produce an aperture field, one surface is not useful for generating fractures with variable apertures and hence for subsequent modelling of flow and transport through heterogeneous aperture fields. We have found that several parameter combinations can produce a generated aperture ensemble that corresponds well with the measured data (Stock and Frampton 2023). However, it is worth to note that although those parameter combinations produce the same aperture ensemble distribution, the surface roughness will change for each combination. This could have a significant impact on flow through different realisations although the distribution remains the same. Thus, further work is required to fully understand which parameter combinations generate suitable ensemble not only for surface roughness and aperture distribution, but also in the context of representing flow and solute transport. This could be achieved by numerical modelling of flow over many different realisations using different input parameters for surface roughness but the same aperture distribution.

It should be noted that changing the mesh resolution whilst representing the same physical size can affect the correspondence between the generated aperture ensemble and the measured aperture distributions. This is another aspect that would benefit from further study, as there might be an optimal mesh resolution for generating apertures depending on the desired physical size. The upscaled aperture ensembles have significantly smaller values, which may change if the mesh resolution is increased for the large scale apertures.

E6.3 Conclusion

The method developed in this study can generate apertures that are representative of natural rock fractures based on high resolution 3D fracture surface scans. During opening of the fracture, rock debris fell out, resulting in abnormally large apertures in the measured aperture distribution, which required filtering before comparison. In work based on the 200 x 200 mm fracture sample from the subsequent Task 10.2.2, the method developed here generates aperture ensemble distributions with very high correspondence with the measured apertures (Stock and Frampton 2023). For the four fracture samples provided here in Task 10.2.1, the method generates aperture distributions that correspond to the measured apertures reasonably well. However, we note that the 75^{th} percentile for Hurst exponent and scaling parameter may not necessarily be the values that best represent the surfaces for these fractures. Also, there are some uncertainties within the correlation structure between the fracture upper and lower surfaces stemming from uncertainties in measurements. The approach to obtaining a correlation between upper and lower fracture surfaces has, however, been improved based on previous published methods by using a third-order polynomial regression. This results in a general trend of change in correlation with scale which is implemented over the required wavenumbers.

The way in which the surfaces are generated and the correlation between them, up-scaling of the generated apertures can be easily achieved. Upscaling from the centimetre scale to the metre scale results in apertures that are significantly smaller for all the cases. Aperture fields generated using this method are representative of a natural fracture aperture and could be implemented within larger DFNs as permeability fields, allowing for simulations to include a representation of aperture internal heterogeneity.

Arkitektkopia AB, Bromma, 2024

SKB is responsible for managing spent nuclear fuel and radioactive waste produced by the Swedish nuclear power plants such that man and the environment are protected in the near and distant future.

skb.se